Earth-Science Reviews 231 (2022) 104072

Contents lists available at ScienceDirect

Earth-Science Reviews

journal homepage: www.elsevier.com/locate/earscirev

Review Article

The 79 CE eruption of Vesuvius: A lesson from the past and the need of a multidisciplinary approach for developments in volcanology

Domenico M. Doronzo [a,*], Mauro A. Di Vito [a], Ilenia Arienzo [a], Monica Bini [b,c,d], Benedetta Calusi [c], Matteo Cerminara [c], Stefano Corradini [e], Sandro de Vita [a], Biagio Giaccio [e,f], Lucia Gurioli [g], Giorgio Mannella [b], Giovanni P. Ricciardi [a], Ilaria Rucco [a,h], Domenico Sparice [a], Micol Todesco [i], Elisa Trasatti [e], Giovanni Zanchetta [b,c,d,f]

[a] Istituto Nazionale di Geofisica e Vulcanologia, Sezione di Napoli, Osservatorio Vesuviano, Italy
[b] Dipartimento di Scienze della Terra, Università di Pisa, Italy
[c] Istituto Nazionale di Geofisica e Vulcanologia, Sezione di Pisa, Italy
[d] Centre for Climatic Change Impact CIRSEC, Università di Pisa, Italy
[e] Istituto Nazionale di Geofisica e Vulcanologia, Sezione di Roma, Osservatorio Nazionale Terremoti, Italy
[f] Istituto di Geologia Ambientale e Geoingegneria, Consiglio Nazionale delle Ricerche, Roma, Italy
[g] Université Clermont Auvergne, CNRS, IRD, OPGC, Laboratoire Magmas et Volcans, Clermont-Ferrand, France
[h] Heriot-Watt University, School of Engineering and Physical Sciences, Edinburgh, United Kingdom
[i] Istituto Nazionale di Geofisica e Vulcanologia, Sezione di Bologna, Italy

ARTICLE INFO

Keywords:
79 CE eruption
Vesuvius
Plinian eruption
Pompeii
Multidisciplinary approach
Pyroclastic succession
Pyroclastic currents
79 CE tephra dispersal

ABSTRACT

A full review of the 79 CE Plinian eruption of Vesuvius is presented through a multidisciplinary approach, exploiting the integration of historical, stratigraphic, sedimentological, petrological, geophysical, paleoclimatic, and modelling studies dedicated to this famous and devastating natural event. All studies have critically been reviewed and integrated with original data, spanning from proximal to ultradistal findings of the 79 CE eruption products throughout the Mediterranean. The work not only combines different investigation approaches (stratigraphic, petrological, geophysical, modelling), but also follows temporally the 79 CE eruptive and depositional events, from the magma chamber to the most distal tephras. This has allowed us first to compile a full database of all findings of those deposits, then to relate the products (the deposits) to the genetic thermomechanical processes (the eruption), and lastly to better assess both the local and regional impacts of the 79 CE eruption in the environment. This information leads to a number of open issues (e.g., regional environmental impact vs. local pyroclastic current impact) that are worthy of further investigations, although the 79 CE eruption of Vesuvius is one of the best studied eruptions in volcanology. The structure of the work follows three macro-categories, the historical aspects, the products, and the processes of the 79 CE eruption. For each investigation approach (from stratigraphy to modelling), all dedicated studies and original data are discussed. The open issues are then synthesized in the discussion under a global view of Plinian eruptions, from the magma setting to its dispersion as pyroclasts flowing on the surface vs. falling from the volcanic plume. In this way, a lesson from the past, in particular from the well-studied 79 CE eruption of Vesuvius, will be of help for a better synchronization of processes and products in future developments. Lastly, various aspects for volcanic hazard assessment of Plinian eruptions are highlighted from the tephra distribution and modelling points of view, as these large natural phenomena can have a larger impact than previously thought, also at other active volcanoes.

1. Introduction

Plinian eruptions are among the most devastating events that can occur in explosive volcanism (Fisher and Schmincke, 1984; Cas and Wright, 1987; Sparks et al., 1997; Cioni et al., 2015). The most famous and first documented Plinian eruption is the one that occurred on the 79 CE at Vesuvius, which gave the name to this type of activity (Pyle, 2000; Cioni et al., 2015) and whose dedicated studies have given a great

* Corresponding author.
E-mail address: domenico.doronzo@ingv.it (D.M. Doronzo).

https://doi.org/10.1016/j.earscirev.2022.104072
Received 21 December 2021; Received in revised form 27 May 2022; Accepted 29 May 2022
Available online 3 June 2022
0012-8252/© 2022 The Author(s). Published by Elsevier B.V. This is an open access article under the CC BY-NC-ND license (http://creativecommons.org/licenses/by-nc-nd/4.0/).

contribution to modern volcanology (e.g., Sigurdsson et al., 1985; Macedonio et al., 1988; Barberi et al., 1990). This eruption is classified as VEI (volcanic explosivity index) 6 (Cioni et al., 2003). Furthermore, the deposits from this eruption have allowed several researchers to investigate the impact effects on inhabited proximal areas (Gurioli et al., 2002, 2005a; Luongo et al., 2003a, 2003b; Zanella et al., 2007; Caricchi et al., 2014). At the time of the eruption, dense infrastructural networks, numerous cities and urban settlements, and a large amount of agricultural activities were present in such areas (e.g., Scandone et al., 2019). The 79 CE event is also one of the ancient eruptions that take the name directly from the date of occurrence; it is also known as the "Pompeii eruption". Various films (e.g., "Pompeii" directed by P.W.S. Anderson, 2014), documentaries (e.g., "Pompeii - Ultima Scoperta" by Radiotelevisione Italiana, 2020), and even a legendary Pink Floyd's concert ("Live at Pompeii", 1972) have been realized in the last fifty years around the 79 CE eruption events. In 2022, Sigma Six (a contemporaneous Pink Floyd cover band) have proposed again "Live at Pompeii" with performances in two locations, S. Giovanni a Teduccio (Naples) and Baia (Bacoli), in the Neapolitan volcanic area. As an example, in the videoclip of "Cities in dust" (1985) of Siouxie and the Banshees (a british punk/new wave band of the eighties) the eruption that destroyed Pompeii has been represented as effusive to strombolian. Another example, in the song lyrics of "Pompeii" (2013) of Bastille (a british pop/rock band of the last decade), the eruption has been characterized by grey clouds bringing darkness, and by damaged walls, with an allusion to consequential social aspects. The iconic painting of "Vesuvius" (1985) of Andy Warhol has been realized in the full spirit of Pop Art, which at those times was also merging with music and film industry. Numerous other painting reproductions of historical eruptions of Vesuvius have been illustrated by Ricciardi (2009). In the poetry "La Ginestra" (1845) of Giacomo Leopardi, the main damages in the coastal towns and in Pompeii have been attributed to ash, blocks and pumice fall coupled with hot flows, with a clear reference to impact and resilience. All the historical, cultural, and scientific attention for the 79 CE eruption and Vesuvius does not preclude the current scientific need to further shed light on the dynamics of Plinian eruptions, which still are among the biggest natural events that may occur at active and populated volcanoes. The 79 CE eruption gives a unique opportunity to merge all the multidisciplinary studies together, and make a picture as complete as possible of the entire eruption from the magma chamber, through the conduit, to the far atmosphere and landscape. This eruption sequence has been reconstructed both by quantifying and integrating physical processes (magma ascent, column dynamics) and geological products (deposits from pyroclastic fall and flow and their associated dynamic phenomenology). The first goal of this paper is to review the several findings that have allowed dating precisely this eruption, which for a longtime was assumed to happen in the summer of 79 CE. Secondly, we will relate the various physical aspects of the 79 CE eruption with each other (stratigraphy, magma chamber, conduit, Plinian column, pyroclastic currents, atmosphere, and climate) as sub-domains of the whole explosive event. Consequently, the multidisciplinary approach used in this review will get to open issues, which will then be useful to shed further light on Plinian eruptions in the future, particularly from the observational, remote sensing, and modelling points of view. The

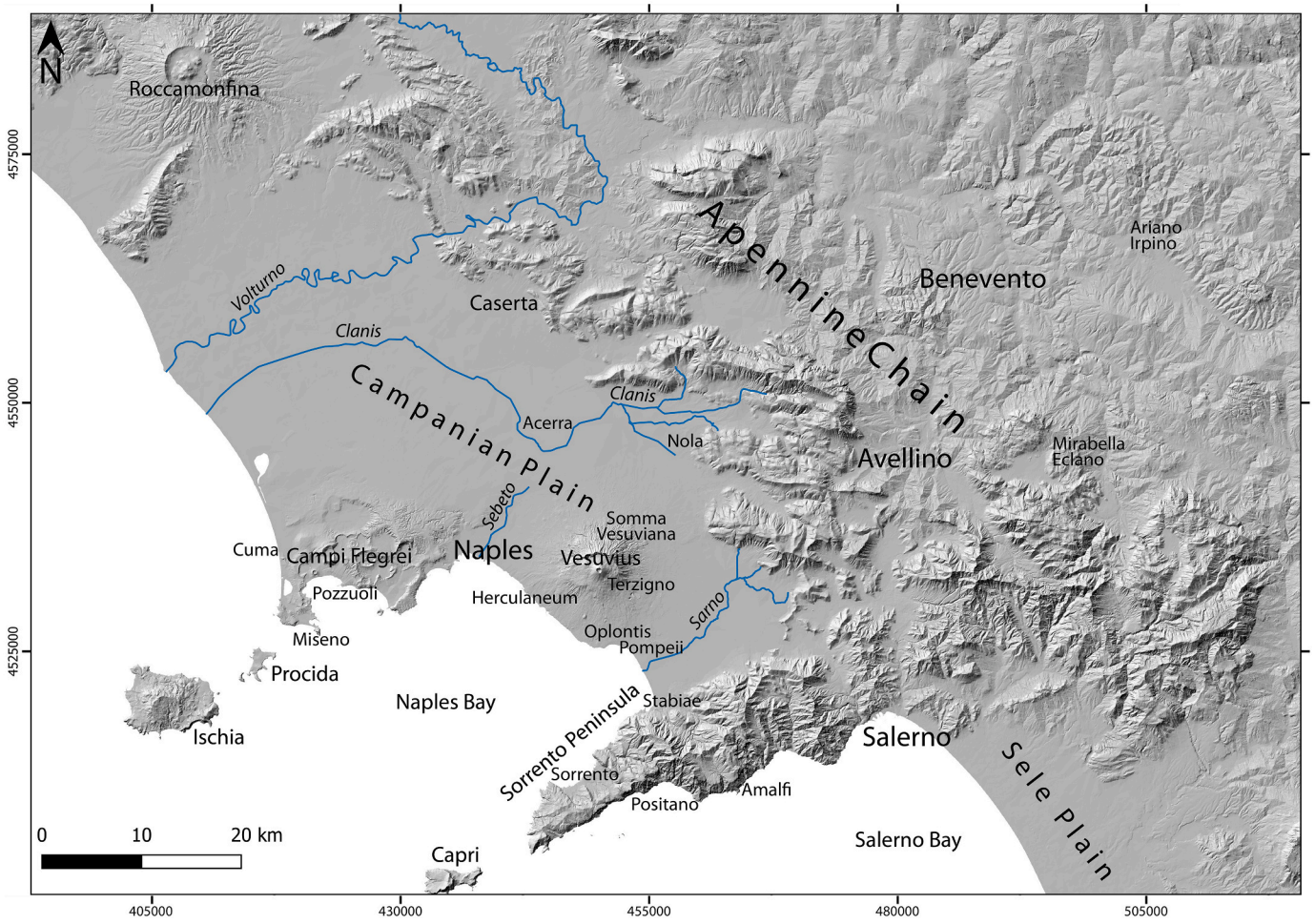

Fig. 1. Digital Terrain Model of the northwestern part of Campania Region, in which the toponyms used in this work are reported. Coordinates and map are in UTM WGS84, data from Tinitaly, software ArcGIS.

present review does not explore in detail the impact that the eruption had on the nearby Roman towns (Fig. 1) and agricultural activities in proximal areas, as for the global (from magma to tephras) integrated methodology adopted for these complex eruptions; only the stratigraphy and the eruption effects at Pompeii are reviewed. On the other hand, some general impact indications on local static load, dynamic pressure, and emplacement temperature are given from the deposit features. A comprehensive contribution of this review is to present, for the first time, a full database with all the GPS coordinates and deposit thicknesses (in the number of 346; see ESM 1), in which the pyroclastic deposits have been reported and/or studied, by extending the available dataset of Gurioli et al. (2010). The new data points, reviewed and attributed to the different eruption units, will be added: i) from medial to ultra-distal settings (Pollino, Calabria, Sicily); ii) from the existing points offshore in both proximal, distal and ultradistal areas; iii) from new points found in numerous archaeological excavations in the City of Naples (previously unknown). Such wide collection and revision of all points in which the 79 CE deposits have been found is a common thread in the review, and this will contribute to deepen the study of the entire sequence of eruptive events in Plinian eruptions, from the magma to the most distal tephras. In this direction, numerical modelling activities on the 79 CE eruption of Vesuvius are reported, which will constrain, using this well studied eruption, the actual impact that Plinian eruptions can have at regional scale. The structure of the manuscript consists of an introduction and chronology of the eruption studies, nine self-consistent sections (one per investigation approach), and conclusions. The latter act as a common thread for the various sections and open to future developments on Plinian eruptions, which we treat as an only natural phenomenon from vent to deposit.

2. Chronology of the eruption studies

The eruptive events occurred on the 79 CE at Vesuvius heavily damaged the Roman towns of Pompeii, Herculaneum, Oplontis, Stabiae (Fig. 1), and a significant part of the perivolcanic area within >10 km (Kent et al., 1981; Sigurdsson et al., 1985; Gurioli et al., 2002, 2005a; Cioni et al., 2004; Zanella et al., 2007; Caricchi et al., 2014). This eruption has become famous since the historical times of Pliny the Younger, when the Latin author observed, and a few decades later described, for the first time the "Plinian" eruption in two letters to Tacitus (Gigante, 1989). During the eruption, Pliny the Younger was at Capo Miseno (Fig. 1), a locality of Campi Flegrei about 30 km west of Vesuvius (Campania region) that allowed Pliny to describe, at a safe distance, the main events of the eruption. For modern times, all references about the main works on the various features of the 79 CE eruption are reported in ESM 2. A first detailed study of the pyroclastic products of the eruption was provided by Lirer et al. (1973). This pioneering work has represented a reference for the following studies. These authors first distinguished the pumices emitted in the 79 CE eruption from the ones emitted during the 3.9 ka Avellino Plinian eruption, the fallout of the latter being dispersed more toward ENE (see Di Vito et al., 2009). Then, they constructed an isopach map of the 79 CE pyroclastic fall deposits, and identified the dispersal area to the southeastern sector of Vesuvius. Lastly, they recognized a change in the colour of the pumices (white vs. grey) in the pyroclastic sequence, with some link to a compositional zonation in the magma chamber, as more deeply investigated petrologically (see section 7 for details). Sheridan et al. (1981) provided complementary information, with the identification of a withdrawal of the 79 CE magma chamber, then a collapse of the sedimentary basement, and the injection of external groundwater from confining aquifer into the chamber as an explanation of an increase in abundance of deep non-juvenile inclusions (metamorphics, skarns) in the upper grey pumice deposits (see Barberi et al., 1989). Sigurdsson et al. (1985) provided a more detailed stratigraphic reconstruction of the eruption sequence, integrating systematic field observations with the chronological accounts of Pliny the Younger. Later, Carey and Sigurdsson (1987) modelled the column height and the magma discharge rate, by using isopleth maps constructed with maximum pumice and lithic dimensions measured at different stratigraphic heights in the pyroclastic fall deposits. These latter two works provided the first quantitative results for the 79 CE eruption, indicating that the sustained Plinian eruption lasted about 19 h, erupted around 4 km^3 of dense rock equivalent (DRE), and caused the emplacement of the white pumices mainly under fallout conditions, followed by the grey pumices under fallout and repeated partial column collapse conditions. These authors calculated the value of the DRE with the method of Rose et al. (1983) (as the product of isopach areas and deposit thicknesses, with an extrapolation beyond the last available isopach to account for very fine ash), and obtained a repartition of 1.0 and 2.7 km^3 for the white and grey pumices, respectively, while the rest of the volume is referred to the initial and final stages of the eruption (0.7 km^3). The calculated values of the column height and magma discharge rate for the white pumices were of 14 to 26 km and of 7.7×10^7 kg/s, respectively, while for the grey pumices were of 26 to 32 km and of 1.5×10^8 kg/s, respectively. To further reconstruct the dynamics of the 79 CE eruptive events, Barberi et al. (1989) and Cioni et al. (1992) produced grain size and componentry data from selected stratigraphic sections, and recognized three main phases of the eruption: an opening phreatomagmatic phase, a dominant Plinian magmatic phase (mostly the fallout sequence), and a final phreatomagmatic phase (mostly the pyroclastic currents sequence). Moreover, Cioni et al. (2003) recalculated the value of the DRE with the method of Pyle (1989) (as an exponential function for the decay of deposit thickness with distance), and found 1.1 and 1.8 km^3 referred to the white and grey pumices, respectively. They also reported the dispersal area within the 10 cm isopach for the two pumice layers, which is of 1540 km^2 for the white pumices, and of 3430 km^2 for the grey pumices, further constraining the highest impact of the grey pumice sub-phase. Considering the variability of the reported DRE values, we were motivated to calculate, in a simple way, the extra volume between the last isopachs and the most distal area representing trace findings of the 79 CE eruption deposits (see section 6). Several other quantitative results have been produced for this well-studied Plinian eruption, which all are useful for a comprehensive quantitative and multidisciplinary reconstruction of the 79 CE eruption (ESM 2). These are presented in the following sections with the rationale enounced in the introduction (from magma to tephras).

3. The date of the eruption

The 79 CE eruption of Vesuvius is very likely the most famous and better studied volcanic eruption in the history of volcanology (cf. Giacomelli et al., 2021). It is considered as the starting point of the modern volcanology, since the description made by Pliny the Younger in the abovementioned letters. However, one of the main open and still debated questions concerns the date of the eruption occurrence. Despite the date of August 24th is widely accepted in the literature, it derives from a medieval translation of the first Pliny's letter, which has been questioned several times since the 17th century (Ricciardi, 2009 and references therein). In this section, we will analyze all the available elements and clues, useful to definitely assert that the 79 CE eruption of Vesuvius could not have occurred on August 24th but, rather, between October and November of that same year, as already suggested by Rolandi et al. (2007) based on pyroclast dispersal and archaeological findings. About two years ago a discovery occurred, during new excavations of the 79 CE deposits: this consists of a wall inscription in Pompeii (Fig. 2) that would confirm the hypothesis, already formulated for some time, that the eruption of Vesuvius in 79 CE took place in autumn and not on August 24th, as reported by the medieval transcription of the famous Pliny's letter (Gaius Plinius Caecilius Secundus, *Epistulae VI, 16*). The inscription, written in charcoal on the wall of a house where restoration work was in progress at the time of the eruption, reports these textual words: *"XVI K Nov in[d] ulsit pro masumis esurit*

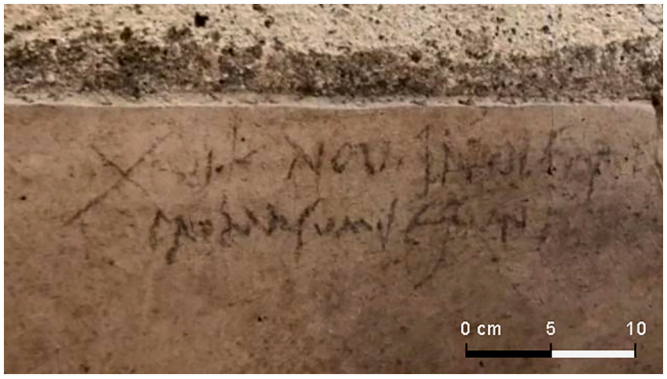

Fig. 2. The inscription found in Pompeii (modified after Avvisati, 2018). It is written in charcoal on the wall of a house and reports the words: "XVI K Nov in [d]ulsit pro masumis esurit[ioni]", which translated means: "The sixteenth day before the kalends of November, he indulged in food in an immoderate way". The sixteenth day before the kalends of November, according to the way in which the days in ancient Rome were indicated, corresponds to the 17th of October.

[ioni]", which translated means: "The sixteenth day before the kalends of November, he indulged in food in an immoderate way". The sixteenth day before the kalends of November, according to the way in which the days in ancient Rome were indicated, corresponds to the 17th of October. In ancient Rome, indeed, the days of the month were indicated by counting backwards with respect to the kalends, nones or ides, depending on which of these dates was closest. The kalends corresponded to the first day of each month, while the nones and ides fell on the fifth or seventh day, and the thirteenth or fifteenth day of the month, respectively, depending on the length of the months (Hannah, 2013, 2016). For example, August 24th was indicated as the ninth day before the kalends of September, including in the count the start and the end days. The obvious implication of the inscription finding is that, if the sentence was written on October 17th, the eruption could not have occurred before this date. Of course, the suspicion that the writing in question may date back to the previous year or before is legitimate, and then, as it is not indisputably demonstrable that the year of the inscription is 79 CE, the uncertainty about the precise date of the eruption still remains. However, some additional elements can be taken into consideration, which suggest the greatest probability that the event happened in the fall. The first element to be evaluated is the source from which the date of August 24th was taken: the first Pliny the Younger's letter to Tacitus. The document itself is universally recognized as reliable, since it was written by a direct witness to the events. Unfortunately, however, we do not have the original writing by Pliny, but only some transcriptions from the medieval era. One of these, in particular, the work of a monk of the 9th century, reported in the "*Codex Laurentianus Mediceus"* bears the date of August 24th (*nonum Kal. Septembres*, the ninth day before the kalends of September). However, already in the 2nd-3rd century A.D., a writing by the historian Dio Cassius seems to indicate a different period for the eruption, which he would place in the second part of the autumn of the first year of the empire of Titus (*DCCCXXXII Ab Urbe Condita*, is that 79 CE; Dione Cassio, 2000), after his fifteenth acclamation. The acclamation was an official act of the Roman Senate, which was registered when an imperial proposal was approved unanimously or on the occasion of important military achievements. It was often celebrated with the minting of a coin, which had the effigy of the emperor and the acclamation number imprinted on it. This is a very important detail since it brings us back to an event that can be considered irrefutable proof that the eruption did not take place on August 24th: the discovery of a coin, a silver denarius that bears the image of the emperor Titus with the inscription XV Imp (Fig. 3; Stefani, 2006). According to other inscriptions that report the date of September 7th or 8th for the Titus' fourteenth acclamation (Cagnat et al., 1927; Merlin, 1962), the following one must have occurred later, and consequently the eruption must necessarily have occurred after the month of August (very likely after the month of September, to give time to the coin to circulate after minting). Another clue that argues against the summer date of August 24th can be deduced from the Pliny's letter itself, in which he said that Admiral Pliny the Elder, having received the request for help from Rectina (the Tascus' wife, a friend of him), drops the quadriremes into the sea (*deducit quadriremes*). The use of the verb "*deducit*", which literally means "leads down", recalls the "*mare clausum*" (literally 'closed sea') of the ancient Romans. The Roman fleet, in charge of the control of the lower Mediterranean, every year in September, close to the autumn equinox, retreated safely to the winter quarters in the port of Miseno. The navigation resumed in springtime, with the festival called "*Navigium Isidis"* in honor of the Egyptian goddess Isis, patroness of the sea, sailors, and maritime activities. Therefore, the fact that it was necessary to lead the ships down into the sea suggests that the "*mare clausum*" had already begun and autumn was started (Ricciardi, 2009). Furthermore, there are other transcriptions of the letter of Pliny the Younger which bear the date of November 1st (Kal. Novembres), such as that of the Codex venetus translated by Pier Alessandro Paravia in 1827 (Ricciardi, 2009), and others that bear the date of October 24th (nonum Kal. Novembres). The abbot Braccini (1632) also reports what was written about a transcription of the Pliny's letter by a Commentator who, considering a printing error the words "Non. Kal. Sept ", said that these should have been reported as "Kal. Novembres". Therefore, the date of August 24th would be an error in the *Laurentianus Mediceus* code, to date the oldest (9th century A.D.) but not the most reliable for this. A plausible hypothesis to justify the choice of this date could be that of a

Fig. 3. Silver denarius of Emperor Titus. Text: "Emperor Titus Caesar Vespasian Augustus Pontiff Maximus; Ninth time with the Tribunicia Potestà, Emperor for the Fifteenth, Consul for the Seventh, Father of the Fatherland" (images from: left, the original - National Museum of Naples, Medal table, Room III, Showcase I, inv. 14,312/176; right, polished collector's coin - Classical Numismatic Group, Inc. cngcoins.com; translation by Stefani, 2006).

symbolic backdating, willingly chosen during the Middle Ages by some monastery chroniclers and scholars, interested in telling about eruptive events for religious or political purposes. In medieval times, it was a common practice to date events modifying both their beginning and duration in order to make them coincide with the striking phenomenon (*mirabilia*), which was the subject of the hagiographic telling. As an example, we can recall the adaptation of the date of birth of Jesus, moved by the emperor Constantine in 330 CE to December 25th, to make it coincide with the Dies Natalis *Solis Invicti* (Day of Birth of the Undefeated Sun) and to superimpose it on the cult of the god Mithras (Ricciardi, 2009). On August 24th the Romans celebrated the "*Vulcanalia*" and the exit of souls from the afterlife through the "*mundus*", a sort of deep and vast pit in the center of the city, which represented a connection point between the Underworld and the world of the living. The foundation of a city or any Roman colony involved a particular ritual action: the excavation of the mundus, which was then covered with a closing stone, called "*lapis manalis*". On August 24th of each year, the "*lapis manalis*" was opened and the ritual of "*mundus patet*" (the mundus is open) was performed. During this ritual the gates of the underworld were opened and the souls of the dead could return to the world of the living and wander through the city. After three days the "*lapis manalis*" was closed and everything returned to normal (Ricciardi, 2009). Therefore, the date of August 24th emphasizes the medieval belief that a volcanic eruption opens the door of Hell, and the day of the "*mundus patet*" of the ancient Roman ritual of the Vulcanalia must have seemed to medieval monks the best date to open the Vesuvius' crater, considered the "funnel of Hell" throughout the Middle Ages. Moreover, Rolandi et al. (2007) demonstrated that the mainly southward-oriented dispersal of the fallout deposits of the 79 CE eruption is compatible with the Autumn-Winter dominant direction of the stratospheric winds, rather than that of the Summer winds (Macedonio et al., 1988). With these elements, it is now possible to definitively establish that the date of the eruption cannot be August 24th but must be limited to an interval that goes from September 7th/8th (date of the silver denarius with the fifteenth acclamation of Tito) to November 1st (the most recent date among those deriving from the various transcriptions of Pliny's letter). This, and particularly the year of occurrence, are corroborated by Ar—Ar datations available by Lanphere et al. (2007). Lastly, if we add to all this complementary information the finding of typically autumn fruits, such as dried figs, walnuts, chestnuts, and pomegranates, that the wine had already been sealed in the "*dolia*" (the large terracotta containers found in many houses in Pompeii), and again that many of the victims wore heavy clothes and in many houses there already were braziers to heating the rooms (Ricciardi, 2009), then it follows that it was late autumn already, and therefore the most probable date must necessarily fall between October 24th and November 1st.

4. Stratigraphy

The main studies on the general stratigraphy of the 79 CE eruption of Vesuvius are mentioned at various degrees of detail in the introductory sections. In the present section, the eruption stratigraphy is reviewed following, in particular, the detailed stratigraphic and sedimentological studies of Cioni et al. (1990, 1992, 2004) on the entire succession of the eruption deposits, complemented by the ones of Gurioli et al. (2002, 2005b) on the Pompeii and Herculaneum impact dynamics, and by the database of Gurioli et al. (2010). The database is integrated with new findings from the City of Naples, Pollino, Velia, Sicily, and revised offshore data, for a total number of 346 points (ESM 1). The term of Eruption Unit (EU) of Cioni et al. (1992) is borrowed here to describe those pyroclastic deposits formed in a single phase of the 79 CE eruption characterized by a distinctive eruptive mechanism and style, in the framework of general volcanic stratigraphy (Manville et al., 2009; Martí et al., 2018; Németh and Palmer, 2019). Also, the general term of pyroclastic current, and not pyroclastic density current, is used to describe lateral flow processes, because such a current does not necessarily behave as a density current, i.e. it can be sustained by eruption dynamics vs. local topography (Doronzo, 2012; Palladino, 2017; Doronzo et al., 2022). In particular, eight Eruption Units (EU1 to EU8) are recognized in the pyroclastic sequence of the eruption, some of which are further subdivided in sub-units emplaced by pyroclastic currents (EUXpf, where X is EU numbering). For the sake of clarity, a correlation of the stratigraphic frameworks of the 79 CE eruption of Vesuvius provided by different authors is reported in Table 1. We reviewed the entire eruption sequence in proximal reaches at Cava Pozzelle, Terzigno (located 4.5 km southeast of the current Vesuvius' crater) (Figs. 1 and 4) and in the Pompeii area (see next section for details). It follows a general

Table 1
Correlation among the stratigraphic units recognized by Sigurdsson et al. (1985), Cioni et al. (1990, 1992), Gurioli et al. (2007), and Scarpati et al. (2020). The empty cells indicate the units not described/recognized, which does not mean that there is a gap in the stratigraphy (each stratigraphic scheme is vertically continuous), but that there is no direct correlation. To be noted that the authors followed different approaches to subdivide the 79 CE deposits sequence: Sigurdsson et al. (1985) reconstructed a composite sequence following a stratigraphic approach, by taking into account all sections exposed all around the volcano, while the reconstruction of Scarpati et al. (2020), also stratigraphic, only focused on the Pompeii area. Instead, the reconstructions of Cioni et al. (1990, 1992) and Gurioli et al. (2007) took into account the sections located around the volcano, but the eruptive units were grouped/separated according to the different eruptive phases (vent to deposit correlation). The letters A, S, and F used by Sigurdsson et al. (1985) indicate fallout, surge, and flow mechanisms of emplacement, respectively. The asterisk means that the unit does not include F4 of Sigurdsson et al. (1985).

	Sigurdsson et al. (1985)	Cioni et al. (1990, 1992) Gurioli et al. (2007)	Scarpati et al. (2020)
STRATIGRAPHIC UNITS			T
			S
			R
			Q
			P
	accretionary lapilli layers	EU8	O
			N
			M
			L
			I
		EU7pf	H
	A10		G3
	S7	EU7	G2
	A9		G1
		EU6	
		EU5	
	C1	EU4 accr. Lapilli-bearing	F
	F6		
	S6	EU4pf	E2
			E1
	A8	EU4bl	D
		EU3pfL	
	F5		
	S5		C3
	A7	EU3pftot *	B3
	F4		
	S4		C2
	A6	EU3f	B2
	F3		
	S3	EU3pfi	C1
	A5	EU3f	B1
	F2		
	S2	EU3pf	
	A4	EU3f	B1
	F1		
	S1	EU3pf	
	A3	EU3f	B1
		EU2/3pf	
	A2	EU2f	A
	A1	EU1	

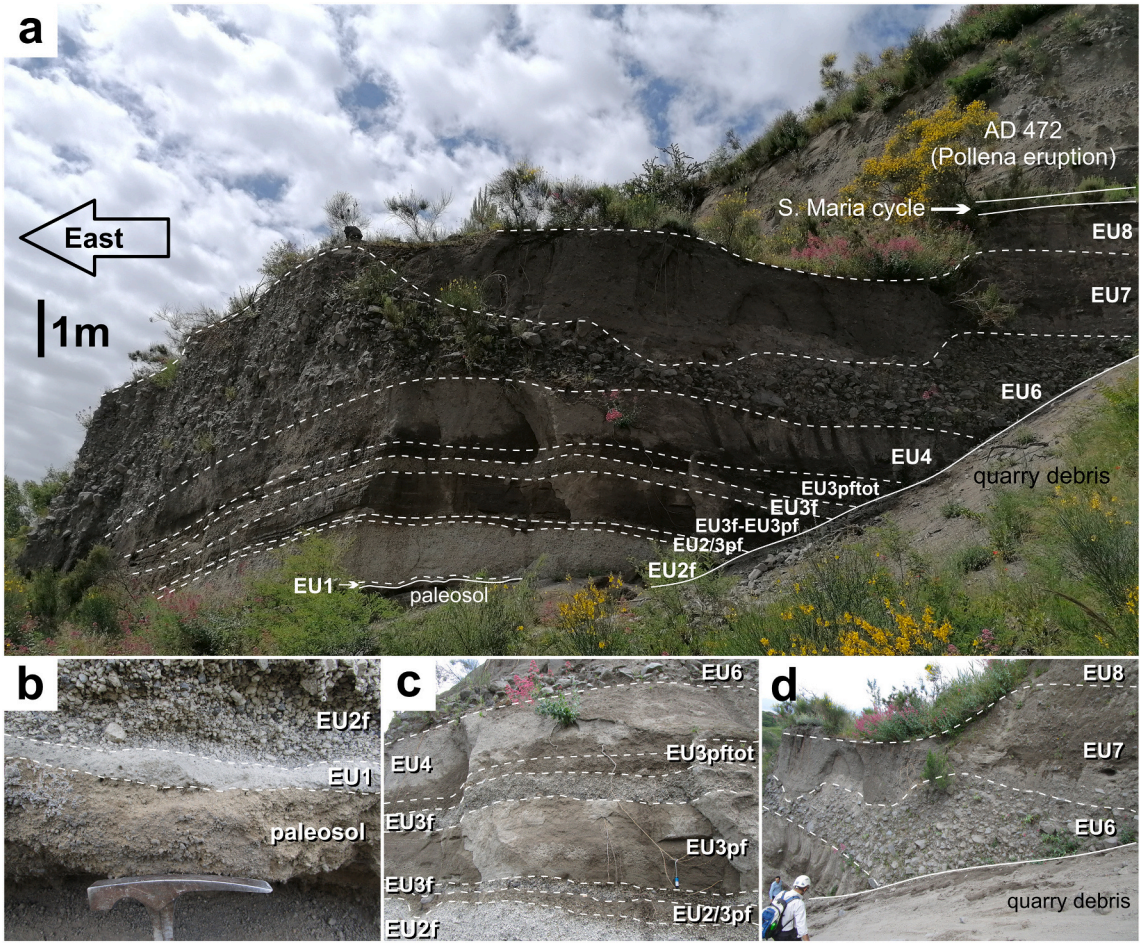

Fig. 4. **a)** Photo of the entire stratigraphic sequence (EU1 to EU8, subvertical wall) of the 79 CE eruption of Vesuvius cropping out at Cava Pozzelle, Terzigno (Fig. 1). Below EU1 there is a paleosoil, while above EU8 there are deposits of the 472 CE Pollena eruption with deposits of the St. Maria cycle in between; **b)** detail of the basal part of the sequence (EU1 to EU2f); **c)** detail of the middle part of the sequence (EU2f to EU6); **d)** detail of the upper part of the sequence (EU6 to EU8).

description of the 79 CE eruption sequence for each EU, from bottom (EU1) to top (EU8), including all details (e.g., lithic % by volume) needed for characterizing the timing and macroscopic impact dynamics of the eruption:

- EU1. It consists of whitish-grey, massive and sometimes normally-graded, accretionary lapilli-bearing fine ash fall deposits, with a dominant distribution toward the East (Fig. 5). This unit is mainly present on the slopes of Vesuvius, where it forms a thin blanket with a maximum thickness of about 15 cm, and more sporadically in the southeastern part of the Campanian Plain at about 20 km from the vent. At some sites on the western slopes of the volcano, this unit is associated with narrowly dispersed, fine-grained pyroclastic current deposits. It records a first transient phreatomagmatic phase, which marked the opening of the conduit. The exact timing of the deposition of EU1 is not very clear, but this event could have triggered the first plea for help to Pliny the Elder from the Vesuvian area, which was reported to have occurred around noon.
- EU2f. It consists of thick, white phonolitic highly-vesiculated pumice lapilli fall deposits (white pumices, with dimensions from a few cm to decimeter), with a distribution toward the South-East (isopach map in Fig. 5). The deposits are massive, reversely-to normally-graded and lithic-poor (minor lavas up to decimeter, limestones and rarer marbles at 10–20% tot.), and roughly represent 25% of the total erupted magma. This unit is present in a southeastern dispersal fan around Vesuvius, with a double maximum thickness of about 1 m close to Pompeii and in the southern part of the volcano. It records a sustained eruptive column phase, and is the second most voluminous unit in the pyroclastic sequence. In more proximal areas, this unit is capped by thin pyroclastic current deposits (described in the next unit).
- EU2/3pf. It consists of thin plane parallel to cross-bedded pyroclastic current deposits, mainly distributed around the vent, but also reaching a distance of about 7 km from the vent in the southern part of Vesuvius (Fig. 5). This unit is faintly laminated, fine-grained with lithic lapilli scattered in lenses of rounded pumice lapilli. It locally thickens in correspondence of topographic lows, still maintaining a thinly stratified facies. Lava ballistics with dimensions up to 25 cm are dispersed (Fig. 6a,b). It records a first phase of partial column collapse, and the first major change in the eruption dynamics, coincident with an important change in magma composition from phonolitic to tephri-phonolitic. The pyroclastic current reached Herculaneum, likely causing the death of the inhabitants, and Terzigno causing partial demolition of the Roman Villae Rusticae and Oplontis.
- EU3f. It consists of thick, grey tephri-phonolitic pumice lapilli fall deposits (grey pumices, with dimensions from a few cm to decimeter), with a distribution toward the South-East (isopach map in Fig. 5). The deposits are massive, reversely-to normally-graded and contain lithic fragments (lavas, limestones, marbles, and rarer cumulitic and metasomatic rocks at 20–25% tot.), and roughly represent 55% of the total erupted magma. Wall-rock lithic blocks are abundant particularly in the upper part of the unit, and also in the form of outsized lava ballistics with dimensions up to 25 cm (Fig. 6a,

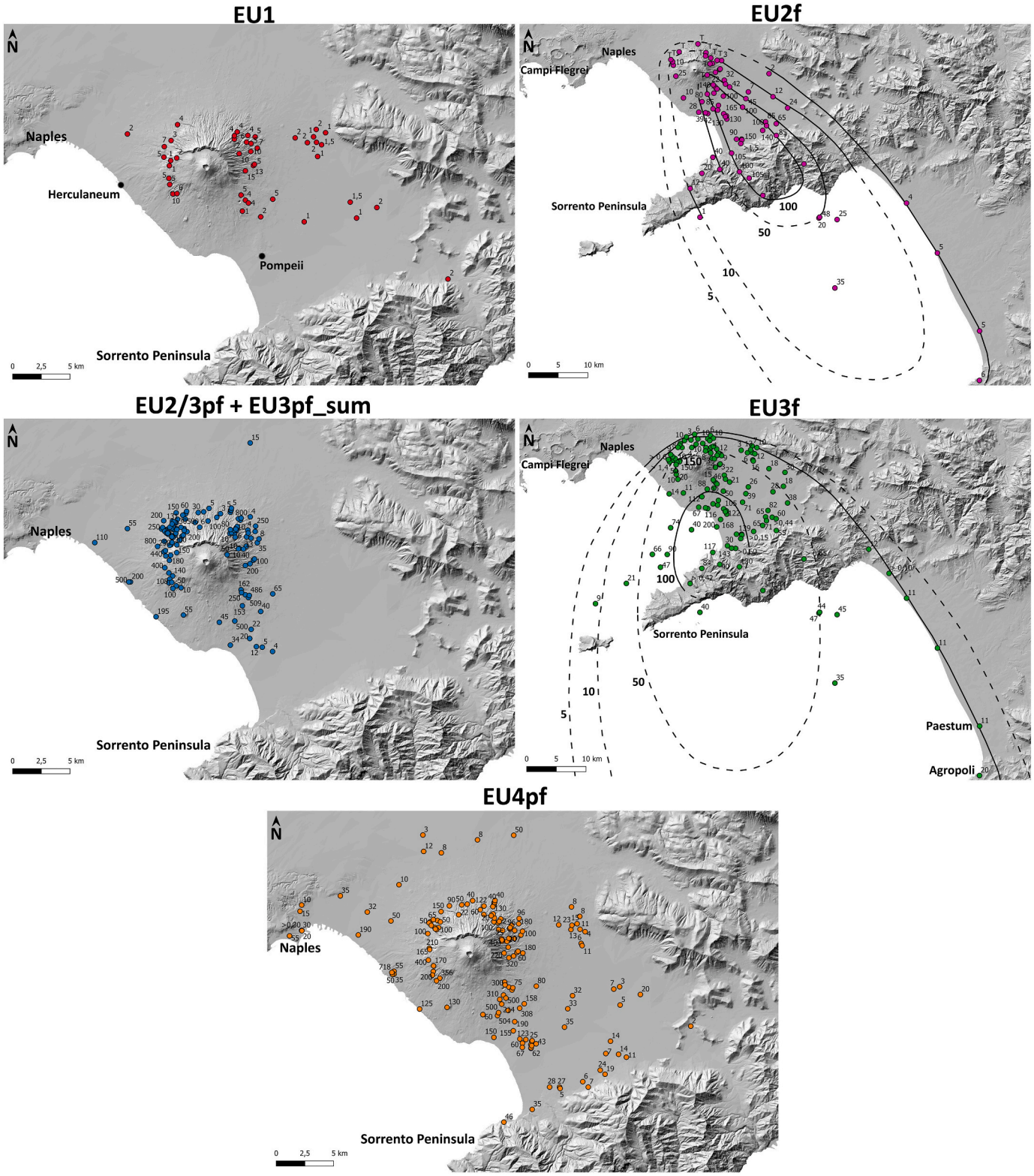

Fig. 5. Local deposit thicknesses (cm) of EU1, EU2f (and related isopachs), EU2/3pf + EU3pf_sum (the latter being the sum of EU3pf, EU3pfi, EU3pftot, and EU3pfL), EU3f (and related isopachs), and EU4pf (the distribution area of this unit on land is of 445 km^2, but a wider area has to be considered, in particular offshore, for the distribution of the most widespread flow unit of the 79 CE eruption).

b). This unit is present in a southeastern dispersal fan around Vesuvius, with an only maximum thickness of about 1.5 m in the Pompeii area, while it is reduced or lacking in the southern part of the volcano. It records a dominant sustained eruptive column phase, and is the most voluminous unit in the pyroclastic sequence. Both EU2f and EU3f reach maximum thicknesses at distances of about 10–15 km from the vent.

- EU3pf. It consists of stratified, undulatory bedded to dune bedded pyroclastic current deposits, locally grading into deposits with a massive facies. The deposits consist of pumice lapilli and coarse to

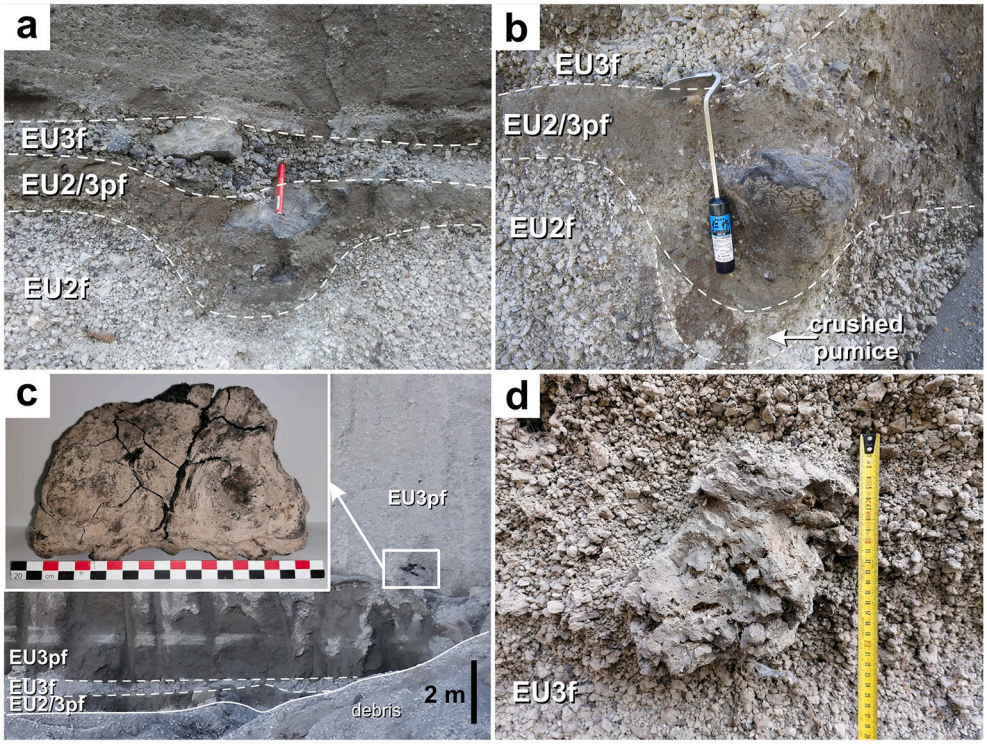

Fig. 6. Ballistic clasts and fragments embedded in the 79 CE pyroclastic sequence at different stratigraphic heights and locations (Cava Pozzelle, Terzigno and Pompeii, at 4.5 and 9.5 km from the current Vesuvius' crater, respectively): **a)** and **b)** lava blocks with dimensions up to 25 cm in EU2/3pf and EU3f. Fragments form deep impact sags even crushing the underlying pumice clasts (Cava Pozzelle); **c)** charred trunk in EU3pf (Cava Pozzelle), in the inset a detail of charred wood; **d)** outsized pumice clast with dimension of 28 cm in EU3f. No impact sag is recognizable (Pompeii).

fine lithics (lavas and minor deep-seated rocks) in a fine to coarse ash matrix, in which there also are dispersed bombs and blocks of several cm. Decimeter-sized fragments of charred trunks are locally dispersed, indicating an emplacement temperature of around 300 °C (Fig. 6c). This unit consists of multiple sub-units that drape the topography, and has an average thickness of about 1–2 m, with a strong thinning in correspondence of topographic highs and thickening in correspondence of topographic lows, and reaches a distance of about 10 km from the vent (Fig. 5). It records at least three phases (one/sub-unit) of partial eruptive column collapse within the dominant EU3f phase, and this makes EU3f more eroded (still thicker) than EU2f in proximal reaches. At Cava Pozzelle, for example, there are at least two partial collapse sub-units, and one total collapse unit. Laterally, the upper EU3pf thickens significantly up to several meters in correspondence of the topographic lows, and acquires a massive pumice-rich facies inglobating charred woods (valley-ponded ignimbrite), with a traction carpet-dominated part at the base. The pyroclastic currents caused the destruction of some Roman Villae Rusticae located on the slopes of the volcano such as in Oplontis, partial demolition of buildings in Herculaneum, and the death of some of the inhabitants. In particular, the last of these pyroclastic currents from partial column collapse emplaced a thin, coarse to fine ash layer (EU3pfi) in proximity of the city walls of Pompeii.

- EU3pftot. This unit corresponds to total eruption column collapse, and generation of a powerful, radially-moving pyroclastic current. The deposits, up to 10 m thick in proximal areas, are stratified but laterally and vertically grade into massive deposits, as the result of a depositional boundary layer subjected to a significant transition from traction-dominated and low accumulation rate to forced deposition and higher accumulation rate (Fig. 5). At Cava di Pollena (4 km from vent), for example, EU3pftot thickens significantly in correspondence of the topographic lows, and acquires a massive pumice-rich facies with charred woods; at the base, the unit is finer and more structured. Although EU3pftot barely reached the southeastern limits of Pompeii with a thickness of only a few cm, it is possible that the EU3pftot phase caused the deaths of some of the inhabitants.
- EU3pfL. The pure magmatic phase (started with EU2f) ceased with the emplacement of lithic-rich pyroclastic current deposits within the first 2 km from the vent to the north and northwest. These narrowly dispersed deposits are matrix-supported and mainly composed by ash with unaltered lava clasts, eroded from the subsurface, and subordinated white and grey pumice fragments. The high temperatures of deposition recorded by these fragments agree with rapid deposition from a slow-moving pyroclastic current directly overflowing from the vent.
- EU4. The base of this unit is composed, where not fully eroded, by a thin, lithic-rich, grain-supported lapilli deposit (EU4bl) dispersed toward the South-East, and emplaced during some short-lived eruptive column dynamics. This deposit is often laminated in the upper part, and is followed by stratified, undulatory bedded to dune bedded pyroclastic current deposits (EU4pf) with a thickness of about 4 m in the proximal part of Vesuvius, changing into deposits with massive to laminated facies at about 6–7 km from the vent, and with a massive accretionary lapilli-bearing facies in the distal part of the volcano (Fig. 5). The deposits are lithic-rich (lavas, marbles, limestones, skarns and cumulites), and consist of pumice and lithic lapilli in a fine to coarse ash matrix, in which there are outsized lava and dense pumice ballistics with dimensions up to a few decimeters, and the deposits are capped by an accretionary lapilli-bearing ash layer of several cm. At Cava di Pollena, for example, EU4pf assumes a well-indurated facies particularly in the topographic lows. This unit is distributed radially from the vent and reaches a distance of about 21 km in the southern part of the volcano, and of >15 km toward the center of the city of Naples. It records a significant phreatomagmatic phase, representing the climactic phase of the eruption through a first destabilization of the magma chamber, external water-magma interaction, and full eruption column collapse; it is the most widespread unit in the pyroclastic current sequence. The pyroclastic current caused partial destruction of buildings and the death of all the surviving inhabitants in Pompeii, and it even reached the

Sorrento Peninsula and the territory presently occupied by the City of Naples. In Fig. 5, an integration of literature data of the deposit thicknesses with more new data collected in archaeological excavations and trenches is presented. This is the widest distributed pyroclastic current EU in the entire sequence of the 79 CE eruption, covering a radial area around Vesuvius of at least 445 km^2 on land.

- EU5. It consists of lithic-rich, massive to dune bedded pyroclastic current deposits (Fig. 4). The deposits are composed by coarse ash, grey pumice lapilli, and abundant lithics at 40–50%. This unit is only present on the slopes and in the main valleys of Vesuvius, reaching north Boscoreale, with a thickening and a strong control in correspondence of the topographic lows. It is completely absent in the southern medial areas. It records a further destabilization phase of the magma chamber, and formation of small pyroclastic currents.
- EU6. It consists of thick (up to 10 m), massive poorly-sorted pyroclastic current deposits, with abundant lithic fragments from the whole basement of Vesuvius (limestones, marbles, syenites, monzonites at about 60% tot.), and showing a very coarse breccia facies with lithic lava blocks and boulders (up to meter-sized) particularly in proximal reaches (Fig. 4). The deposits consist of pumice lapilli and very abundant lithic fragments in a fine to coarse ash matrix. This unit is distributed following the topography, mainly filling topographic lows in the southeastern part of the volcano, and reaching a distance of about 6 km from the vent. It records the culmination of the destabilization of the magma chamber into its definitive roof collapse phase, and formation of a pyroclastic current, i.e. the climax of caldera collapse.
- EU7. The general description of this unit is similar to the one for EU4, with the difference that it consists of a less regular facies variation in pyroclastic current deposits that are thinner (Fig. 4). The deposit sequence, in particular, consists of a lapilli-enriched layer with porphyritic scoriae and lithic fragments (marbles and phlogopite-bearing clinopyroxenites at 50–60% tot.), and a massive to dune bedded fine ash layer, capped by a thick accretionary lapilli-bearing ash layer. This unit is mainly distributed in the southern part of Vesuvius, reaching a distance of about 15 km from the vent. It records a final transient phreatomagmatic phase, and formation of a pyroclastic current, which left an ash deposit in Pompeii.
- EU8. It consists of thick, finely alternating ash-fall and flow deposits, with a stratified accretionary lapilli-bearing facies (Fig. 4). This unit is lithic-rich (with fresh lava fragments), is slightly lithified in the distal reaches, and is mainly distributed in the northern and western parts of Vesuvius following the topography, while in the southern part of the volcano it shows more evidently such fall-and-flow alternation. The maximum distance of finding of this unit, at Stabiae, is about 15 km from the vent. It records the final evolution and the waning stages of the eruption through multiple phreatomagmatic pulses.

5. Volcanic deposits, timing, and related effects at the Roman town of Pompeii

In 79 CE, the ancient city of Pompeii (Fig. 1), located 9.5 km southeast of the current Vesuvius' crater, met its fate being buried under a thick blanket (6–7 m) both of fall and pyroclastic current deposits. Following the early excavations started in 1748 (Maiuri, 1958), systematic archaeological investigations have brought to light a large part of the city, which has become one of the most important archaeological site worldwide, as well as a volcanological heritage and milestone in modern volcanology (Scandone et al., 2019; Giacomelli et al., 2021, and references therein). Strictly from the archaeological excavation point of view (beyond the main goal here), a comprehensive work on recent studies at Pompeii is the volume XXXII - 2021 of Rivista di Studi Pompeiani, which we referred to. On the other hand, numerous volcanological studies conducted in Pompeii have investigated several aspects of the eruption, including: (i) stratigraphy (Sigurdsson et al., 1985; Cioni et al., 1990, 1992; Scarpati et al., 2020); (ii) influence of the urban structure on the pyroclastic current direction and impact (Luongo et al., 2003a; Gurioli et al., 2005a, 2007; Ruggieri et al., 2020); (iii) causes of death of the inhabitants (Giacomelli et al., 2003; Luongo et al., 2003b; Scandone et al., 2019); (iv) temperature of the pyroclastic currents (Cioni et al., 2004; Gurioli et al., 2005a; Zanella et al., 2007, 2014), and sedimentation dynamics of such currents (Dellino et al., 2021); and (v) heat effects on frescoes (Marcaida et al., 2019). In this section, the interplay among local stratigraphy, sequence of volcanic events, damages and victims at Pompeii archaeological site caused by the eruption is reported (Fig. 7), by exploring the available literature (see also section 3). A synthesis of the 79 CE stratigraphy is presented giving a review of the available stratigraphic sections, located both inside and outside the city walls. The most detailed stratigraphic study, based on 39 sections, is reported by Gurioli et al. (2007). Other scattered sections, studied during excavations, are reported by other authors (Marturano and Varone, 1997, 2005; Luongo et al., 2003a; Scarpati et al., 2020). The analysis of the stratigraphic sections gives information on almost the entire sequence of the events occurred during the eruption in medial reaches. Stratigraphy is described according to the EUs presented in the previous section, while the timing of volcanic phenomena and related damages follows the eruption chronology reconstructed by Sigurdsson et al. (1985) and Cioni et al. (2000). Archaeological exploration is still underway in Pompeii, and in the last few years many outstanding findings were unearthed (e.g., the *Termopolium* of Regio V, with a decorated counter or the so-called "Room of the slaves"), giving new priceless information to the archaeologists on many aspects of the culture and lifestyle at Pompeii. In order to pursue the multidisciplinary approach that characterizes this work, the description of the 79 CE stratigraphy is enriched here with some of the latest (2018–2021) archaeological discoveries made in Pompeii, which can have volcanological implications on the effects of the eruption (Rivista di Studi Pompeiani - vol. XXXII, 2021). At Pompeii, the sequence is composed only of five (EU2f, EU3f, EU4, EU7, and EU8) of the 8 EUs generated during the 79 CE eruption (Table 1 and Fig. 7). This event began after noon on October 24th with a phreatomagmatic ash fall spreading toward East, and emplacing an accretionary lapilli-bearing, whitish ash deposit (EU1). This ash fall did not reach Pompeii. The eruption continued, at 1 pm, with the formation of a sustained Plinian column, which gave a pumice lapilli and blocks fall deposit toward South-East that grades vertically from white (EU2f) to grey (EU3f) pumices. This phase of the eruption lasted about 18–19 h. At Pompeii, the pumice fall deposit is crudely stratified due to vertical grain-size variations (EU3f appears coarser and poorer sorted than EU2f), it contains lithic clasts made up of lava, limestone and rare cumulite fragments and attains a maximum total thickness of 2.8 m. Centimeter- to decimeter-sized ballistic blocks and bombs, composed by lava, limestone and pumice fragments, are dispersed throughout the fall deposit (Fig. 6d). Local anomalous thickening, up to 5 m, has been reported inside houses, due to drainage of pumice lapilli from roofs through compluvia (rectangular holes at the center of the roof) and accumulation into impluvia (rectangular basins with the function of rainwater collection coming from compluvia), or alleys, due to rolling and sliding of pumice lapilli in the presence of sloping roofs (Luongo et al., 2003a; Cioni et al., 2000). The thick accumulation of lapilli engulfed the ground floor of the buildings, protecting them from the impact of the multiple pyroclastic currents generated during the following eruption phases. Damages and victims in this phase of the eruption are associated with the overload exerted by the pumice lapilli accumulated on flat or low-sloping roofs. As evidenced by the analysis of the stratigraphic sections, roof collapses occurred during the emplacement of EU2f, at a few hours from the beginning of the fallout, below a deposit thickness of 60 cm (Cioni et al., 1992) corresponding to a static load on the roof exceeding about 500 kg/m^2. These collapses caused hundreds of victims among the inhabitants. In fact, 394 bodies were found below and within the pumice fall deposit as a consequence of the roof collapses (Luongo et al., 2003b). Then,

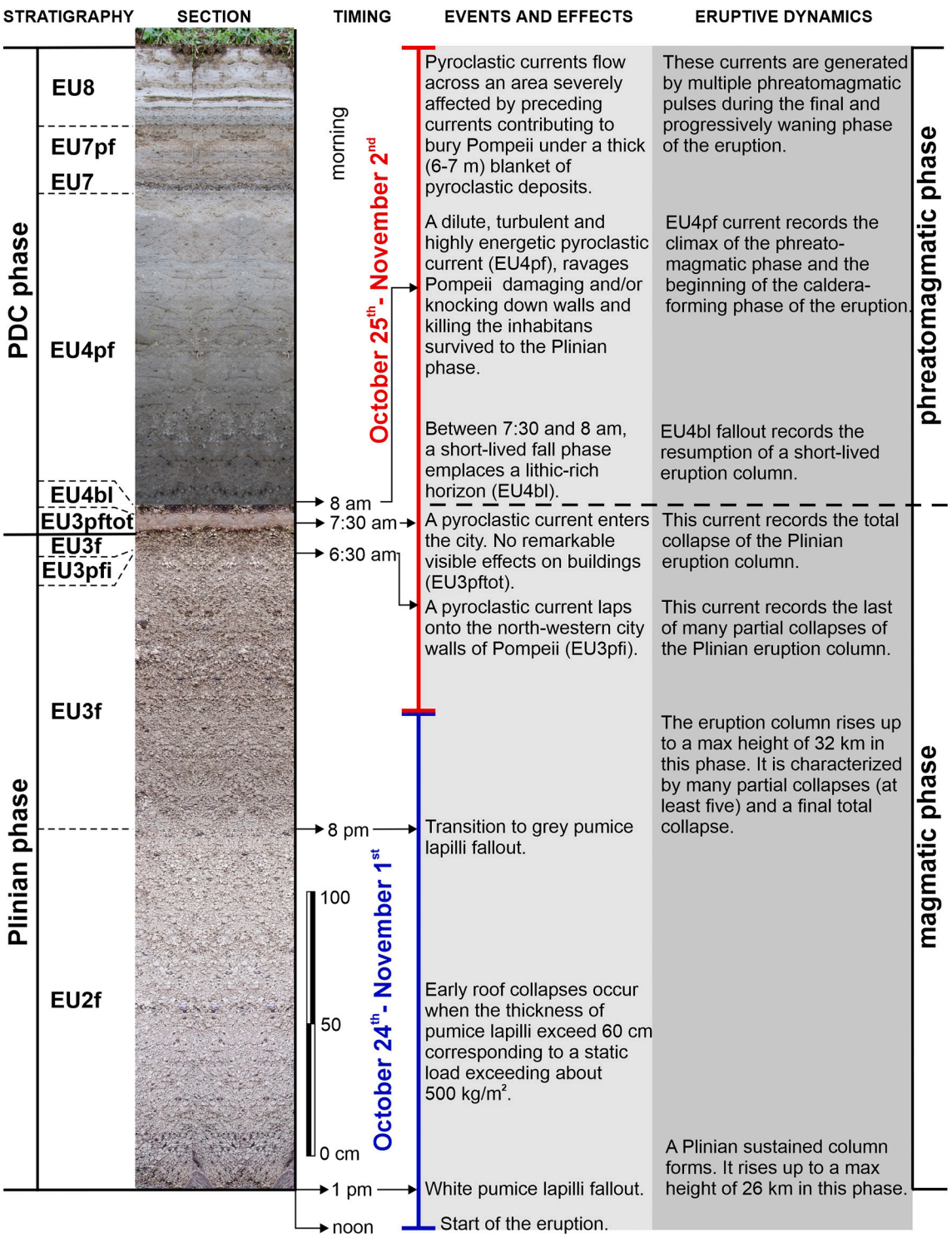

Fig. 7. Composite photo of the stratigraphic sequence of the 79 CE eruption around Pompeii (left), synchronization of the eruptive phases with the historical chronicles (middle), and distinctive eruption effects in the city (right).

partial collapses of the Plinian column generated pyroclastic currents at the transition between the white and the grey pumice phases (EU2/3pf), as well as during the emplacement of the grey pumice phase (EU3pf), in the night of October 24th and early morning of October 25th. The stratigraphic sequence inside and all around Pompei gives evidence that only the last of these pyroclastic currents reached Pompeii, likely around 6:30 am, without entering the city. This pyroclastic current laps onto the northwestern edge of Pompeii, emplacing a thin, massive, coarse- to fine-ash layer (EU3pfi) containing few millimeter-sized lithic lava clasts, a few centimeters below the top of EU3f (Fig. 7). Otherwise, Scarpati et al. (2020) have reported the occurrence of this ash horizon (their unit C1; Table 1) well inside the city, in a restricted sector of Regio V (northern part of Pompeii). According to the experiments and numerical modelling of Doronzo and Dellino (2011) on pyroclastic current-building interaction, urban structures can act as flow baffles depending on how the urbanization is articulated. The top of EU3f is overlain by two, massive to well-stratified, coarse to fine ash layers containing fine pumice lapilli separated by a thin horizon of fine pumice lapilli

(EU3pftot). Total thickness of this unit is usually few centimeters, although it can reach a maximum of 30 cm. The lower ash layer has a predominantly massive structure, while the upper layer is characterized by different lithofacies (Gurioli et al., 2007). It was emplaced around 7:30 am, and is the result of a pyroclastic current that followed the ultimate total collapse of the eruption column marking the end of the magmatic phase. The current reached Pompeii and entered the city by overcoming its walls, without leaving any remarkable visible effects on the buildings, although Cioni et al. (2000) reported the occurrence of tiles and bricks in the resulting deposit. In addition, parts of skeletons were found in a thin unit (Sigurdsson et al., 1985; Cioni et al., 2000) buried by deposits of the overlying unit (EU4), suggesting that some victims were associated to this phase of the eruption. The transition to the caldera-forming and phreatomagmatic phase was marked by the resumption of a short-lived eruption column that lasted about 25 min (Gurioli et al., 2007). The resulting deposit is a basal, grain-supported, mainly massive, lithic lapilli-rich layer (EU4bl) having a maximum thickness of 7 cm in Pompeii (Fig. 7). The fall origin of this horizon is testified by its mantle bedding fashion even on undulated surfaces; such horizon is more laminated at other places (e.g., Cava Pozzelle, Terzigno). Undulations are mainly related to the attitude of the underlying pumice fall deposit to mantle standing walls. Lithic clasts are mainly composed of lavas, minor limestones and marbles. Centimeter-sized, ballistic lava clasts and impact sags can occur at the interbed surface with the underlying EU3pf, while juvenile clasts are subordinate and composed by grey pumices. This basal layer is overlain by a grey, matrix-supported, coarse- to fine-ash deposit containing grey, rounded pumice lapilli, accretionary lapilli and minor lithic clasts set into the matrix (EU4pf). The amount of accretionary lapilli increases upward. Lithic clasts are mainly made up of lavas, minor limestones and rare cumulites. Tiles and bricks are common in this unit. This deposit is characterized by a great thickness variability both inside and outside Pompeii. According to Gurioli et al. (2007), the thickness of EU4pf ranges from a few decimeters to 2.15 m, although thicknesses up to 3.3 m have been reported inside some buildings (Luongo et al., 2003a). This unit shows different lithofacies (Gurioli et al., 2007). The most common vertical lithofacies association varies from a basal massive ash containing rounded pumice lapilli (and locally decimeter-sized lithic clasts and building fragments), emplaced under local accumulation rates of the order of tens of (to a hundred) kg/m^{2}s, through a crudely to diffuse stratified ash containing rounded pumice lapilli to a planar- to undulated to low-angle, cross-stratified fine ash at the top. Fines-depleted lenses composed by fine to coarse pumice lapilli can be found in this unit. Locally, in Pompeii, this deposit rests directly on the grey pumice lapilli deposit due to the erosion of EU4bl and EU3pftot. The sequence of EU4 ends with an accretionary lapilli-bearing, massive to faintly laminated, light grey ash layer up to 20 cm thick. According to Cioni et al. (1990, 1992, 2020), this accretionary lapilli-bearing layer is interpreted as a co-ignimbrite ash fall associated with the emplacement of EU4pf. Alternatively, Scarpati et al. (2020) assume this layer (their unit F) as emplaced directly from a pyroclastic current. The flow unit in EU4 resulted from the most powerful pyroclastic current that got to Pompeii, at around 8 am, during the climax of the phreatomagmatic phase, ravaging the entire city, damaging or knocking down walls and killing the inhabitants who survived during the Plinian phase (Figs. 7 and 8). The energy of this pyroclastic current is even testified by its capacity to erode, locally, the underlying units. According to Doronzo et al. (2012), Roche (2015), Trolese et al. (2019), and Doronzo et al. (2022), that was a fully inertial pyroclastic current not concomitant with eruption column collapse, and the current had a highly-mobile depositional system (fed from the upper transport system) capable of entraining and transporting outsized clasts into the flow. According to Luongo et al. (2003b), 650 victims were found in EU4pf (their unit E) laying a few centimeters above the base of this unit. The recent excavation of a "*villa suburbana*" at Civita Giuliana, 700 m northwest of the ancient Pompeii city walls, has returned further evidence that this pyroclastic current was a relentless killer. Skeletal parts of two victims of the eruption were found in a 2.2 m wide room, probably having the function of passageway from the *cryptoporticus* to the upper floor, in the noble part of the villa (Toniolo et al., 2021). Casts of the victims were obtained according to a technique developed in the second half of the 19th century by Giuseppe Fiorelli (see Osanna, 2021), by pouring liquid plaster into the void left by the decomposition of the corpses. The analysis of the stratigraphic position of the casts (Toniolo et al., 2021) shows that the victims rest about 10 cm above the base of

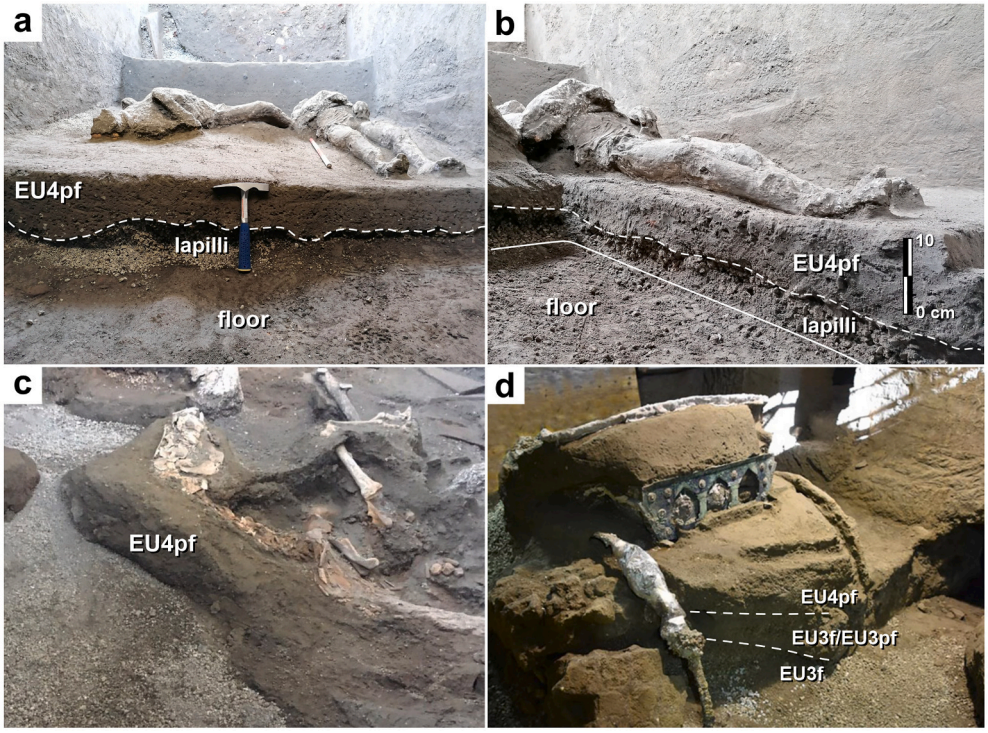

Fig. 8. Photos of recent (2018–2021) archaeological findings during the excavation of a "*villa suburbana*" at Civita Giuliana, 700 m northwest of ancient Pompeii: **a)** and **b)** plaster casts of two victims of the eruption resting few centimeters above the base of EU4pf (modified after Toniolo et al., 2021); **c)** skeleton of a horse found in the stable and entombed in EU4pf (from pompeiisites.org); **d)** four-wheeled chariot found in a sheltered portico buried by deposits emplaced during different phases of the eruption (from pompeiisites.org).

EU4pf, in turn resting on few centimeters of pumice lapilli (Fig. 8a,b). The absence of the ash layers of EU3pf suggests that the early pyroclastic currents reaching Pompeii were not able to penetrate inside this room. In 2018, three horses (Fig. 8c), one of them still with its harness, were found in a stable, located in the servants' part of the same villa, most likely killed by the same pyroclastic current. Furthermore, in 2021, a four-wheeled processional chariot (Fig. 8d) with well-preserved bronze decorations was found in a portico, just outside the stable, probably overlooking an open courtyard. From the evidence in Fig. 8d, we can argue that the burial of the chariot started during the fallout phase, with emplacement of the grey pumice (EU3f) and likely the ash layers of EU3pf, and ended with the emplacement of EU4pf. The pumice lapilli deposit appears to thin left to right, probably as a consequence of rolling and/or sliding of pumice lapilli on the sloping canopy of the portico, and forming a heap along the edge of the canopy. Successively, the EU4pf pyroclastic current interacted with the structure emplacing an ash deposit (that thickens on the heap of lapilli) and entombed the chariot, preserving it from full deterioration. The interaction between this pyroclastic current and the urban structure of Pompeii has been studied in detail by Luongo et al. (2003a) and Gurioli et al. (2005a, 2007), and can be compared with the general experimental and modelling results of Doronzo and Dellino (2011) on pyroclastic current-building interaction. From the analysis of the 79 CE deposits in Pompeii, the dense basal part of the parental pyroclastic current was partially deflected by the buildings, while the more dilute upper part was not particularly affected by the urban structure of Pompeii. In terms of damage assessment, we can conclude that the orientation of the walls appears to be a fundamental parameter during flow-building interaction. Walls parallel to the current direction were minimally damaged, while walls perpendicular to the current direction were strongly impacted under locally-variable flow pressures (cf. Zuccaro and Ianniello, 2004; Doronzo and Dellino, 2011). In many sections at Pompeii, damaged walls show a channel-shaped profile (Luongo et al., 2003a). Where successive walls (two or more) are closely spaced, the depth and amount of the damage to the walls is lower downcurrent. This observation, along with the distribution of the deposits around the buildings, suggest that the removal of the pyroclasts from the current by forced deposition is a key factor for the impact of the local flow. On the other hand, the presence of decimeter-sized building and lava fragments incorporated in EU4pf is evidence, through quantitative sedimentology, that the pyroclastic current had the capacity to entrain and transport outsized external clasts under flow dynamic pressures of 5–10 kPa (cf. Roche, 2015; Martí et al., 2019). EU5 and EU6, representing the deposits emplaced during the climax of the caldera collapse (see section 4), are completely lacking at Pompeii. EU7 is a stratified deposit, up to 13 cm thick, composed by two, clast-supported, massive, lithic lapilli-rich horizons separated by a cohesive ash horizon containing few mm-sized lithic lava clasts set into the matrix. EU7 is overlain by a massive to faintly laminated accretionary lapilli-bearing layer (EU7pf; Gurioli et al., 2007). The transition to EU8 is marked by a very thin (below 0.5 cm) clast-supported horizon composed by coarse ash to very fine lapilli, made up of lava fragments, overlain by a sequence of accretionary lapilli-bearing layers, having a total thickness <1 m, emplaced during the final and waning phase of the eruption (Fig. 7). EU8 is composed by an alternation of ash layers, up to 10 cm thick. Each layer is characterized by a massive to crudely stratified base overlain by an accretionary lapilli-rich top. EU8 records multiple phreatomagmatic pulses that generated pyroclastic currents, and minor fallout, flowing over an already ravaged and almost completely buried area (no artefacts are reported for this unit), which contributed to the burial of the ancient Pompeii.

6. Distal and ultra-distal deposits

The pyroclastic products emitted during the 79 CE explosive eruption are distributed all around Vesuvius, but particularly in the southern and southeastern parts of the volcano. Although the 79 CE deposits have a radial distribution with respect to the vent, they show a preferential dispersion in the fan-shaped area south of the volcano, bordered by the surrounding mountains (Gurioli et al., 2010). The pyroclastic current deposits are quite well distributed in such a fan on land, on the other hand they have been found in marine cores off the coastline of the Naples Bay (Sacchi et al., 2005, 2009; Insinga et al., 2008). These are decimeters-thick primary deposits resulting from the entrance of the pyroclastic currents into the sea, locally showing some reworking and interaction-with-water processes in the form of distal turbidity current deposits. They are quite thick close to the coast, particularly in correspondence of the Sarno River mouth (Fig. 1), where they reach a couple of meters (Sacchi et al., 2005). The most distal sites in which the 79 CE pyroclastic current deposits have been found are in the Sorrento Peninsula, which acted as a topographic barrier for the pyroclastic currents that entered the sea, and in the city of Naples (Fig. 5). Among the latter is Municipio Square, at a distance of >15 km from the vent in which decimeters-thick deposits have been found during archaeological excavations (Di Donato et al., 2018). Instead, the 79 CE pyroclastic fall deposits have been found in much more distal areas in the southern and particularly in southeastern directions (Fig. 9). In particular, by distal here we refer to the area between the limit of pyroclastic current propagation/ballistic impact and the 5 cm isopach, while by ultra-distal we refer to the area between the 5 cm isopach and the furthest trace findings (cryptotephra). These are primary deposits that reach thicknesses of decimeter up to a meter, passing over the Sorrento Peninsula in the Salerno Bay (Fig. 1). They have been found offshore in marine cores, and show the presence of both the white and grey pumice layers (Sacchi et al., 2005, 2009; Insinga et al., 2008; Crocitti et al., 2018). At Pontecagnano near Salerno, the white and grey pumices stand on Roman plowing traces. The pyroclastic fall deposits have even been also found offshore in marine cores west of Calabria (Cosentino et al., 2017; Crocitti et al., 2018), in the Policastro Bay (Munno and Petrosino, 2004), and in the Taranto Bay (Cini Castagnoli et al., 1990; Crocitti et al., 2018; Pepe et al., 2018; Di Donato et al., 2019). At these localities, the eruption deposits occur as thin but significant primary tephra layers or cryptotephra, and are geochemically representative only of the most energetic phase corresponding to EU3f, i.e. the grey pumices. On the other hand, the grey pumices have been found in the northern and central part of Calabria on land (Pollino and Sila, respectively), in which they have a significant primary thickness of the order of centimeters (Galli and Scionti, 2006; Sevink et al., 2020). Other evidences of the grey pumices have been found as cryptotephra in marine cores in the Adriatic Sea (Jalali et al., 2018), in Sicily, in the Ionian Sea up to offshore Greece and Crete (Keller et al., 1978), and even in Greenland (Barbante et al., 2013; cf. Plunkett et al., 2022). On the whole, the dispersal area and main directions are indicative of the size and intensity of the 79 CE Plinian eruption, which heavily impacted proximal-to-distal areas (up to tens of km from the vent) under pyroclastic current dynamics, and proximal-to-ultradistal areas throughout the Mediterranean (up to thousands of km from the vent) under pyroclastic fallout and seasonal wind dynamics, particularly in the grey pumices phase. In Fig. 9, all evidences (as of today) of proximal-to-ultradistal tephra attributed to the 79 CE eruption are reported, while in ESMs 3 and 4 further details of medial-to-ultradistal tephras are specified (see also ESM 1). Fig. 9 also reports the 5 cm and 2 cm isopachs within the whole ash cloud represented by all trace findings of the grey pumices (T area). We recalculated the erupted volume for such pumices, with respect to the volumes reported in the literature by Sigurdsson et al. (1985) and Cioni et al. (2003), by adding the volumes relative to the areas between the 5 cm and 2 cm isopachs, and between the 2 cm isopach and T area. Roughly, the new calculation is the product of the GIS surface area and average deposit thickness (3.5 cm for the first area of about 11,000 km^2, and assumed 2 mm for the second area of about 290,000 km^2), which gives a minimum extra volume of erupted magma of 0.5 km^3 corresponding to around 20% more than the volumes reported in the literature. The tables reported in ESM 3 and 4 show the state of the art on the location,

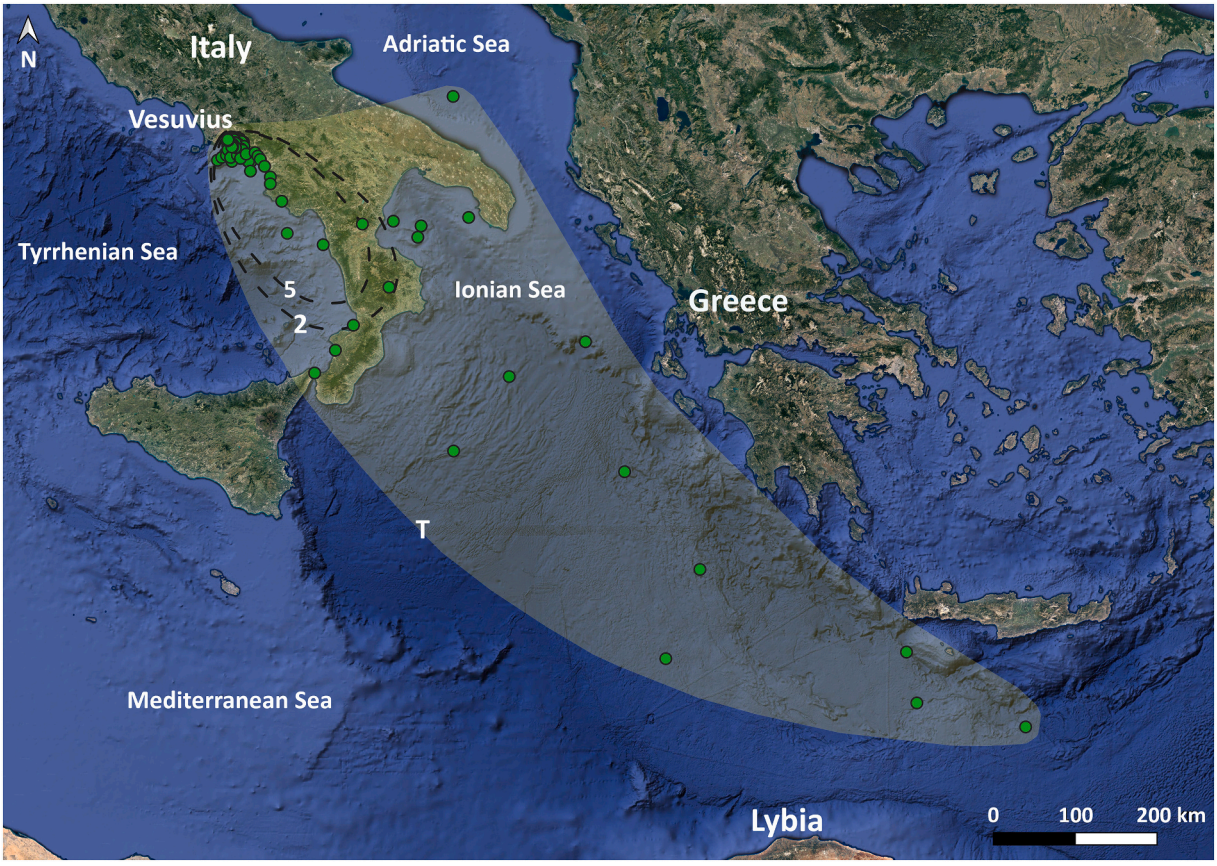

Fig. 9. Distribution of EU3f from proximal to ultradistal areas miming the volcanic cloud dispersal that occurred during the 79 CE eruption of Vesuvius. The 5 cm and 2 cm isopachs, and trace area (T) are shown, while all deposit characteristics are reported in ESM 1, 3 and 4.

thickness, juvenile chemistry (white vs. grey pumice), methodology, and general stratigraphic features of the 79 CE tephra, which have been found in the above mentioned localities, and have been described in the literature. These points, along with the new ones in Naples, Pollino, Velia, and Sicily, are all included in the integrated database for the distribution maps. The recent attributions of the tephra have been based on convincing geochemical data and chronostratigraphic constraints, with the remarkable exception of the tephra Z-1 of Keller et al. (1978) found in the most distal sites of the Ionian Sea. This tephra was originally attributed to the "Pomici di Avellino" eruption (c. 3.9 ka), and for sure it is of Vesuvian origin for its XRF composition, which is not suitable for a confident individual correlation but enough for a convincing identification of the volcanic source. In fact, based on its stratigraphic position above the tephra Z-2 of the Minoan eruption of Santorini (c. 3.6 ka), the attribution of Z-1 was reappraised to the stratigraphically consistent 79 CE eruption (Wulf, 2000). Future geochemical analyses on samples from this tephra, and from others found in some lacustrine basins in Puglia and Basilicata regions and the Adriatic Sea will allow a precise provenance attribution, and consequently a refined distribution map of the ultra-distal deposits.

7. Magma chamber

The magma chamber and the pre-eruptive conditions of the 79 CE eruption have been studied by integration of petrological and stratigraphic investigations. A distinctive feature in the stratigraphy of the 79 CE pyroclastic deposits is a marked change of chemical composition and particle density passing from the white to the grey pumices (Carey and Sigurdsson, 1987; Cioni et al., 1995). The white pumices are K-phonolitic and have a homogeneous density distribution with a mode at about 600 kg/m^3. In contrast, the grey pumices are K-tephri-phonolitic and have a more heterogeneous density distribution with higher modes at about 700 kg/m^3 and 1100 kg/m^3, and show broader density distributions with coarse tails (Gurioli et al., 2005b; Shea et al., 2012). Such variations are correlated to variations of the column height and magma discharge rate (Carey and Sigurdsson, 1987; Sigurdsson et al., 1990; Shea et al., 2011), and all have been ascribed to a compositional zonation of the 79 CE magma chamber (Sigurdsson et al., 1990; Cioni et al., 1995; Cioni, 2000; Scaillet et al., 2008). A study of the pyroclastic deposits of the 79 CE eruption was conducted by Cioni et al. (1995). This study allowed reconstructing the thermal, compositional and isotopic features of the pre-eruptive magma, as well as investigating *syn*-eruptive mixing among different magmas and recognizing the variability of the magma batches feeding the chamber. The authors suggested that during the different phases of the eruption about 25–30% of magma was erupted as white k-phonolitic pumices, while c.a. 75–70% as grey k-tephry-phonolitic pumices. The total volume of the erupted magma was estimated at 4.4 km^3: 1 km^3 as white pumices, 2.7 km^3 as grey pumices, and 0.7 km^3 as phreatomagmatic products (Sigurdsson et al., 1985; Civetta et al., 1991). These early works already suggested that the white pumices resulted from tapping of progressively deeper magma with a body at T = 850–900 °C that represents a pre-existing tephritic-phonolitic, crystal-rich magma reservoir, possibly a residue from the previous "Avellino" Plinian eruption (c. 3.9 ka; Sevink et al., 2020). Moreover, this magma body consisted of distinct layers. The basal "grey" magma was formed by syn-eruptive mixing between the phonolitic white magma, mafic cumulates and a crystal poor, phono-tefritic grey magma (Cioni et al., 1995). The periodic arrival of hot mafic magma batches was considered the main engine for the growth of the 79 CE magma chamber. This mafic magma had k-tephritic to k-basanitic composition, homogeneous Sr isotopic composition ($^{87}Sr/^{86}Sr$ of c.a. 0.70729), high temperature (T = 1100 °C) and was characterized by high volatile

contents (ca. 2 wt% H_2O, Cl, F and S), low viscosity (10–20 Pa·s) and relatively low densities (c.a. 2500 kg/m^3). Cioni et al. (1995) suggested an ellipsoidal or cylindrical chamber geometry and a minimum volume of c.a. 5 km^3 for the magma chamber, taking into account for c.a. 1 km^3 of unerupted mafic cumulates. The minimum, vertical extent of the chamber was suggested to be between 1.5 and 1.0 km. Marianelli et al. (1995) analyzed melt inclusions (MIs) in olivine and diopside crystals from pyroclasts of the 79 CE eruption. MIs were found to be relatively primitive, silica undersaturated, basaltic to tephritic compositions and were considered as representative of the composition of magma batches that supplied the Vesuvius Plinian and sub Plinian magma chamber(s) from the 3.9 ka Avellino eruption to the 472 CE Pollena eruption. Based on these reconstructions, the 79 CE magma chamber chemically evolved to form a two-fold layering consisting of a highly evolved body at T = 850–900 °C, overlying a less evolved, homogeneous body of greater mass (1–2 km^3) and temperature of c.a. 1000 °C. However, the most "primitive" magma batches supplying the chamber were characterized by much higher temperature (< 1200 °C). Balcone-Boissard et al. (2008) focused on the pumice- fallout deposits that were emitted during the 79 CE eruption and which represent the 80% of the erupted magma (Cioni et al., 1995). The authors performed a systematic sampling of a representative section of the fallout deposit in the Terzigno quarry, where six units crop out. The authors found that melt inclusion and matrix glass compositions in both the white pumices and the grey pumices define two distinct, continuous differentiation trends. These trends are characterized by enrichment in Na_2O and CaO and depletion in K_2O at approximately constant Al_2O_3 content. Moreover, SiO_2, Fe_2O_3 and MgO vs Na_2O contents for the white pumices and grey pumices diverge. These data were interpreted as the evidence of *syn*-eruptive magma mingling between the white and the grey magmas during ascent in the feeder conduit and not in the magma chamber as suggested by Cioni et al. (1995). The authors performed several estimates of H_2O contents in MIs using the "by difference method" and compared their results with those available from literatures and obtained by using different techniques (e.g. FTIR, SIMS). In products from the 79 CE eruption, sanidine displays the most differentiated MIs composition and has H_2O contents ranging from 3.5 to 6.5 wt%. Major elements content of MIs in pyroxene spans a wider range, which extends toward a less differentiated melt composition. Moreover, MIs feature H_2O contents between 5 and 1 wt%. Finally, MIs in leucite crystals display the lowest H_2O content (0.7–2.6 wt%), which is consistent with the late, syn-eruptive crystallization of leucite. Based on their work and on data from literature, Balcone-Boissard et al. (2008) suggested that white pumice magma stored in the upper part of the chamber was saturated at pressures of c.a. 185 MPa considering 5 wt % of H_2O. Similar results were obtained by considering Cl solubility. They calculated that the white pumice magma chamber was emplaced at c.a. 7.5 km depth, in agreement with Scaillet et al. (2008), and suggested it had a vertical extent <500 m. The grey pumice reservoir extended from just below the white pumice reservoir. No constraint was given on the vertical extension of this latter. Assuming that fractional crystallization, dissolution-regrowth as well as recharge and mixing occurred before the 79 CE eruption, the timescale of such processes can be determined by investigating diffusion profiles within individual crystals. Morgan et al. (2006) presented data on sanidine crystals from the 79 CE eruption. Crystals display abrupt changes in Ba concentration that were suggested to be caused by magma chamber recharge events prior to the eruption. Based on the results of their analyses the authors identified three distinct recharge events, the most recent of which occurred 20 years before the eruption. Given the relatively large uncertainty, this time information is very close to the time of the 62 CE earthquake. For such a reason, Morgan et al. (2006) suggested that significant magmatic recharge occurred around the time of the earthquake. At least two more recharging phases were identified 30 and 80 years before the 79 CE eruption, suggesting that episodic recharge occurred at Vesuvius in the last century prior to this Plinian eruption.

8. Modern geophysical observations and past evidences

Somma-Vesuvius is a stratovolcano consisting of a central cone, Vesuvius, grown after the 79 CE eruption, and an external older caldera, Mt. Somma. The cone as we know today was not formed yet at the time of the eruption. At the Roman time indeed, only one, truncated and asymmetrical volcano, without an intracaldera cone, was present, as shown by the Roman painting of the "Love of Venus and Mars", now at "Museo Archeologico Nazionale" in Naples. In this mythological picture, the Somma-Vesuvius caldera (at the time called Vĕsŭvĭus, Vesevius, Vesvius, or Vesbius) is visible on the background where a deep notch probably cut the southeastern caldera rim, showing the stratified structure of the Mt. Somma caldera walls. The new cone grew discontinuously (with minor summit collapses) during periods of open conduit, persistent activity (both strombolian and effusive), the last of which happened recently in 1631–1944 (Arrighi et al., 2001). The NE-SW tectonic lineament controlling the activity of Vesuvius is in accordance with the general lineament trend of the southern Apennine (Cassano and La Torre, 1987). The occurrence of normal fault-like sliding along the contact zones confirms the extensional tectonic regime in the area (Montone et al., 1995), while radial and en-echelon fractures are related to the volcanic inflations and caldera collapse (Tramparulo et al., 2018). The Vesuvius dynamics has been interpreted as joint effects of gravitational sliding and extensional tectonic stress occurring at the contact between different lithological units (De Natale et al., 2000; Lanari et al., 2002; Borgia et al., 2005). Static deformation measurements performed by terrestrial and satellite techniques over the last 50 years evidence a current subsidence of the central cone of few mm/yr (e.g., Bonasia et al., 1985; Lanari et al., 2002). The subsidence of the central cone agrees with the local seismicity clustered below the cone, possibly driven by gravitational stress due to the weight of the topographic relief and the sedimentary substratum (De Natale et al., 2000; Borgia et al., 2005; D'Auria et al., 2014). Subsidence larger than 2 mm/yr is also found at regional scale, as a result of the sediment compaction of the Campanian Plain (Lanari et al., 2002). However, paleontological and petrochemical analyses since the last glacial era constrain 5 mm/yr uplift, suggesting that the volcanic component prevailed over the long-term subsidence of the entire Campanian Plain (Marturano et al., 2011, 2013). Little was known about shallow crustal structure beneath Vesuvius until the '90s. The knowledge of the internal structure of Vesuvius has increased in the last decades, after several active seismic experiments carried out at Vesuvius, disclosing the strong velocity heterogeneity of its shallow structure (see details in Principe et al., 1987; Zollo et al., 1996a, 1996b, 2002; Gasparini et al., 1998; De Natale et al., 2000, 2004; Auger et al., 2001; Lomax et al., 2001; Di Stefano and Chiarabba, 2002; Scarpa et al., 2002; De Natale et al., 2006; D'Auria et al., 2014). A teleseismic tomography was obtained by merging seismic data recorded by the Italian Seismic Network located on the southern Apennines with stations deployed in a temporary broad-band experiment around Vesuvius volcano (De Gori et al., 2001). A sharp transition at 10 km depth from a high-velocity to a low-velocity medium was already inferred by Zollo et al. (1996a), identified as a discontinuity consistent with the occurrence of magmatic melt within a high-permeability host rock. The large-scale tomography by De Gori et al. (2001) infers an almost continuous high-velocity body in the upper mantle, interpreted as the signature of the Adriatic lithosphere subducting westward toward the back-arc Tyrrhenian basin. Therefore, the low-velocity anomaly beneath Vesuvius evidenced by Zollo et al. (1996a), and later by Auger et al. (2001), is located above this high-velocity zone dipping in the mantle, and De Gori et al. (2001) suggest that magma is generated by the subducting slab at depths 15–30 km. The complex interaction among the volcanic edifice, fluids circulation and seismicity are matter of study to depict the recent, but also the past, dynamics of Vesuvius and the relation among the hydrothermal/magmatic systems. Recently, Ricco et al. (2021) evidenced a close relation between episodic seismic swarms and ground tilting. Also,

episodes of surface deformation are related to thermal pulses of fluids, due to hot injections within the deep carbonate basement. All these geophysical studies shed light on the past behaviour of Vesuvius, as they are the result of the volcanic activity through the centuries. Bouguer gravity anomalies were computed to infer the depth of the basement at larger scale (down to 2.3 km in the western side of the volcano; Santacroce, 1987). A complete reconstruction of the top of the carbonate basement was carried out by Cella et al. (2007), evidencing an annular volume of dense rocks around Mt. Somma extending down to the basement. A minimum depth of about 3 km for the top of the reservoir was inferred using mineral equilibrium of metamorphic carbonate ejecta (Barberi et al., 1981). Civetta et al. (1991) found evidence from xenolithic ejecta of the top of the chamber to be located within the Mesozoic calcareous sequence, at a depth ranging from 3 and 5 km. Scaillet et al. (2008) provided evidence, from experimental phase equilibria from the main explosive events at Vesuvius, that the reservoirs migrated from 7 to 8 km to 3–4 km depth between the 79 CE and 472 CE events. Volcanological and archaeological studies in the Roman towns provided information regarding phenomena preceding the 79 CE eruption. The eruption caught the inhabitants in their every-day life, suggesting different response to early seismic events and ground deformation as recorded by historical accounts and archaeological excavations. Seismic activity continued during the eruption as reported in the Pliny's second letter, and that likely occurred through the first destabilizations of the magma chamber, also in analogy with the eruption of Mount St. Helens observed in 1980 (Scandone and Giacomelli, 2001; Scandone et al., 2019). Archaeological sources document several water crises in Pompeii. Civil aqueducts have ceased to supply water due to the change in slope of the slight inclination typical of these Roman artefacts. The uplift had compensated the gentle slope (Marturano, 2008). A minimum 30 cm uplift was documented on the flanks of Vesuvius, at about 10 km from vent, prior to the eruption (Keenan-Jones, 2015). Russo et al. (1997) performed one of the first attempts to simulate the mechanical response of the local crust to the action of the pressurization of the magmatic source at Vesuvius. These models are aimed at evaluating the current hazard level at Vesuvius and understanding the conditions of the plumbing system of the 79 CE eruption. The numerical models by means of the Finite Element Modelling (FEM) technique were used to evaluate the stability of the reservoir's walls, considering the slopes of the volcano and the regional stress (Russo et al., 1997). The reservoir characteristics are chosen according to the conditions of the 79 CE eruption and the medium includes the basement evidenced by Zollo et al. (1996a). Simulations are performed with several spherical and ellipsoidal reservoirs with top at 2 km b.s.l. whose volumes range from 0.1 km^3 to 4 km^3. Considering an overpressure amounting to 10 MPa, surface displacements of the order of cm were obtained. Also, all the results show that the shallow reservoir is below its critical conditions for gravitational collapse of the Vesuvius flanks. In a second study, Russo and Giberti (2004) evidenced that the effect of the rigid structure and the carbonate basement is to focus the deformation field around the summit area of the volcano. Further simulations by FEM models were carried out by Meo et al. (2008) to analyze in greater detail the impact of topography and crustal layering (e.g., the carbonate basement) on the ground deformations with comparisons between homogenous and heterogeneous media. The 3D topography deviates surface displacement patterns from the axial symmetry of the spherical and/or vertical ellipsoidal reservoirs employed. Recently, Tammaro et al. (2021) developed new FEM models accounting for the 3D elastic structure as deployed from the tomography, along with the real topography. The reservoir is placed at 2 km depth, and it is compatible with the tomography resolution that did not constrain low-velocity zones larger than 0.5 km. As in Meo et al. (2008), significant differences respect to flat and homogeneous modelling are obtained as result of the simulations. These models highlight the complex interpretation of geodetic signals at volcanic areas in general and at Vesuvius in particular, due to the relevant topography and the highly heterogeneous local crust. To conclude, a strong interaction among seismic and ground deformation data, along with petrological and historical data are needed at those monitoring active volcanoes capable to give, in particular, Plinian eruptions.

9. The climate at the time of the 79 CE eruption

In recent years, the impact produced by large volcanic eruptions on climate and environment at regional to global scale is a matter of careful investigation and discussion (e.g. Sigl et al., 2015; Muschitiello et al., 2017). In this section, the climate condition at the time of (or close to) the 79 CE eruption is investigated, not only to detect possible climatic anomalies potentially related to the effect of the eruption, but also to investigate how local climate might have played a role in the following environmental recovery. For instance, thick debris flow deposits due to remobilization of the primary pyroclastic deposits of the 79 CE eruption are common around Vesuvius, as a consequence of heavy rains, at least locally. There also are thick sequences of these deposits even in Amalfi and Positano, at about 50 km from vent (Fig. 10; see also Cinque and Robustelli, 2009). Such debris flows could have had a high frequency, from months to years. On the other hand, compared to the other three Plinian eruptions of Somma-Vesuvius, the 79 CE eruption is the only to have the major axis of tephra dispersal elongated in southeast direction (toward Crete), which can give information of specific atmospheric circulation at that time related to some prevailing conditions (e.g., seasonal impact; Rolandi et al., 2007). It is useful to remember that the Roman time has been traditionally considered a period of general "benign" climate (the so-called "Roman Warm Period", e.g., Lamb, 1995, or "Roman Climatic Optimum", e.g., Harper, 2017). The "Roman

Fig. 10. Sequence of multiple flow units emplaced by debris flows in the Canneto valley, Amalfi (about 50 km from Vesuvius), and composed almost exclusively by fragments of the 79 CE products. The lower part of the sequence is dominated by the grey pumices, while in the upper part by the white pumices. Interestingly, such secondary deposits "restore" the chemical zonation of the magma chamber (double reverse). The whole sequence overlies the 79 CE fallout deposits (lower white pumices and upper grey pumices, single reverse).

Climatic Optimum" lasted between ca. 200 BCE and 450 CE (McCormick et al., 2012; Harper, 2017), and was followed by a phase of climatic deterioration during the Late Antiquity (e.g. McCormick et al., 2012; Büntgen et al., 2016; Zanchetta et al., 2020). Starting from the analyses of many proxy records, McCormick et al. (2012) reported favorable and exceptionally stable conditions across the Roman Empire from ca. 100 BCE to ca. 200 CE, which, they inferred, fostered the Roman Empire's unparalleled rise. However, the climatic signal during this period is organized regionally following the main atmospheric modes of the North Atlantic and Mediterranean (Dermody et al., 2012), making general statements on the climatic condition to the whole Empire probably not applicable. However, McCormick et al. (2012) highlight that in the heart of the Roman Empire, that is Italy, there is a substantial absence of significant studies on this period. This does not mean that studies have not been performed, but their chronological anchoring and resolution are not adequate for the purposes of this kind of research. In addition, many archives were investigated with pollen and/or proxies, which are sensitive to human impact giving preeminently environmental information instead of genuine climatic information (e.g. Mensing et al., 2015). The situation in the last years has surely changed but not substantially improved. In particular, it would be fundamental to have archives which directly contain the physical evidence of the 79 CE eruption (i.e. in form of visible tephra layer or as cryptotephra), which could also avoid misalignment related to the use of different age model (Zanchetta et al., 2011, 2012a, 2012b, 2019). However, this evidence is rare and when the case is, the records available do not possess significant resolution. Aware of these limitations we select some archives in the western Mediterranean, which can be representative (in a very broad sense) of the condition prevailing on the Tyrrhenian side of Italy (Fig. 11). Bini et al. (2020) investigated the relation between flood events recognized in archaeological sites in northern Tuscany and hydrological condition inferred from stable isotopes and trace elements on speleothems collected in the Apuan Alps caves (Renella and Corchia, Fig. 11e,f). According to these authors, the very end of the I century B.C. and almost of the whole I century A.D. are characterized by an increase of precipitation associated to evidences of increased fluvial floods, which is substantially mimicked by the historical reconstruction of the Tiber river flood (e.g. Aldrete, 2007). They suggest that this may have corresponded to a phase of Negative North Atlantic Oscillation (NAO) index, favoring penetration of the Westerlies and cyclones from the Atlantic into the Mediterranean during autumn and winter months. However, the speleothems proxy indicates for the very end of the I century A.D. a progressive return to drier condition even if not particularly prominent. This is not perfectly coincident with some proposed reconstruction of the NAO index (Fig. 11), even if this can be considered within the errors of the Apuan Alps speleothems age models. As shown in Fig. 11e,f, the year 79 CE occurred during the trend of decreasing precipitation. As indicated by the sea surface temperature (SST) record, obtained using alkenones in the sediment of the core KSGC-31, average annual temperature seems relatively stable during this period, and the Roman Period does not stand as particularly prominent phase of high temperature (Jalali et al., 2016, Fig. 11c). Summer temperatures reconstructed from lake Verdarolo on the Northern Apennine (Samartin et al., 2017) indicate a cooler condition during the first part of the Roman Period, which terminates at the end of the I century A.D. with a slow increase in temperature. The oxygen isotope composition of the shell of the planktonic foraminifera *Globigerodinoides ruber* ($\delta^{18}O$ in core SW104, Fig. 11d) in the Gulf of Gaeta (Fig. 11) shows during the similar period higher values potentially indicating lower temperature, and an interesting trend toward lower values during the time corresponding, according to the age model, to the occurrence of the eruption (Margaritelli et al., 2016). However, the interpretation of this record is ambiguous. The isotopic signal could indeed be related to changes in local salinity (i.e. higher contribution of freshwater) or to an increase in temperature at time of shell calcification (or both). For comparison, in Fig. 11a are reported the high-resolution dendroclimatological study of the summer temperature in central Europe (Büntgen et al., 2016). The error associated to this kind of study probably allows, with a low degree (decadal) of uncertainty, to place the 79 CE eruption during a period of progressive reduction of temperature at the end of the first maximum warming of the "Roman Climatic Optimum" (Fig. 11). However, this cannot be mechanically translated in higher summer temperatures over the Mediterranean region; indeed, Verdarolo and core SW104 seems to suggest an opposite trend. Overall, the selection of data from Fig. 11 clearly shows inconsistencies and divergent trends. Speleothems from the Apuan Alps indicate that the 79 CE eruption occurred during a transition to a period of progressive (even if not extreme) drying; whereas $\delta^{18}O$ values from Gulf of Gaeta suggest a possible decrease in sea surface salinity (i.e. increase in freshwater input) and/or transition to trend of temperature increase. Whereas the Gulf of Lyon SST does not show temperature change (Jalali et al., 2016). However, some of these differences could be probably only a result of discrepancies between age models. It is also important to note that proxies displayed in Fig. 11 are indicative of different climatic parameters like precipitation (for speleothems in the Apuan Alps these should be mostly a winter precipitation signal, e.g. Bini et al., 2019), temperature (SST obtained from alkenone in the Mediterranean Sea is considered to be close to mean average temperature, e.g. Sicre et al., 2016), and changes in sea salinity, which can roughly be related to changes in hydrological budget. Despite the very common use of terms to indicate the Roman Climate, a clear and objective picture of climate over the Italian peninsula during roman times is still far to be obtained from the available proxy records. The same applies if we want to understand the possible climatic and (more probable) environmental impact of the eruption at regional scale.

10. Numerical modelling of explosive eruptions

10.1. Modelling of explosive eruptions: General aspects and the 79 CE simulation

In this section, we review the available numerical models that have been used to describe the 79 CE eruption of Vesuvius over the years. Given the complexity of modelling explosive eruptions and the evolution of the models particularly in recent years, we briefly introduce the general problem of physical modelling of such eruptions (see Neri et al., 2022 for a comprehensive review). This will provide a measure of the great development that was prompted by the study of the 79 CE eruption in the field of numerical modelling of volcanic eruptions. The ascent of magma toward the ground surface, its fragmentation and emission into the atmosphere as a mixture of hot gas and solid particles involve a variety of thermodynamic processes. Outside the volcano, the solid particles (after fragmentation) can eventually decouple from the volcanic plume and fall to the ground, where they can form widespread fallout deposits that mantle extended areas around the vent, and all along the direction of prevailing winds. On the other hand, partial or total collapses of the eruption column, or the failure of a volcanic dome can cause the development of pyroclastic currents, which can quickly propagate down the slope of the volcano. These currents are capable of overcoming obstacles (both topographic and urban) and reach distances of tens of km. The dynamics of the flow depends on several features including, in particular, not only the relative proportion between gas and particles but also the interaction with topographic and urban obstacles (Sulpizio et al., 2014, and references therein). This extraordinary complexity combines with our limited capacity to observe and directly measure many of these phenomena, affecting our ability to model explosive eruptions. It is just to imagine all complexities, but at the same time the investigation needs, which are related to a large and so impacting event like the 79 CE eruption of Vesuvius, to understand how such studies should be systematic. To overcome all these difficulties, a common practice is to separate and address one single process at a time, identifying its driving mechanisms and governing equations. Depending on the processes considered, different time- or length-scales can be

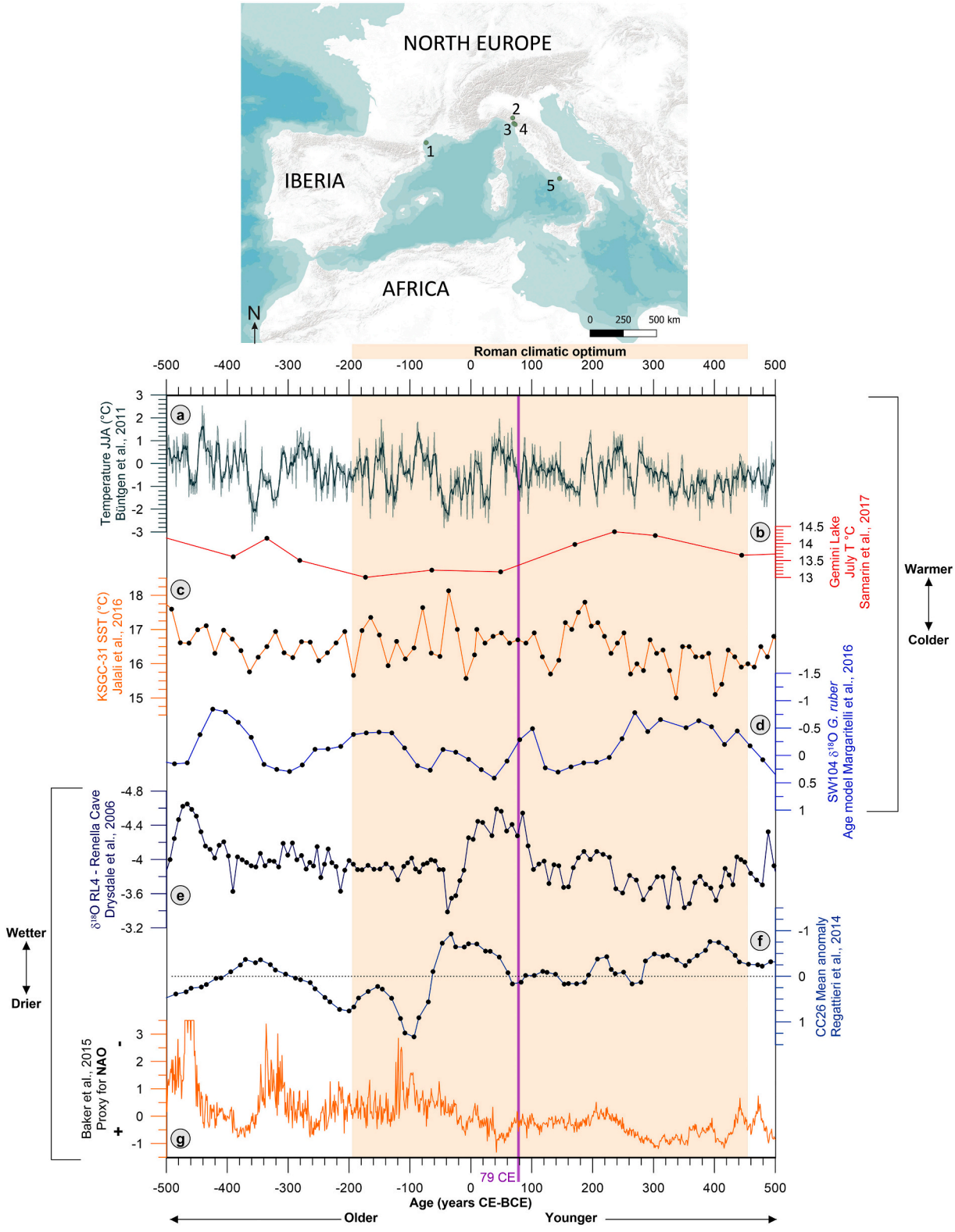

Fig. 11. Top: Location map of the Western Mediterranean sites reported in the text. Site 1 - Core KSGC-31, sea surface temperature (Jalali et al., 2016); site 2 - Lake Verdarolo average summer temperature (Samartin et al., 2017); site 3 - Antro del Corchia Cave, CC26 speleothem anomaly index (Regattieri et al., 2015); site 4 - Grotta della Renella, RL4 $\delta^{18}O$ record (Zanchetta et al., 2016); site 5 - Core SW104, $\delta^{18}O$ record in the test of the foraminifera *Globigerodinoides ruber*. Bottom: Proxy records discussed in the text. **a)** Dendroclimatological data for summer temperature for central Europe (Büntgen et al., 2016); **b)** Average summer temperature from Lake Verdarolo (Samartin et al., 2017); **c)** Core KSGC-31, sea surface temperature (Jalali et al., 2016); **d)** Marine core SW104, $\delta^{18}O$ record in the test of the foraminifera *Globigerodinoides ruber;* **e)** Grotta della Renella, RL4 $\delta^{18}O$ record (Zanchetta et al., 2016); **f)** Antro del Corchia Cave, CC26 speleothem anomaly index (Regattieri et al., 2015); **g)** NAO-index from speleothems proxy records (Baker et al., 2015).

relevant. Regardless of the process considered, model setup and validation require input parameters and, commonly, specific assumptions concerning the natural system. This has promoted specific field studies and observations aimed at collecting the data needed to set up and constrain model parameters and assumptions. All the stratigraphic and petrological studies described in the first half of this work are intended as the actual constraints of an explosive eruption (products), the 79 CE one, that already happened. Then, the numerical modelling makes a full circle, allowing us to better understand what might have happened during the eruption (processes). Despite these difficulties, the need to provide a quantitative assessment of volcanic hazards gave a strong motivation to develop models capable of describing specific features of volcanic eruptions. Vesuvius has always been a natural target for these modelling efforts, given the high volcanic risk, the symbolic relevance of the Roman towns buried in 79 CE, and due to the large amount of information available about its volcanic history. First attempts to model explosive activity at Vesuvius began as early as 1988, with the description of ash fallout during the 79 CE eruption (Macedonio et al., 1988). Considering the eruptive phases responsible for the deposition of the white and grey pumices (EU2f and EU3f), Macedonio et al. (1988) applied an advection-diffusion model describing the distal ash fallout, based on a continuity equation for mass concentration that considers wind field, atmospheric diffusion and gravity settling (input parameters in ESM 5). The same model was later applied to perform a first assessment of the hazard posed by ash accumulation. The model output describes the total particle concentration at the ground and, given particle density and grain size distribution, the corresponding deposit thickness. The model validation featured a comparison between calculated (Macedonio et al., 1988) and measured (Sigurdsson et al., 1985) deposit thicknesses at different locations. A good correspondence was found for the grey phase, for which a better reconstruction of the grain size and componentry distribution was available. Also, the comparison between the calculated and observed (Lirer et al., 1973) grain size distribution resulting at different locations provided a good match for the grey pumice deposit. A complementary modelling study was carried out within a given eruptive scenario corresponding to the maximum expected event, and exploring the effects of wind variability (Barberi et al., 1990). On the other hand, Macedonio et al. (1990) explored the possible outcome of future events at Vesuvius, considering three different eruptive scenarios, ranging from small-size "ultra-strombolian" to large scale Plinian. The authors first assessed the eruption column behaviour based on the plume theory (Wilson and Walker, 1987). The theory describes the changes of the eruption column properties (density, temperature, velocity and radius) at different heights as a function of input parameters, which include (among others) the column radius at the vent, the gas weight fraction and mass eruption rate (ESM 5). The authors used the plume theory to constrain the vent radiuses and corresponding column heights that are expected for a given mass eruption rate. In this case, there is no direct comparison with data from real observations, but modelling results show the effect of column heights on particle distribution on the ground, especially when the more variable summer winds are considered. It was found that as column height increases, the maximum distance reached by heavier particles is reduced, while isomass lines pertaining to lighter particles extend further. The same model was later applied by Cioni et al. (2003) to perform a probabilistic assessment of the hazard related to ash fallout. Macedonio et al. (1990) also accounted for column collapse and pyroclastic current propagation. At the time, however, specific models to describe pyroclastic current propagation and deposition were not available, and Macedonio et al. (1990) limit their considerations to an estimate of maximum runout distance. Results were based on the energy cone method (Malin and Sheridan, 1982; Sheridan and Malin, 1983), even though Macedonio et al. (1990) highlighted the oversimplified approach of such method. A first description of the dynamics of pyroclastic currents along the slopes of Vesuvius was carried out only a few years later by Dobran et al. (1994). In this work, two different models were employed. A first 1-D model (Papale and Dobran, 1993) was used to simulate magma ascent along the volcanic conduit, in order to compute vent conditions based on mass eruption rate, conduit length, magma chamber temperature and pressure, magma composition, gas and crystal content, and grain size after fragmentation. The outputs of this first model constrained the conditions at the vent, which were then used as input parameters (ESM 6) for a second transient model, which was meant to describe the evolution of the eruptive mixture once injected into the atmosphere within a 2-D axisymmetric domain (Dobran et al., 1993). In this second model, the eruptive material was described as a multiphase mixture of solid particles and water vapor, entering a standard atmosphere composed by air. Both gas components (vapor-air multispecies) were assumed to follow the ideal gas law, while the solid phase was made by spherical particles of equal diameter (100 μm). The model accounted for mechanical and thermal disequilibrium between gas and solid particles, described the effects of particle-particle interactions, and implemented a turbulent sub-grid scale model to represent gas turbulence. In their application to Vesuvius, Dobran et al. (1994) considered three different scenarios referred to large-, medium- and small-scale events. The large-scale event was tailored to represent the 79 CE eruption. The authors also explored the effect of different volcano slopes, although under the simplifying assumption of axial symmetry. Two topographic profiles were implemented, one across Mt. Somma along the northern sector of the volcano, and a smoother one, representative of the southern sector. Performed simulations described the collapse of the volcanic column and the generation of pyroclastic currents that quickly swept the computational domain. For the considered largest scenario, simulated pyroclastic currents were capable of overcoming the topographic obstacle characterizing the northern profile. A coarse model validation was carried out through a comparison with volcanological evidence and historical accounts, suggesting similar runout distances and timing for the pyroclastic current propagation, and confirming that the currents could indeed overcome Mt. Somma. The modelling results of Dobran et al. (1994) were later analyzed to explore the impact of pyroclastic currents on inhabited areas (Baxter et al., 1998; Doronzo and Dellino, 2011). These authors focused on the evolution of selected flow variables that are found to be critical for human survival (in particular, ash concentration > 0.1 kg/m^3, temperature > 200 °C) or building resistance (dynamic pressure $>$ 5–10 kPa). As field constraints, the findings of numerous charred woods in EU3pf at Cava Pozzelle and in EU3pftot at Cava di Pollena, and decimeter-sized lithic fragments in EU4pf at Pompeii indicate a high thermo-mechanical impact of the pyroclastic currents in proximal to medial reaches. Results showed that pyroclastic currents generated by large-scale events like the 79 CE eruption of Vesuvius, can cause destruction and unsurvivable conditions along their entire path, and within minutes from their generation after column/caldera collapse. Also, minutes or less is the order of magnitude for the emplacement of depositional flow units (lamina, layer, bed; see Doronzo, 2012; Roche, 2015; Martí et al., 2019). In case of slower flows (i.e., smaller eruptions or in the presence of obstacles), air entrainment may lower the flow temperature below a critical threshold, at distances greater than a few km from the vent. Ash concentration in the areas reached by the flow is always to be considered as unsurvivable, therefore the flow runout is a reliable indicator for the hazard associated with respiratory problems. Also, the model of Dobran et al. (1993) was further refined to introduce the description of solid particles with different sizes and properties (Neri and Macedonio, 1996), and to account for terrain roughness and its effects on flow turbulence and runout (Todesco et al., 2002). The application to Vesuvius confirmed the expected high impact of the pyroclastic currents, and highlighted the transient nature of the simulated hazard variables. In particular, results showed the complex dynamics that leads to significant pressure changes and peaks of the dynamic pressure, regardless of the steady discharge rate fixed at the vent (Esposti et al., 2002). Simulations also showed that even in case of short-lasting feeding (i.e., with discharge from vent interrupted after 2 min), the currents were capable to reach urban

settlements around Vesuvius, highlighting the inertial behaviour of such currents (Todesco et al., 2002; Doronzo et al., 2022). A substantial advancement was achieved by Neri et al. (2007) and Esposti Ongaro et al. (2007, 2008), who implemented a parallel code for the simulation of transient dispersal of pyroclasts into the atmosphere. The implementation of the parallel code on a supercomputer allowed the simulation of 3-D eruptive scenarios featuring the real topography of the volcano. The application to Vesuvius described a medium-scale sub-Plinian eruption, and showed the role of column collapse regimes on the generation and impact of the pyroclastic currents (Neri et al., 2007; Esposti Ongaro et al., 2008; see Fig. 12). Such application gives a clear idea of the importance of eruptive dynamics on pyroclastic current generation, transport, and emplacement, i.e. the density contrast between the flow and atmosphere is not the only driving mechanism in explosive eruptions (cf. Trolese et al., 2019; Doronzo et al., 2022). Ongoing research is also considering simpler models that allow a statistically sound assessment of volcanic hazard and associated uncertainty (Tierz et al., 2018; Tadini et al., 2021). Future developments of numerical modelling will aim at improving the description of the physical phenomena that take place during explosive eruptions in general, as the 79 CE eruption of Vesuvius had a number of similarities with other eruptions at monitoring volcanic areas, such as for example Mount St. Helens, Pinatubo, Tenerife, Fogo, and others worldwide (see next sections).

10.2. Recent developments and future perspectives

In this section, we compiled a set of information to complement the recent advances that are ongoing in the modelling of explosive eruptions. From the 79 CE eruption of Vesuvius, we have learned how to pass from "reading" pyroclastic deposits of past eruptions (products) to implement equations to explain the processes. It is indeed a unique opportunity to use this well-known eruption to extend the comprehensive approach that we propose to explosive volcanoes in general. An effort was done here in that sense, considering the substantial improvement of the models in recent years. Concerning volcanic plumes, maximum height and time-averaged vertical profiles of density, entrainment, gas and solid mass fraction, plume bending and radius, temperature, and velocity have recently been focused on (Costa et al., 2016; Suzuki et al., 2016a). Such studies have shown that the entrainment processes are of paramount importance to accurately relate mass eruption rate with maximum plume height. When simulating Plinian eruptions with mass eruption rate $> 10^7$ kg/s, the complex buoyancy reversal process undergoing from the crater, up to the suspended region 1–5 km above (Neri and Dobran, 1994; Suzuki et al., 2016b; Costa et al., 2018), is difficult to capture with 1-D models, and a better understanding of the process is needed to relate eruption source parameters with total/partial column collapse, and with the dynamics of the buoyant part of the volcanic column (Degruyter and Bonadonna, 2013; Koyaguchi and Suzuki, 2018; Koyaguchi et al., 2018; Trolese et al., 2019; Aubry et al., 2021). Some of the existing modern 3-D models for volcanic plumes and pyroclastic currents have been presented in that sense, in particular SK-3D (Suzuki et al., 2005), ATHAM (Herzog et al., 2003), ASHEE (Cerminara et al., 2016a, 2016b), and PDAC (Neri et al., 2003). Other existing 3-D models are, for example, MFIX (e.g., Dufek and Bergantz, 2007), Plume-SPH (Cao et al., 2017), and Ansys Fluent (Doronzo et al., 2011), which have been experimentally-validated (see Sulpizio et al., 2014). In general terms, the governing equations for mass, momentum and energy conservation can be solved in their full transient 3-D shape, or averaged horizontally and temporally to obtain integral 1-D models, or averaged vertically to obtain shallow water models. Alternatively, only some of these equations can be solved, using observations and one-way coupling, like in Volcanic Ash Transport and Dispersion Models (VATDM), where atmospheric conditions and mass conservation are used for the transport of volcanic ash and gas. The degree of accuracy, resolution and dynamic phenomena that is possible to resolve depends on computational resources and performances, the accuracy of empirical relationships obtained from laboratory and large-scale experiments, the knowledge and observation of the volcano, of its products and dynamical behaviour, above and below ground (Sulpizio et al., 2014; Esposti Ongaro et al., 2020). To model the dynamics of a volcanic column in explosive eruptions, the first step is to define the eruption source parameters produced by underground dynamics, the magma chamber, and the volcanic conduit. In that sense, we did an effort in this multidisciplinary work to provide all needed information about the 79 CE eruption of Vesuvius. This input information can define the so-called independent eruption source parameters (Trolese et al., 2019), for which it has recently been published a database (Aubry et al., 2021), and which are: mass eruption rate, magma temperature, mass fraction of exsolved gases in the magma, magma overpressure, grain-size, density and shape distribution. Other parameters are needed increasing the accuracy of the simulation, such as the specific heat distribution of the pyroclasts (Moitra et al., 2018), the initial presence of ice and rocks above the volcanic conduit, or the chemical and petrological properties of the fragmented magma (see section 7). It should be kept in mind that all of these parameters typically change in time and space, starting from the mass eruption rate, which is one of the most important parameters (cf. Carey and Sigurdsson, 1987). Recently, remote sensing techniques have enabled the observation of such variations (Marzano et al., 2020; Freret-Lorgeril et al., 2021; see also next section). When only the subaerial dynamics is of interest, different eruption source parameters are used to model the eruption dynamics. For example, inputs for pyroclastic current vertical profiles can be reconstructed from large-scale experiments (Doronzo and Dellino, 2011; Sulpizio et al., 2014; Shimizu et al., 2021; Cerminara et al., 2021; Brosch et al., 2021), while for ash transport and dispersion maximum plume height and vertical profiles of ash components should be prescribed (Suzuki, 1983; Pfeiffer et al., 2005; Devenish and Cerminara, 2018; Aubry et al., 2019; Folch et al., 2020; Cao et al., 2021). One way to prescribe these vertical profiles (to be used as input for VATDM simulations) is to average results from 3-D numerical simulations in time and horizontally in space. In Fig. 13, the averaged vertical profiles of pyroclasts going into the atmosphere from a volcanic plume are shown based on the 79 CE eruption scenario for Vesuvius, simulated by using the ASHEE code (Cerminara et al., 2016a, 2016b). The approach enables dispersion models to have an initial condition taking into account of the turbulent multiphase non-

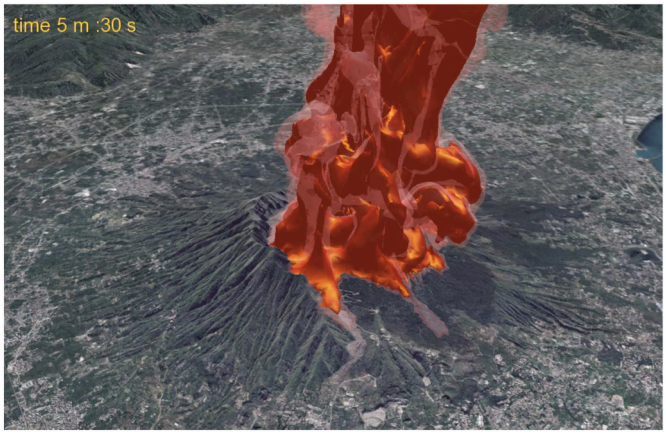

Fig. 12. Results from 3-D modelling of an explosive volcanic eruption at Vesuvius. The figure illustrates isosurfaces of mixture temperature after 330 s of flow time. The inner darker surface corresponds to a temperature of 350 °C, while the lighter outer surface represents a temperature of 100 °C. The mass eruption rate imposed at the vent (5×10^7 kg/s) corresponds to a medium scale, sub-Plinian eruption (Esposti Ongaro et al., 2008). The top view of the sumulation results is from the west, and shows some barrier effect of Mt. Somma visible toward the northeast. Such effect is reflected in the distribution maps of Fig. 5.

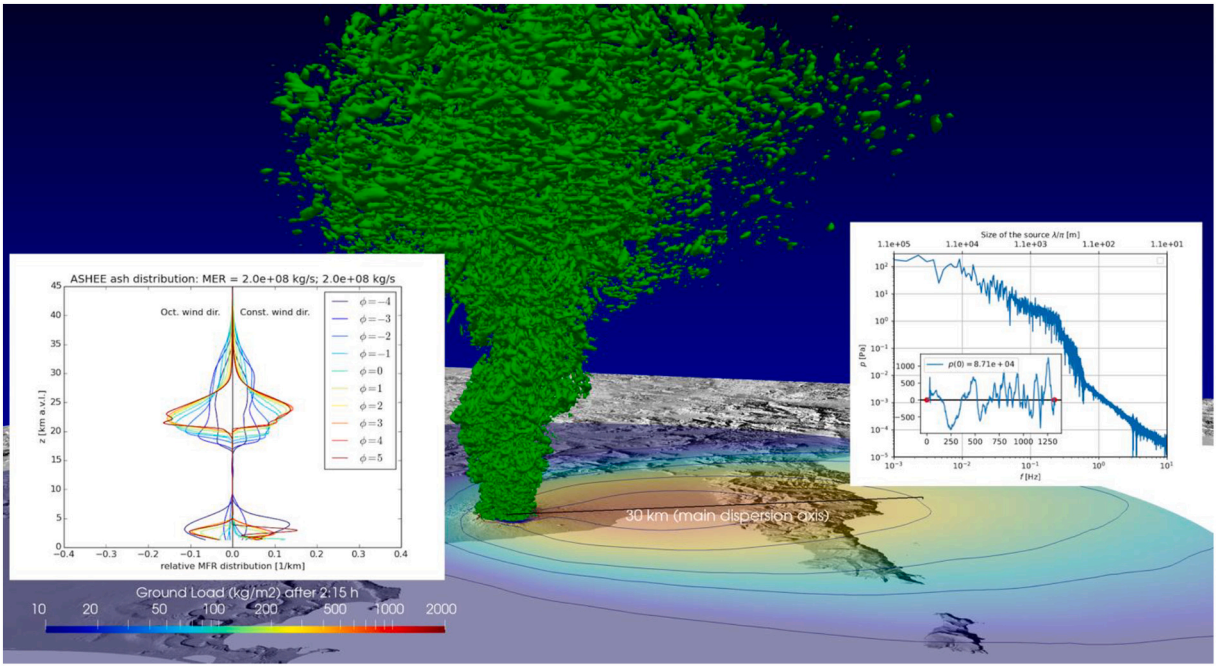

Fig. 13. Turbulence isosurface (Q-criterion) of the mixture velocity field (green). Deposit ground load is represented by the colormap and contour lines drawn in 10, 50, 100, 250, 500 kg/m^2 (and, not visible, 750, 1000, 1500, 2000 kg/m^2). The 30 km long black line starting from the center of the Vesuvius' crater is pointing along the main dispersion axis to the southeast. The left inbox shows the averaged mass flow rate vertical distributions for all the 10 solid phases, obtained with the average October Vesuvius wind (left), and with a wind field of constant direction (right). The right inbox shows the infrasonic acoustic signal and spectrum produced by the eruption, at a distance of 10 km from the vent. (For interpretation of the references to colour in this figure legend, the reader is referred to the web version of this article.)

equilibrium phenomena occurring in the volcanic plume. Modern High-Performance Computing (HPC) infrastructures enables the numerical simulation of explosive eruptions with unprecedented resolution. Volcanic eruptions are multiscale. Indeed, the smallest scale is of the order of the finest ash particles, and of the smallest turbulent eddy developing in the column, i.e. 1 μm. On the other hand, the largest scale to be captured is of the order of hundreds (when not thousands) of km. Even if we still are abundantly far from being able to numerically solve for all of these scales, modern supercomputers and codes enable to reach numerical simulations with hundreds of millions to billions of degrees of freedom. A number of physical processes and mathematical problems are involved in the long road to understanding and reproducing as accurately as possible the 3-D dynamics of volcanic plumes, pyroclastic currents, and ash dispersion. The presence of multiscale dynamics and complex topographies makes discretization far from being trivial, even if modern developments in numerical analysis and information technology allow to deal with it. Since it is impossible to resolve all the relevant scales, subgrid models are necessary to close the equations for turbulence, like LES and dynamic LES models (Moin et al., 1991; Cerminara et al., 2016a, 2016b). The strong advantage of dynamic LES models is that they do not need any empirical parameter (like the Smagorinsky coefficient), as the equation closure is based directly on the self-similarity of the local turbulent spectrum. In this way, air entrainment of volcanic plumes can be calculated by 3-D models without the need of any prescribed parameter (Cerminara et al., 2016b). In Fig. 16, we show the turbulent eddies inducing air entrainment tentatively for the 79 CE eruption scenario are shown. Atmospheric stratification, moisture, and wind conditions pose problems regarding boundary conditions, data assimilation (Pardini et al., 2020; Osores et al., 2020), water phase change (Folch et al., 2015), and extremely low pressure and density regions (Costa et al., 2018). Such complexity is reflected by the distribution of the 79 CE pyroclastic fall deposits, as the reconstruction of EU2f points to the southeast, while the one of EU3f to the south (Fig. 5). On the whole, the mimic of the 79 CE volcanic cloud points to the southeast, along the Vesuvius-Crete axis (Fig. 9), indicating some rotation of the dispersal axis as a function of the plume height over time. Volcanic mixtures are multiphase, in which each particle moves with a velocity and temperature different from that of the surrounding gas species. Two-way coupling, i.e. the momentum and energy exchanges between solid particles and gas is of paramount importance when the particle volumetric concentration increases up to around 1%, so it is important in particle settling and sedimentation. Finally, particle-particle interactions (four-way coupling) start to become important when the particle volumetric concentration exceeds 1%, and it is important in hindered settling and deposition. Eulerian multiphase dynamics is computationally extremely expensive because in principle, every grain size classes have a different velocity to be found through a dedicated Navier-Stokes equation. However, for fine to medium ash (pyroclasts finer than 1 mm) it is the optimal approach, while for coarser ash, lapilli, and bombs a Lagrangian approach is preferable (Balachandar and Eaton, 2010; Valentine et al., 2011). Approximations allows to simplify the problem keeping a good accuracy for ash decoupling, preferential concentration, and settling (Ferry and Balachandar, 2001; Balachandar and Eaton, 2010; Cerminara et al., 2016a). In Fig. 17, we show the difference in the 3-D distribution of 1 mm ash and 16 mm lapilli. In Cerminara et al. (2016b), it is shown the effect of spatial resolution, turbulence sub-grid model, and ash decoupling for Plinian and sub-Plinian plume averaged profiles. A key parameter for modelling particle decoupling in dilute systems is the Stokes time, depending on particle size, density and shape, measured in the laboratory through the particle settling velocity (e.g., Bagheri et al., 2015). An additional complication is particles aggregation, changing their size and shape while they are moving in wet atmosphere (Folch et al., 2015; Rossi and Bonadonna, 2021), and particle deceleration through Lagrangian trajectory in denser systems (Doronzo et al., 2012). Plume rise influences the surrounding atmosphere, pushing it away from the plume head, and sucking it from the edges of the plume due to turbulent entrainment. The vertical profiles shown in Fig. 16 are strongly influenced by the air

entrainment rate modelled by the 3-D plume simulation. Once the plume reaches its maximum height, its top starts to oscillate creating gravity waves (Suzuki et al., 2016a). Turbulence and conduit exit dynamics create infrasound (Ripepe et al., 2010; Matoza et al., 2019; Cerminara et al., 2016b). In Fig. 16, the infrasonic signal and spectrum that would be measured from a synthetic microphone located in Naples and generated by turbulence is shown. Moving to the bottom of the domain, the multiphase fluid-dynamics of the boundary layer above the topography is important to accurately reproduce pyroclastic current sediment mechanics (Doronzo et al., 2012). In these types of flow, concentration increases due to particle decoupling and a dense layer typically forms below the upper layer that characterizes the transport system (Valentine, 1987; Shimizu et al., 2021). The dense layer may still move also depending on topography (Druitt et al., 2002; Doronzo, 2012). Such interplay between transport and depositional system in pyroclastic currents can be inferred from the deposit characteristics at Cava Pozzelle and Cava di Pollena (see section 4). In topographic lows, the depositional boundary layer first reacts to substrate through a low accumulation rate, then succumbs to forced deposition through a higher accumulation rate (vertical facies variation); a reaction to substrate can also occur on topographic highs (lateral facies variation) (Doronzo et al., 2012). The presented high resolution 3-D numerical simulation of eruption scenarios based on the 79 CE eruption of Vesuvius are being simulated with the ASHEE model (Cerminara et al., 2016a, 2016b). Results from a scenario with MER equal to $2 \cdot 10^8$ kg/s are shown in Figs. 13, 14 and 15. A smaller scenario is shown in Fig. 16 (MER $= 3 \cdot 10^7$ kg/s). Interestingly, it is possible to extract from numerical simulations quantities that may be monitored during real volcanic eruptions, such as deposit ground load and grain size distribution (Fig. 17), volcanic infrasound (once turbulence is modelled with enough accuracy; Cerminara et al., 2016b) and shocks (related to compressibility effects), infrared emission (Cerminara et al., 2015; Calusi et al., 2020; see Figs. 18 and 19), and electromagnetic wave backscattering (once optical properties of particles are given; Gouhier and Donnadieu, 2008; Marzano et al., 2020). In Fig. 18, the signal that would be measured by a synthetic radar in Naples is shown. This result was produced by using the information contained in the 3-D simulation, such as the density and velocity fields. In this way, it is possible to evaluate the total backscattering power P_{tot}, the backscattering power of particles moving away from and toward the radar P_+ and P_-, the plume reflectivity factor Z, the maximum velocity of particles moving away from the radar V_{max}, and the particle volumetric concentration C. To better constrain inversion algorithms used to monitor volcanoes, it would be useful to compare these synthetic observations with field data. The decay of the deposit ground load with distance follows the classical deposition from volcanic plumes (cf. Pyle, 1989), which in our case gets to the Sorrento Peninsula and well beyond (Figs. 13 and 14). Curiously, the contemporary eruption of Hunga Tonga occurred in 2022 has shown a number of these phenomena, confirming the reliability of the numerical modelling approach of explosive eruptions.

11. Satellite remote sensing

The technological advances of satellite remote sensing systems made over the last 20 years marked a major step forward both in the proximal and distal monitoring of volcanic eruptions in real time. This approach represents a powerful tool able to significantly improve the risk mitigation on local population and air traffic, and to gain insight into processes of volcanic unrest (see for example, Prata and Kerkmann, 2007; Corradini et al., 2018, 2020; Theys et al., 2019). Today, many different instruments, working at different spectral ranges with different spatial/temporal resolutions and placed in geostationary and polar orbits, offer a unique opportunity to track the whole evolution of the volcanic eruptions, extending the monitoring capabilities both during day and night. Since the beginning of this "new satellites era", there (fortunately) were no large-scale eruptions like the 79 CE one of Vesuvius, so no direct measurements of an event of this magnitude are available. An exception (with due proportions) is the Hunga Tonga eruption occurred beginning

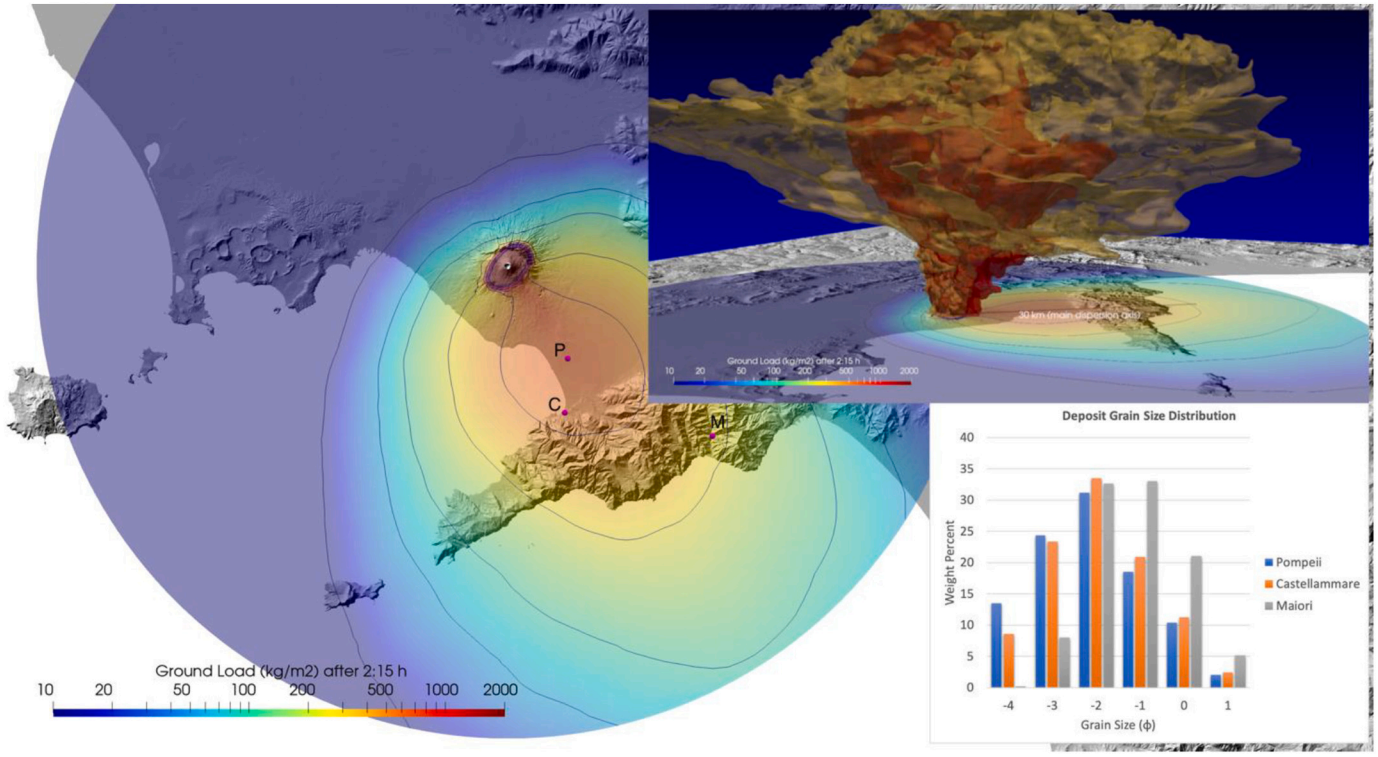

Fig. 14. Deposit ground load as in Fig. 13, vertical view. The lower inbox shows the grain size distribution of the deposit in Pompeii (P), Castellammare (C), and Maiori (M). The upper one shows mass fraction isosurfaces of 16 mm lapilli (red) and 1 mm ash (yellow) above the Vesuvian and Neapolitan area, 2:15 h after the beginning of the eruption. (For interpretation of the references to colour in this figure legend, the reader is referred to the web version of this article.)

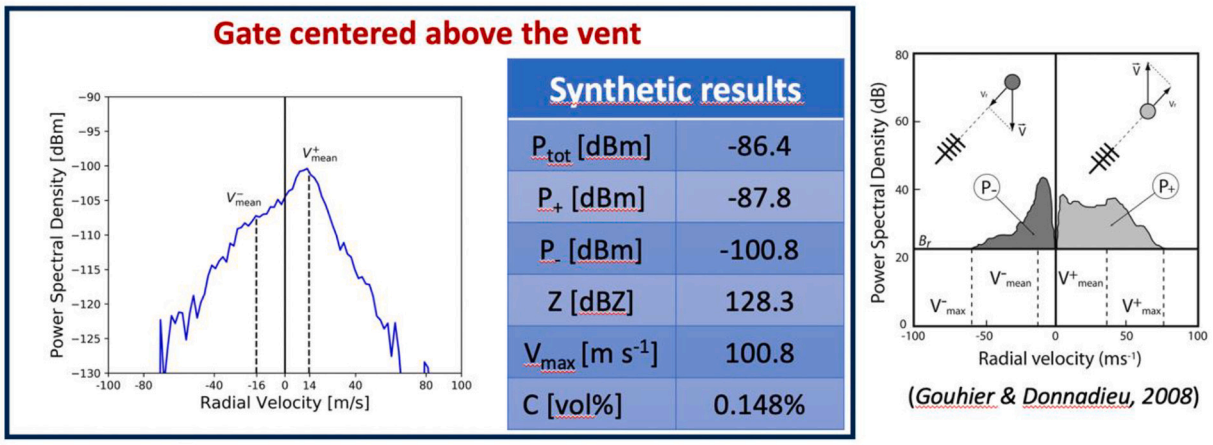

Fig. 15. Radar power spectral density as obtained from the Vesuvius numerical simulation (left) and from an eruption at Mount Etna (right; Gouhier and Donnadieu, 2008). P_{tot} is the total backscattering power (BSP), P_+ is the total BSP of the particles moving away from the radar, P_- is that of the particles moving toward the radar, Z is the reflectivity factor, V_{max} is the maximum velocity of the particles in the gate and C is the particle concentration in the gate.

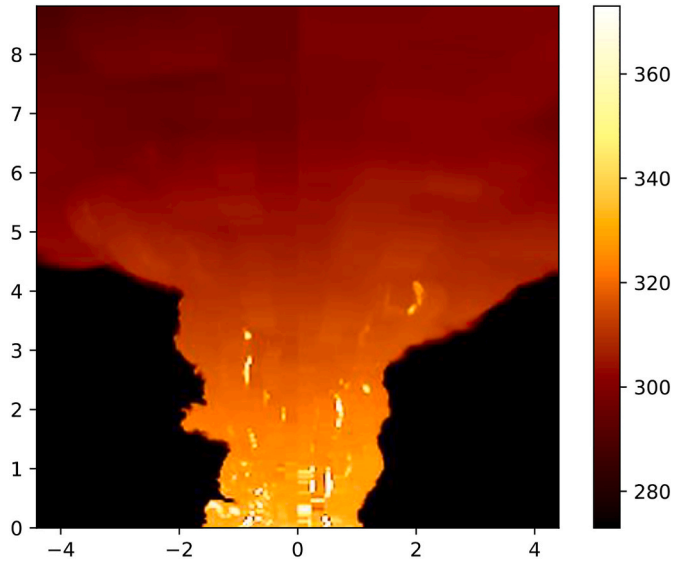

Fig. 16. Infrared image of a numerically simulated Plinian eruption (in Kelvin). In this case, the synthetic average temperature of the plume top seen from satellite is 215 K.

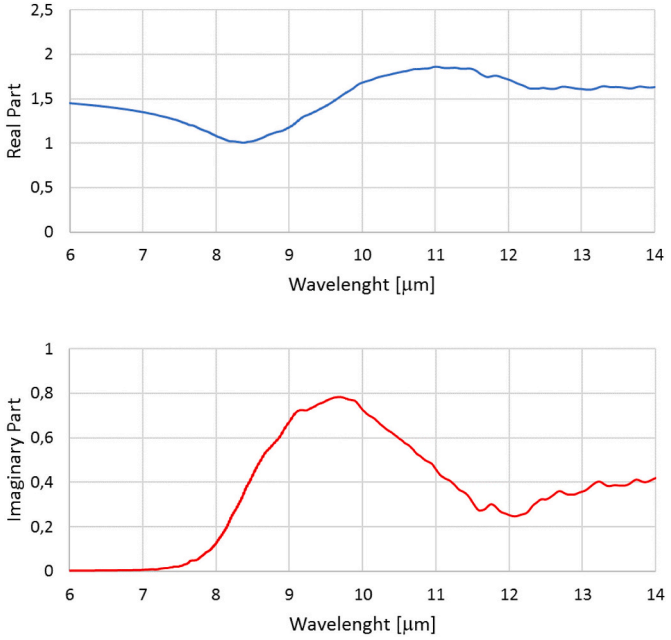

Fig. 17. Vesuvius ash refractive index computed considering a percentage of SiO_2 of 56%; real part (top) and imaginary part (bottom).

of 2022. To test the reliability of the algorithms already developed, particularly for the estimation of gases and particles in the volcanic cloud under such extreme conditions, it is therefore necessary to simulate what the satellite would see in those cases. Among the capabilities described in the previous section, numerical modelling can also be used to simulate the upper atmosphere (TOA) radiance, at different wavelengths, as seen by a satellite sensor orbiting the Earth. These TOA radiances depend on surface characteristics (temperature and emissivity), volcanic cloud geometry (altitude and thickness), atmospheric profiles (temperature, pressure and humidity) and ash optical properties (extinction coefficients, single scattering albedos and asymmetry parameters). These latter parameters are those with higher uncertainties leading to higher errors in the retrievals (Prata and Grant, 2001; Corradini et al., 2008). The optical properties can be obtained by knowing the particle refractive index and the size distribution. Generally, if the size distribution can be fixed, the refractive index is unknown and highly variable. Recently, a novel procedure has been introduced for the refractive index computation, based on the percentage of SiO_2 present in the ash sample (Prata et al., 2019). The importance of the analysis of samples from the 79 CE eruption deposits is that it allows to estimate the percentage of SiO_2 present, then to compute the refractive index of ash particles of the volcanic cloud. These investigations indicate a variation between 54.5 and 57.5% for the white pumices (EU2f), and between 54.0 and 56.5% for the grey pumices (EU3f) (Civetta et al., 1991). Fig. 17 shows the real and imaginary part of the ash refractive index, computed by considering a percentage of SiO_2 of 56% in the thermal infrared (TIR) spectral range (6–14 μm). From the computed refractive index, and considering a defined size distribution, the optical properties can be obtained. Fig. 18 shows the extinction coefficient, single scattering albedo and asymmetry parameter for particles effective radii between 0.5 and 10 μm (computed considering a log-normal size distribution). By knowing the optical properties, simulations of the TOA radiative effect of ash clouds considering different configurations (i.e., different volcanic cloud altitudes, ash mass etc.…) can be realized. This will help us to understand the validity limits of the retrieval procedures in case of Plinian eruptions, and to understand how to improve and

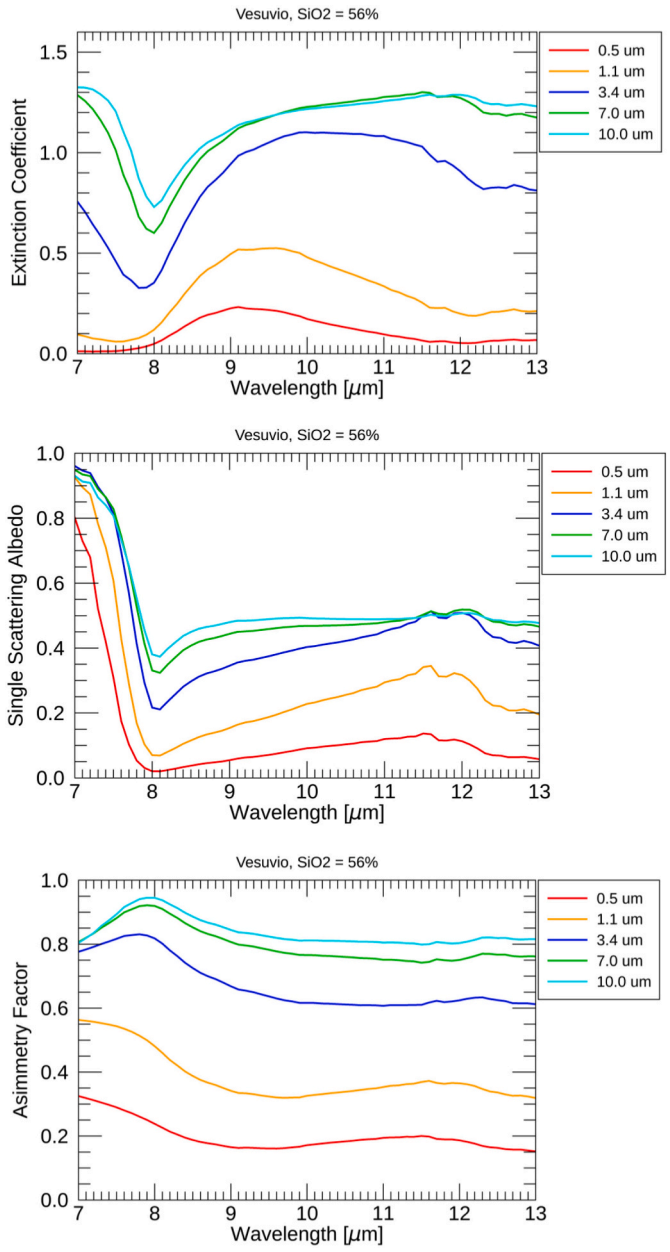

Fig. 18. Extinction coefficients (top), single scattering albedo (middle), and asymmetry parameter (bottom) computed for different particles effective radii and considering the Vesuvius ash refractive index and log-normal distribution.

make them even more effective. Such knowledge strengthens our preparedness, and then increases effectiveness and responsiveness of our actions in case of similar events. Another type of sensors onboard of remote sensing aircrafts is the radar. Today, a huge number of observations based on Synthetic Aperture Radar (SAR) are available, and the InSAR (Interferometric SAR) technique is able to process such data and constrain ground deformations with spatial resolution of few meters and sub-millimeter accuracy. Also, missions such as Sentinel-1 from the European Space Agency (ESA) provide SAR data with revisit time of 6 days, allowing for a dense temporal sampling of the surface deformations. The satellite constellations launched by global space agencies have different capabilities to capture large or small deformations, and are affected by coherence issues in different ways. As an example, X-band SAR sensors (3.1 cm wavelength, e.g., COSMO-Skymed from the Italian Space Agency ASI) have very high spatial resolution, but can decorrelate easily for intense deformations or in vegetated areas. On the other hand, L-band (24 cm wavelenght, e.g., ALOS-2 from the Japanese Space Agency JAXA) are capable of high coherence in case of large displacements and presence of vegetation, but cannot map small displacements. In between, there are the C-band SAR sensors (5.4 wavelength, e.g., Sentinel-1). With reference to the 79 CE eruption, pre-eruptive surface displacements are expected to have taken place (Biggs et al., 2014), that might have been detected by InSAR data in X- and C- bands. Modelling of such deformations would give insights on the position, depth and volume variation of the magmatic source or feeding dyke in case of a similar eruption in the future. Very short-time pre-eruptive and *syn*-eruptive deformations are expected to be intense due to magma ascent toward the surface, and InSAR processing might present decorrelation issues, so C- and L- bands are more suitable. Patterns of lava and pyroclastic currents results to be incoherent with standard InSAR processing, but innovative techniques such as automatic change detection can estimate the lava field and its temporal evolution, combining the InSAR coherence and the InSAR intensity during an eventual emergency phase (e.g., Bignami et al., 2020).

12. Conclusions and future perspectives

The present work on the 79 CE Plinian eruption of Vesuvius reviewed all available information (both from the literature and original) from a multidisciplinary perspective, by discussing the eruption sequence not only with different investigation approaches, but also following ideally the eruption from the magma chamber to the most distal tephras. The work has revised the historical, stratigraphic, sedimentological, petrological, geophysical, paleoclimatic, and modelling aspects of the eruption, which for the first time are combined all together to give a full picture of the 79 CE eruption. With reference to the eruption deposits, a total of 346 stratigraphic sections have been reviewed not only in the Campanian Plain but also farther, both from the literature and as original data. For Pompeii, 39 stratigraphic sections have been reviewed with a focus on the eruption effects in the urban area, plus some other scattered sections. In particular, the database of Gurioli et al. (2010) has been integrated with new medial-to-ultradistal observational points in which the 79 CE pyroclastic deposits have been found (City of Naples, Pollino, Calabria, Sicily, offshore data), in order to show the global environmental impact of the eruption. A large database and a detailed stratigraphy are fundamental not only for the reconstruction of past explosive eruptions, but also for the set up, along with surveillance, of statistical models for probabilistic volcanic hazard assessment, particularly at monitoring volcanoes. With reference to the petrology and modelling, the information from the literature has provided a general but complete picture of the eruption sequence, which reflected a compositional zonation into the magma chamber. Such zonation is something that has also been detected at other explosive volcanic areas worldwide that gave variably large volume eruptions, such as for example Tenerife (Bryan et al., 2000; Martí et al., 2020) and Novarupta (Hildreth and Fierstein, 2012), among others.

On the other hand, some open issues have arisen from the project, each one emerged from the various approaches, and will be addressed in the future in the more general framework of Plinian eruptions. One thing will be to constrain the timing and various phases of the eruption, including the description of ongoing phenomena (e.g., fine ash dispersal into the atmosphere and environmental impact) that might occur during Plinian events similar to the 79 CE eruption of Vesuvius. This can have important implications both on direct and indirect effects of atmospheric ash dispersal in the environment at various scales. As it occurred for other similar large explosive eruptions, such as for example at Mount Pinatubo in 1991 and Popocatépetl in Prehispanic time, the ash dispersal and gas emission can impact directly the climate then (in) directly the agriculture, by modifying the atmospheric temperature and precipitation of acid rains due to significant fine ash and volcanic gas emissions, and the soil fertility and water availability (Siebe et al., 1996; Dartevelle et al., 2002; Costa et al., 2018; Aubry et al., 2021), as well as

can impact civil aviation (Sulpizio et al., 2012; Gouhier et al., 2019). Compared with other Plinian eruptions of Vesuvius, such as the "Avellino" one, the total duration of the eruption (both fall and pyroclastic current phases) could be better constrained, because different pulses feeding the pyroclastic currents may be separated by variably-short quiescence states (Di Vito et al., 2009). Such instants could occur at fragmentation scale by discrete explosive events, particularly during phreatomagmatic phases, as well as at deposition scale (Vazquez and Ort, 2006; Németh and Cronin, 2009; Sohn et al., 2011; Agustin-Flores et al., 2014), and this may not be so evident in proximal areas due to concomitant fall and pyroclastic current processes. As a general case, in a specific site a pyroclastic current can emplace a deposit while the eruption has already ceased at the vent, or vice versa the current does not emplace a deposit (for topographic reason and/or deposition timing) but the eruption is still ongoing, which is something that could be addressed from the deposits in distal areas (Sorrento Peninsula or new sites for future investigations). Also, refined interpretations of the distal and ultradistal tephras will help further constraining the modelling of volcanic column in explosive eruptions. Distal and ultradistal deposits can give insights about the concentration of fine ash present in the umbrella cloud at the time of eruption. As an example, assuming a threshold of ash concentration of 2 mg/m^3 for aircraft's turbines damaging and an umbrella cloud 1 km thick, we get a corresponding threshold of 2 mm the deposit of fine ash (Gouhier et al., 2019), vice versa the 2 mm thick area would imply a volcanic hazard for civil aviation. Following comparison, ashes of the "Avellino" eruption have been found up to Tuscany Region and Adriatic Sea (Sulpizio et al., 2008), and the ones of the sub-Plinian 472 "Pollena" eruption have been found up to Constantinople (Marcellino Comite' Chronicon in Ricciardi, 2009), testifying the regional impact that large eruptions of Vesuvius can have.

Another thing will be constraining the definition of the evolutionary mechanisms (physical, geochemical and petrological) that determined the passage from one phase of the eruption to the next. This has implications on new geochemical and tephrostratigraphic constraints in distal and ultradistal areas to further refine the calculation of the 79 CE erupted magma, and in more proximal areas (e.g., Cava Pozzelle, Terzigno) for fine geochemical analyses over the entire stratigraphic sequence. Another issue will be constraining the definition of the eruption source parameters for Plinian eruptions, by increasing the number and type of simulated observables (e.g., satellite data), and using the simulated satellite data to assess the uncertainties and improve the retrieval algorithms for the volcanic ash cloud. On this side, remote sensing real-time data can help volcanic hazard assessment and risk procedures. Comparison with synthetic data from numerical simulations can refine and better constrain such kind of data. A need of the future community of scientists tasked with monitoring active volcanoes – in light of the present comprehensive work on the 79 CE eruption of Vesuvius – will be to detect the mass eruption rate in quasi real-time for plume dynamics (Dürig et al., 2015), then assess the local impact for pyroclastic current dynamics (Esposti Ongaro et al., 2008) such as for example from Cava di Pollena. This can have implications on the forecasting of ash dispersion into the atmosphere in terms of environmental, aviation, agricultural, and hydric impacts, and of ash distribution and accumulation on landscape.

Further issues will be integrating earth and satellite instruments with the use of different wavelengths (from VIS to MW), and forecasting the impact of similar Plinian eruptions in the future, including precursory to sin-eruptive (e.g., ground deformation via FEM models, seismicity, sin-eruptive debris flows) and post-eruptive (e.g., post-eruptive debris flows via reverse engineering) phenomena. In particular, secondary phenomena, such as debris flows generated by the remobilization of ash and fine lapilli deposits, can significantly impact the local landscape over long periods of time. This is because a thicker, but local, debris flow deposit can form after variably-fast remobilization of a thinner primary pyroclastic deposit, particularly along ravines and inside valleys. Such a phenomenon can occur multiple times, also depending on seasonal local weather, and this has a heavy impact on landscape, hence on local human activities, as it has occurred in the Sorrento Peninsula after the 79 CE eruption of Vesuvius.

Lastly, other issues will be reconstructing and synchronizing the climatic phases (through archives) at the time of the 79 CE eruption, in order to generally assess the environmental impact of Plinian eruptions at regional scale, and studying and measuring systematically the outsized clasts (ballistics, boulders, charred trunks, walls) found both in the fall and pyroclastic current deposits of the 79 CE eruption of Vesuvius, in order to assess the ballistic impacts and flow dynamic pressures on landscape and urban areas. Systematic studies and mapping of spatial distribution of fall and pyroclastic current impact parameters are lacking for this eruption, and they will be done to further improve the knowledge of products vs. processes related to Plinian eruptions. Such need is indeed related to the lesson learned from the 79 CE eruption, and its impacting feature on landscape. By imagining to zoom in the eruption at the scale, for example, of Roman towns, we find general aspects that can be applied to many explosive volcanoes worldwide, particularly when inhabited areas are directly exposed to eruption impact (e.g., at Merapi; see Jenkins et al., 2013). By also keeping in mind the principles of thermodynamics, and the governing equations that model volcanic processes, we find at Vesuvius that locally-enhanced flow dynamic pressures and velocities, forced deposition against obstacles vs. shadow zones with no deposition, and thermal effects can be extremely important during pyroclastic current-building interaction, not only in proximal reaches (Luongo et al., 2003a; Zuccaro and Ianniello, 2004; Gurioli et al., 2005a; Di Vito et al., 2009; Doronzo and Dellino, 2011; Scandone et al., 2019). The archaeological excavations that have been made over the years in the Roman towns around Vesuvius, and very likely the ones that will be made in the future, shed an alarm in volcanic hazard assessment at the scale of city, as modern architecture could take advantage from what happened in 79 CE. On the other hand, a multiphase fluid dynamic approach is necessary for constraining the interaction between pyroclastic currents and local topographies/urban structures.

All these points could contribute to address quantitatively each of the different but contiguous phenomena occurring in Plinian eruptions, without neglecting the ensemble view of the explosive event from the magma chamber to the most distal tephras. A complete knowledge of these eruptions, of the factors governing their dynamics and phases, and of all source and impact parameters is of paramount importance also in risk evaluation and mitigation, especially in densely inhabited and urbanized areas, but also in distal and ultradistal ones, in consideration of the vulnerability of our structures and infrastructures. This is a further lesson also for the next-generation models of explosive eruptions, which will take advantage from a more precise timing of the different eruptive phases, from a global evolution of the volcanic cloud at regional scale, and from a local impact of the pyroclastic currents at municipal scale. We would like to conclude with the Ascanio Filomarino's words about the importance of systematically collecting data before, during, and after an eruption. When he was describing his pioneeristic seismograph, now in exhibition at the Museum of Osservatorio Vesuviano - INGV, he concluded that "…*By observing these together with the external signs of the volcano, it may sometimes be possible, if not to clearly foresee a new eruption, at least to conjecture it*" (Filomarino, 1797).

CRediT authorship contribution statement

Domenico M. Doronzo: Conceptualization, Methodology, Validation, Investigation, Data curation, Writing – original draft, Writing – review & editing, Visualization, Supervision. **Mauro A. Di Vito:** Conceptualization, Methodology, Validation, Investigation, Data curation, Writing – original draft, Writing – review & editing, Visualization, Supervision. **Ilenia Arienzo:** Writing – original draft, Visualization. **Monica Bini:** Writing – original draft, Visualization. **Benedetta Calusi:**

Writing – original draft, Visualization. **Matteo Cerminara:** Writing – original draft, Visualization. **Stefano Corradini:** Writing – original draft, Visualization. **Sandro de Vita:** Writing – original draft, Visualization. **Biagio Giaccio:** Writing – original draft, Visualization. **Lucia Gurioli:** Writing – original draft, Visualization. **Giorgio Mannella:** Writing – original draft, Visualization. **Giovanni P. Ricciardi:** Writing – original draft, Visualization. **Ilaria Rucco:** Writing – original draft, Visualization. **Domenico Sparice:** Writing – original draft, Visualization. **Micol Todesco:** Writing – original draft, Visualization. **Elisa Trasatti:** Writing – original draft, Visualization. **Giovanni Zanchetta:** Writing – original draft, Visualization.

Declaration of Competing Interest

The authors declare that they have no known competing financial interests or personal relationships that could have appeared to influence the work reported in this paper.

Acknowledgements

This work was supported by the INGV project Pianeta Dinamico - Working Earth (CUP 1466 D53J19000170001 - "Fondo finalizzato al rilancio degli investimenti delle 1467 amministrazioni centrali dello Stato e allo sviluppo del Paese", legge 145/2018) - Task V3, and with the financial support of Presidenza del Consiglio dei Ministri and Dipartimento della Protezione Civile DPC-INGV project, resp. Di Vito M.A. This is Laboratory of Excellence ClerVolc contribution number 545. We thank Ente Parco Nazionale del Vesuvio, la Soprintendenza Archeologia, Belle Arti e Paesaggio per il Comune di Napoli e per le Province di Salerno e Avellino, Parco Archeologico di Paestum e Velia, and Parco Archeologico di Pompeii. We really thank the revisions provided by Ray Cas, Karoly Nemeth, and an anonimous reviewer, and the editorial work by Gillian Foulger. Doronzo D.M. dedicates this work to Diana.

Appendix A. Supplementary data

Supplementary data to this article can be found online at https://doi.org/10.1016/j.earscirev.2022.104072.

References

Agustin-Flores, J., Németh, K., Cronin, S.J., Lindsay, J.M., Kereszturi, G., Brand, B.D., Smith, I.E.M., 2014. Phreatomagmatic eruptions through unconsolidated coastal plain sequences, Maungataketake, Auckland Volcanic Field (New Zealand). J. Volcanol. Geotherm. Res. 276, 46–63.

Aldrete, G.S., 2007. Flood of the Tiber in Ancient Roma, Baltimore.

Aubry, T.J., Cerminara, M., Jellinek, A.M., 2019. Impacts of climate change on volcanic stratospheric injections: comparison of 1-D and 3-D plume model projections. Geophys. Res. Lett. 2019GL083975.

Anderson, P.W.S., 2014. Pompeii. FilmDistrict, Constantin Film Produktion, Don Carmody Productions. Impact Pictures.

Arrighi, S., et al., 2001. Violent strombolian and subplinian eruptions at Vesuvius during post-1631 activity. Bull. Volcanol. 63, 126–150.

Aubry, T.J., et al., 2021. The Independent Volcanic Eruption Source Parameter Archive (IVESPA, version 1.0): a new observational database to support explosive eruptive column model validation and development. J. Volcanol. Geotherm. Res. 417.

Auger, E., Gasparini, P., Virieux, J., Zollo, A., 2001. Seismic evidence of an extended magmatic sill under Mt. Vesuvius. Science (80) 294, 1510–1512. https://doi.org/10.1126/SCIENCE.1064893.

Avvisati, C., 2018. Il Mattino, Giovedì 18 Ottobre 2018.

Bagheri, G.H., Bonadonna, C., Manzella, I., Vonlanthen, P., 2015. On the characterization of size and shape of irregular particles. Powder Technol. 270, 141–153.

Baker, A., Hellstrom, J.C., Kelly, B.F.J., Mariethoz, G., Trouet, V., 2015. A composite annual-resolution stalagmite record of North Atlantic climate over the last three Millennia. Sci. Rep. 5, 10307.

Balachandar, S., Eaton, J.K., 2010. Turbulent Dispersed Multiphase Flow. Annu. Rev. Fluid Mech. 42, 111–133.

Balcone-Boissard, H., Villemant, B., Boudon, G., Michel, A., 2008. Non-volatile vs volatile behaviours of halogens during the AD 79 plinian eruption of Mt. Vesuvius. Earth Planet. Sci. Lett. 269, 66–79.

Barbante, C., Kehrwald, N.M., Marianelli, P., Vinther, B.M., Steffensen, J.P., Cozzi, G., Hammer, C.U., Clausen, H.B., Siggaard-Andersen, M.-L., 2013. Greenland ice core evidence of the 79 AD Vesuvius eruption. Clim. Past 9, 1221–1232.

Barberi, F., Bizouard, H., Clocchiatti, R., Metrich, N., Santacroce, R., Sbrana, A., 1981. The somma-vesuvius magma chamber: a petrological and volcanological approach. Bull. Volcanol. 1981 443 44, 295–315. https://doi.org/10.1007/BF02600566.

Barberi, F., Cioni, R., Rosi, M., Santacroce, R., Sbrana, A., Vecci, R., 1989. Magmatic and phreatomagmatic phases in explosive eruptions of Vesuvius as deduced by grain-size and compositional analysis of pyroclastic deposits. J. Volcanol. Geotherm. Res. 38, 287–307.

Barberi, F., Macedonio, G., Pareschi, M.T., Santacroce, R., 1990. Mapping the tephra fallout risk: an example from Vesuvius, Italy. Nature 344 (6262), 142–144. https://doi.org/10.1038/344142a0.

Baxter, P.J., Neri, A., Todesco, M., 1998. Physical modelling and human survival in pyroclastic flows. Nat. Hazards 17, 163–176.

Biggs, J., Ebmeier, S.K., Aspinall, W.P., Lu, Z., Pritchard, M.E., Sparks, R.S.J., Mather, T. A., 2014. Global link between deformation and volcanic eruption quantified by satellite imagery. Nat. Commun. https://doi.org/10.1038/ncomms4471.

Bignami, C., Chini, M., Amici, S., Trasatti, E., 2020. Synergic use of multi-sensor satellite data for volcanic hazards monitoring: the fogo (Cape Verde) 2014–2015 effusive eruption. Front. Earth Sci. 8, 22. https://doi.org/10.3389/feart.2020.00022.

Bini, M., Zanchetta, G., Perşoiu, A., Cartier, R., Català, A., Cacho, I., Dean, J.R., Di Rita, F., Drysdale, R.N., Finnè, M., Isola, I., Jalali, B., Lirer, F., Magri, D., Masi, A., Marks, L., Mercuri, A.M., Peyron, O., Sadori, L., Sicre, M.A., Welc, F., Zielhofer, Brisset E., 2019. The 4.2 ka BP event in the mediterranean region: an overview. Clim. Past 15, 555–577.

Bini, M., Zanchetta, G., Regattieri, E., Isola, I., Drysdale, R.N., Fabiani, F., Genovesi, S., Hellstrom, J.C., 2020. Hydrological changes during the Roman Climatic Optimum in Northern Tuscany (Central Italy) as evidenced by speleothem records and archeological data. J. Quat. Sci. 35, 791–802. https://doi.org/10.1002/jqs.3224.

Bonasia, V., Del Pezzo, E., Pingue, F., Scandone, R., Scarpa, R., 1985. Eruptive history, seismic activity and ground deformations at Mt. Vesuvius, Italy. Ann. Geophys. 3, 395–406.

Borgia, A., Tizzani, P., Solaro, G., Manzo, M., Casu, F., Luongo, G., Pepe, A., Berardino, P., Fornaro, G., Sansosti, E., Ricciardi, G.P., Fusi, N., Di Donna, G., Lanari, R., 2005. Volcanic spreading of Vesuvius, a new paradigm for interpreting its volcanic activity. Geophys. Res. Lett. 32, 1–4. https://doi.org/10.1029/2004GL022155.

Braccini, G.C., 1632. Dell'incendio fattosi nel Vesuvio a XVI di Dicembre MDCXXXI, Napoli, Secondino Roncagliolo.

Brosch, E., et al., 2021. Destructiveness of pyroclastic surges controlled by turbulent fluctuations. Nat. Commun. 12, 7306.

Bryan, S.E., Cas, R.A.F., Martí, J., 2000. The 0.57 Ma plinian eruption of the Granadilla Member, Tenerife (Canary Islands): an example of complexity in eruption dynamics and evolution. J. Volcanol. Geotherm. Res. 103, 209–238.

Büntgen, U., Myglan, V.S., Ljungqvist, F.C., McCormick, M., Di Cosmo, N., Sigl, M., Jungclaus, J., Wagner, S., Krusic, P.J., Esper, J., Kaplan, J.O., de Vaan, M.A.C., Luterbacher, J., Wacker, L., Tegel, W., Kirdyanov, A.V., 2016. Cooling and societal change during the late Antique Little Ice Age from 536 to around 660 AD. Nat. Geosci. 9, 231–237.

Cagnat, R., Feignon, J.G., Besnier, M., 1927. Année epigraphique, 0096. http://db.edcs.eu/epigr/epi_einzel.php?s_sprache=it&p_belegstelle=AE+1927,+00096&r_sortierung=Belegstelle.

Calusi, B., Andronico, D., Pecora, E., Biale, E., Cerminara, M., 2020. PyTirCam-1.0: a python model to manage thermal infrared camera data. Remote Sens. 12, 4056.

Cao, Z., Patra, A., Bursik, M., Pitman, E.B., Jones, M., 2017. Plume-SPH 1.0: a three-dimensional, dusty-gas volcanic plume model based on smoothed particle hydrodynamics. Geosci. Model Dev. Discuss. 1–37.

Cao, Z., Bursik, M., Yang, Q., Patra, A., 2021. Simulating the transport and dispersal of volcanic ash clouds with initial conditions created by a 3D plume model. Front. Earth Sci. 9, 1–18.

Carey, S., Sigurdsson, H., 1987. Temporal variations in column height and magma discharge rate during the 79 A.D. eruption of Vesuvius. Geol. Soc. Am. Bull. 99, 303–314.

Caricchi, C., Vona, A., Corrado, S., Giordano, G., Romano, C., 2014. 79 AD Vesuvius PDC deposits' temperatures inferred from optical analysis on woods charred in-situ in the Villa Dei Papiri at Herculaneum (Italy). J. Volcanol. Geotherm. Res. 289, 14–25.

Cas, R.A.F., Wright, J.V., 1987. Volcanic successions: Modern and Ancient. Chapman & Hall, p. 528.

Cassano, E., La Torre, P., 1987. Geophysics, in: Santacroce, R. (Ed.), Somma-Vesuvius. Quaderni de "La Ricerca Scientifica", CNR, Roma, pp. 175–195.

Cassio, Dione, 2000. Storia romana LXVI, 21–24. Testo Greco a fronte, vol. 7. Libri 64-67. Ed. BUR.

Cella, F., Fedi, M., Florio, G., Grimaldi, M., Rapolla, A., 2007. Shallow Structure of the Somma-Vesuvius Volcano from 3D Inversion of Gravity Data. https://doi.org/10.1016/j.jvolgeores.2006.12.013.

Cerminara, M., Esposti Ongaro, T., Valade, S., Harris, A.J.L., 2015. Volcanic plume vent conditions retrieved from infrared images: a forward and inverse modeling approach. J. Volcanol. Geotherm. Res. 300, 129–147.

Cerminara, M., Esposti Ongaro, T., Berselli, L.C., 2016a. ASHEE-1.0: a compressible, equilibrium–Eulerian model for volcanic ash plumes. Geosci. Model Dev. 9, 697–730.

Cerminara, M., Esposti Ongaro, T., Neri, A., 2016b. Large eddy simulation of gas-particle kinematic decoupling and turbulent entrainment in volcanic plumes. J. Volcanol. Geotherm. Res. 326, 143–171.

Cerminara, M., Brosch, E., Lube, G., 2021. A theoretical framework and the experimental dataset for benchmarking numerical models of dilute pyroclastic density currents. ArXiv 2106.14057, 1–17.
Cini Castagnoli, G., Bonino, G., Caprioglio, F., Provenzale, A., Serio, M., Guang-Mei, Z., 1990. The carbonate profile of two recent Ionian Sea cores: evidence that the sedimentation rate is constant over the last millennia. Geophys. Res. Lett. 17, 1937–1940.
Cinque, A., Robustelli, G., 2009. Alluvial and coastal hazards caused by long-range effects of Plinian eruptions: the case of the Lattari Mts. After the AD 79 eruption of Vesuvius. Geol. Soc. Lond. Spec. Publ. 322, 155–171.
Cioni, R., 2000. Volatile content and degassing processes in the AD 79 magma chamber at Vesuvius (Italy). Contrib. Mineral. Petrol. 140, 40–54.
Cioni, R., Marianelli, P., Sbrana, A., 1990. L'eruzione del 79 d.C.: stratigrafia dei depositi ed impatto sugli insediamenti romani nel settore orientale e meridionale del Somma-Vesuvio. Rivista di Studi Pompeiani IV, pp. 179–198.
Cioni, R., Marianelli, P., Sbrana, A., 1992. Dynamics of the A.D. 79 eruption: stratigraphic, sedimentological and geochemical data on the successions from the Somma-Vesuvius southern and eastern sectors. Acta Vulcanol. 2, 109–123.
Cioni, R., Civetta, L., Marianelli, P., Metrich, N., Santacroce, R., Sbrana, A., 1995. Compositional layering and syneruptive mixing of a periodically refilled shallow magma chamber: the AD 79 Plinian eruption of Vesuvius. J. Petrol. 36, 739–776.
Cioni, R., Gurioli, L., Sbrana, A., Vougioukalakis, G., 2000. Precursory phenomena and destructive events related to the late Bronze Age Minoan (Thera, Greece) and 79 AD (Vesuvius, Italy) Plinian eruptions: Inferences from the stratigraphy in the archaeological areas. Geol. Soc. Spec. Publ. 171, 123–141.
Cioni, R., Longo, A., Macedonio, G., Santacroce, R., Sbrana, A., Sulpizio, R., Andronico, D., 2003. Assessing pyroclastic fall hazard through field data and numerical simulations: example from Vesuvius. J. Geophys. Res. 108, B22063.
Cioni, R., Gurioli, L., Lanza, R., Zanella, E., 2004. Temperatures of the AD 79 pyroclastic density current deposits (Vesuvius, Italy). J. Geophys. Res. 109, 1–18. https://doi.org/10.1029/2002JB002251.
Cioni, R., Pistolesi, M., Rosi, M., 2015. Plinian and Subplinian Eruptions. In: Encyclopedia of Volcanoes, 2nd Ed. Elsevier Science Publishing.
Cioni, R., Tadini, A., Gurioli, L., Bertagnini, A., Mulas, M., Bevilacqua, A., Neri, A., 2020. Estimating eruptive parameters and related uncertainties for pyroclastic density currents deposits: worked examples from Somma-Vesuvius (Italy). Bull. Volcanol. 82, 65. https://doi.org/10.1007/s00445-020-01402-7.
Civetta, L., Galati, R., Santacroce, R., 1991. Magma mixing and convective compositional layering within the Vesuvius magma chamber. Bull. Volcanol. 1991 534 53, 287–300. https://doi.org/10.1007/BF00414525.
Corradini, S., Spinetti, C., Carboni, E., Tirelli, C., Buongiorno, M.F., Pugnaghi, S., Gangale, G., 2008. Mt. Etna tropospheric ash retrieval and sensitivity analysis using Moderate Resolution Imaging Spectroradiometer measurements. J. Appl. Remote. Sens. 2, 023550 https://doi.org/10.1117/1.3046674.
Corradini, S., Guerrieri, L., Lombardo, V., Merucci, L., Musacchio, M., Prestifilippo, M., Scollo, S., Silvestri, M., Spata, G., Stelitano, D., 2018. Proximal monitoring of the 2011-2015 Etna lava fountains using MSG-SEVIRI data. Geosci. Special Issue on Volcanic Plumes: Impacts on the Atmosphere and Insights into Volcanic Processes 8, 140. https://doi.org/10.3390/geosciences8040140.
Corradini, S., Guerrieri, L., Stelitano, D., Salerno, G., Scollo, S., Merucci, L., Prestifilippo, M., Musacchio, M., Silvestri, M., Lombardo, V., Caltabiano, T., 2020. Near real-time monitoring of the Christmas 2018 etna eruption using SEVIRI and products validation. Remote Sens. 12, 1336. https://doi.org/10.3390/rs12081336.
Cosentino, C., Molisso, F., Scopelliti, G., Caruso, A., Insinga, D., Lubritto, C., Pepe, F., Sacchi, M., 2017. Benthic foraminifera as indicators of relative sea-level fluctuations: Paleoenvironmental and paleoclimatic reconstruction of a Holocene marine succession (Calabria, South-Eastern Tyrrhenian Sea). Quat. Int. 439, 79–101.
Costa, A., et al., 2016. Results of the eruptive column model inter-comparison study. J. Volcanol. Geotherm. Res. 326, 2–25.
Costa, A., Suzuki, Y.J., Koyaguchi, T., 2018. Understanding the plume dynamics of explosive super-eruptions. Nat. Commun. 9.
Crocitti, M., Sulpizio, R., Insinga, D., De Rosa, R., Donato, P., Iorio, M., Zanchetta, G., Barca, D., Lubritto, C., 2018. On ash dispersal from moderately explosive volcanic eruptions: examples from Holocene and Late Pleistocene eruptions of Italian volcanoes. J. Volcanol. Geotherm. Res. 385, 198–221.
Dartevelle, S., et al., 2002. Origin of the Mount Pinatubo climactic eruption cloud: implications for volcanic hazards and atmospheric impacts. Geology 30, 663–666.
D'Auria, L., Massa, B., De Matteo, A., 2014. The stress field beneath a quiescent stratovolcano: the case of Mount Vesuvius. J. Geophys. Res. Solid Earth 119, 1181–1199. https://doi.org/10.1002/2013JB010792.
De Gori, P., Cimini, G.B., Chiarabba, C., De Natale, G., Troise, C., Deschamps, A., 2001. Teleseismic tomography of the Campanian volcanic area and surrounding Apenninic belt. J. Volcanol. Geotherm. Res. 109, 55–75. https://doi.org/10.1016/S0377-0273(00)00304-8.
De Natale, G., Petrazzuoli, S.M., Troise, C., Pingue, F., Capuano, P., 2000. Internal stress field at Mount Vesuvius: a model for background seismicity at a central volcano. J. Geophys. Res. Solid Earth 105, 16207–16214. https://doi.org/10.1029/2000jb900031.
De Natale, G., Troise, C., Trigila, R., Dolfi, D., Chiarabba, C., 2004. Seismicity and 3-D substructure at Somma-Vesuvius volcano: evidence for magma quenching. Earth Planet. Sci. Lett. 221, 181–196. https://doi.org/10.1016/S0012-821X(04)00093-7.
De Natale, G., Troise, C., Pingue, F., Mastrolorenzo, G., Pappalardo, L., 2006. The Somma-Vesuvius volcano (Southern Italy): Structure, dynamics and hazard evaluation. Earth-Sci. Rev. 74, 73–111. https://doi.org/10.1016/j.earscirev.2005.08.001.
Degruyter, W., Bonadonna, C., 2013. Impact of wind on the condition for column collapse of volcanic plumes. Earth Planet. Sci. Lett. 377-378, 218–226.
Dellino, P., Dioguardi, F., Isaia, R., et al., 2021. The impact of pyroclastic density currents duration on humans: the case of the AD 79 eruption of Vesuvius. Sci. Rep. 11, 4959. https://doi.org/10.1038/s41598-021-84456-7.
Dermody, B.J., Boer, H.J., Bierkens, M.F.P., Weber, S.L., Wassen, M.J., Dekker, S.C., 2012. A seesow in Mediterranean precipitation during the Roman Period linked to millennial-scale changes in the North Atlantic. Clim. Past 8, 637–651.
Devenish, B.J., Cerminara, M., 2018. The transition from Eruption Column to Umbrella Cloud. J. Geophys. Res. Solid Earth 123, 2018JB015841.
Di Donato, V., Ruello, M.R., Liuzza, V., Carsana, V., Giampaola, D., Di Vito, M.A., Morhange, C., Cinque, A., Ermolli, E.R., 2018. Development and decline of the ancient harbor of Neapolis. Geoarchaeology 33, 1–16.
Di Donato, V., Insinga, D.D., Iorio, M., Molisso, F., Rumolo, P., Cardines, C., Passaro, S., 2019. The palaeoclimatic and palaeoceanographic history of the Gulf of Taranto (Mediterranean Sea) in the last 15 ky. Glob. Planet. Chang. 172, 278–297.
Di Stefano, R., Chiarabba, C., 2002. Active source tomography at Mt. Vesuvius: Constraints for the magmatic system. J. Geophys. Res. Solid Earth 107, ESE 4-1. https://doi.org/10.1029/2001JB000792.
Di Vito, M.A., Zanella, E., Gurioli, L., Lanza, R., Sulpizio, R., Bishop, J., Tema, E., Boenzi, G., Laforgia, E., 2009. The Afragola settlement near Vesuvius, Italy: the destruction and abandonment of a Bronze Age village revealed by archeology, volcanology and rock-magnetism. Earth Planet. Sci. Lett. 277, 408–421.
Dobran, F., Neri, A., Macedonio, G., 1993. Numerical simulation of collapsing volcanic columns. J. Geophys. Res. 98 (B3), 4231–4259. https://doi.org/10.1029/92JB02409.
Dobran, F., Neri, A., Todesco, M., 1994. Assessing the pyroclastic flow hazard at Vesuvius. Nature 367 (6463), 551–554. https://doi.org/10.1038/367551a0.
Doronzo, D.M., 2012. Two new end members of pyroclastic density currents: Forced convection-dominated and inertia-dominated. J. Volcanol. Geotherm. Res. 219-220, 87–91.
Doronzo, D.M., Dellino, P., 2011. Interaction between pyroclastic density currents and buildings: Numerical simulation and first experiments. Earth Planet. Sci. Lett. 310, 286–292.
Doronzo, D.M., de Tullio, M.D., Dellino, P., Pascazio, G., 2011. Numerical simulation of pyroclastic density currents using locally refined Cartesian grids. Comput. Fluids 44, 56–67.
Doronzo, D.M., Martí, J., Sulpizio, R., Dellino, P., 2012. Aerodynamics of stratovolcanoes during multiphase processes. J. Geophys. Res. 117, B01207.
Doronzo, D.M., Giordano, G., Palladino, D.M., 2022. *Energy facies*: a global view of pyroclastic currents from vent to deposit. Terra Nova 34, 1–11.
Druitt, T., Calder, E.S., Cole, P.D., Hoblitt, R.P., Loughlin, S.C., Norton, G.E., Ritchie, L.J., Sparks, R.S.J., Voight, B., 2002. Small-volume, highly mobile pyroclastic flows formed by rapid sedimentation from pyroclastic surges at Soufrière Hills Volcano, Montserrat: An important volcanic hazard. In: Druitt, T., Kokelaar, P. (Eds.), The Eruption of Soufrière Hills Volcano, Montserrat, from 1995 to 1999. Geological Society, London, Memoirs, vol. 21, pp. 263–279.
Dufek, J., Bergantz, G.W., 2007. Suspended load and bed-load transport of particle-laden gravity currents: the role of particle–bed interaction. Theor. Comput. Fluid Dyn. 21, 119–145.
Dürig, T., Gudmundsson, M.T., Karmann, S., Zimanowski, B., Dellino, P., Rietze, M., Büttner, R., 2015. Mass eruption rates in pulsating eruptions estimated from video analysis of the gas thrust buoyancy transition—a case study of the 2010 eruption of Eyjafjallajökull, Iceland. Earth Planets Space 67, 180.
Esposti Ongaro, T., Neri, A., Menconi, G., de Michieli Vitturi, M., Marianelli, P., Cavazzoni, C., Erbacci, G., Baxter, P.J., 2008. Transient 3D numerical simulations of column collapse and pyroclastic density current scenarios at Vesuvius. JVGR 178, 378–396. https://doi.org/10.1016/j.jvolgeores.2008.06.036.
Esposti Ongaro, T., Cerminara, M., Charbonnier, S.J., Lube, G., Valentine, G.A., 2020. A framework for validation and benchmarking of pyroclastic current models. Bull. Volcanol. 82.
Esposti, Ongaro T., Neri, A., Todesco, M., Macedonio, G., 2002. Pyroclastic flow hazard assessment at Vesuvius (Italy) by using numerical modeling. II. Analysis of flow variables. Bull. Volcanol. 64, 178–191.
Esposti, Ongaro T., Cavazzoni, C., Erbacci, G., Neri, A., Salvetti, M.V., 2007. A parallel multiphase flow code for the 3D simulation of volcanic explosive eruptions. Parallel Comput. 33, 541–560. https://doi.org/10.1016/j.parco.2007.04.003.
Ferry, J., Balachandar, S., 2001. A fast Eulerian method for disperse two-phase flow. Int. J. Multiphase Flow 27, 1199–1226.
Filomarino, A., 1797. Gabinetto Vesuviano del Duca della Torre (III ed.). Talani, Napoli.
Folch, A., Costa, A., Macedonio, G., 2015. FPLUME-1.0: an integrated volcanic plume model accounting for ash aggregation. Geosci. Model Dev. Discuss. 8, 8009–8062.
Fisher, R.V., Schmincke, H.U., 1984. Pyroclastic Rocks. Springer Berlin, Heidelberg, p. 472.
Folch, A., et al., 2020. FALL3D-8.0: a computational model for atmospheric transport and deposition of particles, aerosols and radionuclides - part 1: Model physics and numerics. Geosci. Model Dev. 13, 1431–1458.
Freret-Lorgeril, V., et al., 2021. Examples of multi-sensor determination of eruptive source parameters of explosive events at Mount Etna. Remote Sens. 13.
Galli, P., Scionti, V., 2006. Two unknown M > 6 historical earthquakes revealed by palaeoseismological and archival researches in eastern Calabria (southern Italy). Seismotectonic implications. Terra Nova 18, 44–49.
Gasparini, P., Zollo, A., Auger, E., Bobbio, A., Emolo, A., Frattini, M., Herrero, A., Iannaccone, G., Improta, L., Nielsen, S., Simini, M., Achauer, U., Jordan, M., Chiarabba, C., Ciaccio, M.G., Lucente, P.F., De Franco, R., Biella, G., Del Pezzo, E., De Matteis, R., La Rocca, M., De Natale, G., Capuano, P., Godano, C., Martini, M.,

Pingue, F., Troise, C., Dietrich, M., Coutant, O., Guerra, I., Kissling, E., Marsella, E., Milana, G., Gorini, A., Marcucci, A., Zambonelli, E., Mirabile, L., Buonocore, B., Nowack, R., Scarpa, R., De Luca, G., Filippi, L., Solarino, S., Eva, E., Virieux, J., Bertrand, E., Charvis, P., Deschamps, A., Deverchere, J., Lomax, A., Montelli, R., Bongiovanni, G., 1998. Looking Inside Mt. Vesuvius. Eos (Washington. DC), 79, pp. 229–232. https://doi.org/10.1029/98EO00165.

Giacomelli, L., Perrotta, A., Scandone, R., Scarpati, C., 2003. The eruption of Vesuvius of 79 AD and its impact on human environment in Pompeii. Episodes 26, 235–238.

Giacomelli, L., Scandone, R., Rosi, M., 2021. The loss of geological memory of past catastrophes: the case of Pompeii. Ann. Geophys. 64, V0547.

Gigante, M., 1989. Il Fungo sul Vesuvio secondo Plinio il Giovane. Lucarini Ed. 38.

Gouhier, M., Donnadieu, F., 2008. Mass estimations of ejecta from Strombolian explosions by inversion of Doppler radar measurements. J. Geophys. Res. Solid Earth 113, 1–17.

Gouhier, M., et al., 2019. Low efficiency of large volcanic eruptions in transporting very fine ash into the atmosphere. Sci. Rep. 9, 1449.

Gurioli, L., Cioni, R., Sbrana, A., Zanella, E., 2002. Transport and deposition from pyroclastic flows over densely inhabited areas: Herculaneum (Italy). Sedimentology 49, 929–953.

Gurioli, L., Pareschi, M.T., Zanella, E., Lanza, R., Deluca, E., Bisson, M., 2005a. Interaction of pyroclastic currents with human settlements: evidences from ancient Pompeii. Geology 33 (6), 441–444.

Gurioli, L., Houghton, B., Cashman, K., Cioni, R., 2005b. Complex changes in eruption dynamics and the transition between Plinian and phreatomagmatic activity during the 79AD eruption of Vesuvius. Bull. Volcanol. 67, 144–159. https://doi.org/10.1007/s00445-004-0368-4.

Gurioli, L., Zanella, E., Pareschi, M.T., Lanza, R., 2007. Influences of urban fabric on pyroclastic density currents at Pompeii (Italy): flow direction and deposition (part I). J. Geophys. Res. 112 (B5) https://doi.org/10.1029/2006JB004444.

Gurioli, L., Sulpizio, R., Cioni, R., Sbrana, A., Luperini, W., Santacroce, R., Andronico, D., 2010. Pyroclastic flow hazard assessment at Somma-Vesuvius based on the geological record. Bull. Volcanol. 72 (9), 1021–1038. https://doi.org/10.1007/s00445-010-0379-2.

Hannah, R., 2013. Greek and Roman Calendars. A&C Black.

Hannah, R., 2016. Roman Calendars. A Companion to Science, Technology & Medicine in Ancient Greece and Rome, pp. 906–922.

Harper, K., 2017. The Fate of Rome. Climate, Disease and the End of an Empire. Princeton University.

Herzog, M., Oberhuber, J.M., Graf, H.-F., 2003. A Prognostic Turbulence Scheme for the Nonhydrostatic Plume Model ATHAM. J. Atmos. Sci. 2783–2796.

Hildreth, W., Fierstein, J., 2012. The Novarupta-Katmai eruption of 1912—largest eruption of the twentieth century; centennial perspectives: U.S. Geological Survey Professional Paper 1791, p. 259.

Insinga, D., Molisso, F., Lubritto, C., Sacchi, M., Passariello, I., Morra, V., 2008. The proximal marine record of Somma-Vesuvius volcanic activity in the Naples and Salerno bays, Eastern Tyrrhenian Sea, during the last 3 kyrs. J. Volcanol. Geotherm. Res. 177, 170–186.

Jalali, B., Sicre, M.-A., Bassetti, M.-A., Kallel, N., 2016. Holocene climate variability in the North-Western Mediterranean Sea (Gulf of Lions). Clim. Past 12, 91–101.

Jalali, B., Sicre, M.-A., Klein, V., Schmidt, S., Maselli, V., Lirer, F., Bassetti, M., Toucanne, S., Jorry, S.J., Insinga, D.D., Petrosino, P., Châles, F., 2018. Deltaic and coastal sediments as recorders of mediterranean regional climate and human impact over the past three millennia. Paleoceanogr. Paleoclimatol. 33, 579–593.

Jenkins, S., Komorowski, J.C., Baxter, P.J., Spence, R., Picquout, A., Lavigne, F., Surono, 2013. The Merapi 2010 eruption: an interdisciplinary impact assessment methodology for studying pyroclastic density current dynamics. J. Volcanol. Geotherm. Res. 261, 316–329.

Keenan-Jones, D., 2015. Somma-vesuvian ground movements and the water supply of pompeii and the bay of Naples. Am. J. Archaeol. 119, 191–215. https://doi.org/10.3764/AJA.119.2.0191.

Keller, J., Ryan, W.B.F., Ninkovich, D., Altherr, R., 1978. Explosive volcanic activity in the Mediterranean over the past 200,000 yrs as recorded in deep-sea sediments. Geol. Soc. Am. Bull. 89, 591–604.

Kent, D.V., Ninkovich, D., Pescatore, T., Sparks, R.S.J., 1981. Palaeomagnetic determination of emplacement temperature of Vesuvius AD 79 pyroclastic deposits. Nature 290, 393–396.

Koyaguchi, T., Suzuki, Y.J., 2018. The condition of eruption column collapse: 1. A reference model based on analytical solutions. J. Geophys. Res. Solid Earth 123, 7461–7482.

Koyaguchi, T., Suzuki, Y.J., Takeda, K., Inagawa, S., 2018. The condition of eruption column collapse: 2. Three-dimensional numerical simulations of eruption column dynamics. J. Geophys. Res. Solid Earth 123, 7483–7508.

Lamb, H.H., 1995. Climate History and the Modern World, Second edition. Routledge, London, p. 433.

Lanari, R., De Natale, G., Berardino, P., Sansosti, E., Ricciardi, G.P., Borgstrom, S., Capuano, P., Pingue, F., Troise, C., 2002. Evidence for a peculiar style of ground deformation inferred at Vesuvius volcano. Geophys. Res. Lett. 29 https://doi.org/10.1029/2001gl014571, 6-1-6–4.

Lanphere, M., et al., 2007. 40Ar/39Ar ages of the AD 79 eruption of Vesuvius, Italy. Bull. Volcanol. 69, 259–263.

Lirer, L., Pescatore, T., Booth, B., Walker, G.P.L., 1973. Two Plinian pumice-fall deposits from Somma-Vesuvius, Italy. Geol. Soc. Am. Bull. 84, 759–772.

Lomax, A., Zollo, A., Capuano, P., Virieux, J., 2001. Precise, absolute earthquake location under Somma-Vesuvius volcano using a new three-dimensional velocity model. Geophys. J. Int. 146, 313–331. https://doi.org/10.1046/j.0956-540X.2001.01444.x.

Luongo, G., Perrotta, A., Scarpati, C., 2003a. Impact of the AD 79 explosive eruption on Pompeii, I. Relations amongst the depositional mechanisms of the pyroclastic products, the framework of the buildings and the associated destructive events. J. Volcanol. Geotherm. Res. 126, 201–223.

Luongo, G., Perrotta, A., Scarpati, C., De Carolis, E., Patricelli, G., Ciarallo, A., 2003b. Impact of the AD 79 explosiv eruption on Pompeii, II. Causes of death of the inhabitants inferred by stratigraphic analysis and areal distribution of the human casualties. J. Volcanol. Geotherm. Res. 126, 169–200.

Macedonio, G., Pareschi, M.T., Santacroce, R., 1988. A numerical simulation of the plinian fall phase of 79 AD eruption of Vesuvius. J. Geophys. Res. B: Solid Earth 93 (B12), 14817–14827. https://doi.org/10.1029/JB093iB12p14817.

Macedonio, G., Pareschi, M.T., Santacroce, R., 1990. Renewal of explosive activity at Vesuvius: models for the expected tephra fallout. J. Volcanol. Geotherm. Res. 40, 327–342.

Maiuri, A., 1958. Pompeii. Sci. Am. 198 (4), 68–82.

Malin, M.C., Sheridan, M.F., 1982. Computer assisted mapping of pyroclastic surges. Science 217, 637–639.

Manville, V., Németh, K., Kano, K., 2009. Source to sink: a review of three decades of progress in the understanding of volcaniclastic processes, deposits, and hazards. Sediment. Geol. 220, 136–161.

Marcaida, I., Maguregui, M., Morillas, H., Perez-Diez, S., Madariaga, J.M., 2019. Raman imaging to quantify the thermal transformation degree of Pompeian yellow ochre caused by the 79 AD Mount Vesuvius eruption. Anal. Bioanal. Chem. 411 (28), 7585–7593.

Margaritelli, G., Vallefuoco, M., Di Rita, F., Capotondi, L., Bellucci, L.G., Insinga, D.D., Petrosino, P., Bonomo, S., Cacho, I., Cascella, A., Ferraro, L., Florindo, F., Lubritto, C., Lubritto, C., Lurcock, P.C., Magri, D., Pelosi, N., Rettori, R., Lirer, F., 2016. Marine response to climate changes during the last five millennia in the Central Mediterranean Sea. Glob. Planet. Chang. 142, 53–72.

Marianelli, P., Métrich, N., Santacroce, R., Sbrana, A., 1995. Mafic magma batches at Vesuvius: a glass inclusion approach to the modalities of feeding stratovolocanoes. Contrib. Mineral. Petrol. 120, 159–169.

Martí, J., Groppelli, G., da Silveira, A.B., 2018. Volcanic stratigraphy: a review. J. Volcanol. Geotherm. Res. 357, 68–91.

Martí, J., Doronzo, D.M., Pedrazzi, D., Colombo, F., 2019. Topographical controls on small-volume pyroclastic flows. Sedimentology 66, 2297–2317.

Martí, J., Zafrilla, S., Andujar, J., Jimenez-Mejias, M., Scaillet, B., Pedrazzi, D., Doronzo, D.M., Scaillet, S., 2020. Controls of magma chamber zonation on eruption dynamics and deposits stratigraphy: the case of El Palomar fallout succession (Tenerife, Canary Islands). J. Volcanol. Geotherm. Res. 399, 106908.

Marturano, A., 2008. Sources of ground movement at Vesuvius before the AD 79 eruption: evidence from contemporary accounts and archaeological studies. J. Volcanol. Geotherm. Res. 177, 959–970. https://doi.org/10.1016/J.JVOLGEORES.2008.07.017.

Marturano, A., Varone, A., 1997. L'eruzione vesuviana del 24 agosto del 79 dC attraverso le lettere di Plinio il Giovane e le nuove evidenze archeologiche, pp. 57–72.

Marturano, A., Varone, A., 2005. The AD 79 eruption: seismic activity and effects of the eruption on Pompeii. In: Cultural responses to the volcanic landscape: the Mediterranean and beyond. Archaeological Institute of America, AIA colloquia and conference papers, Vol. 8, pp. 241–260.

Marturano, A., Aiello, G., Barra, D., 2011. Evidence for Late Pleistocene uplift at the Somma-Vesuvius apron near Pompeii. J. Volcanol. Geotherm. Res. 202, 211–227. https://doi.org/10.1016/j.jvolgeores.2011.02.010.

Marturano, A., Aiello, G., Barra, D., 2013. Somma-Vesuvius ground deformation over the last glacial cycle. J. Volcanol. Geotherm. Res. 255, 90–97. https://doi.org/10.1016/j.jvolgeores.2013.02.007.

Marzano, F.S., Mereu, L., Scollo, S., Donnadieu, F., Bonadonna, C., 2020. Tephra mass eruption rate from ground-based x-band and l-band microwave radars during the November 23, 2013, Etna Paroxysm. IEEE Trans. Geosci. Remote Sens. 58, 3314–3327.

Matoza, R.S., Fee, D., Green, D., Mialle, P., 2019. Volcano Infrasound and the International Monitoring System. In Infrasound Monitoring for Atmospheric Studies, vol. 5. (Springer International Publishing, pp. 1023–1077.

McCormick, M., Büntgen, U., Cane, M.A., Cook, E.R., Harper, K., Huybers, P., Litt, T., Manning, S.W., Mayewski, P.A., More, A.F.M., Nicolussi, K., Tegel, W., 2012. Climate Change during and after the Roman Empire: Reconstructing the past from Scientific and Historical evidence. J. Interdiscip. Hist. 43 (2), 169–220.

Mensing, S.A., et al., 2015. 2700 years of Mediterranean environmental change in central Italy: a synthesis of sedimentary and cultural records to interpret past impacts of climate on society. Quat. Sci. Rev. 116, 72–94.

Meo, M., Tammaro, U., Capuano, P., 2008. Influence of topography on ground deformation at Mt. Vesuvius (Italy) by finite element modelling. Int. J. Non. Linear. Mech. 43, 178–186. https://doi.org/10.1016/J.IJNONLINMEC.2007.12.005.

Merlin, A., 1962. Année Epigraphique, 288. http://db.edcs.eu/epigr/epi_einzel.php?s_sprache=it&p_belegstelle=AE+1962,+00288&r_sortierung=Belegstelle.

Moin, P., Squires, K.D., Cabot, W.H., Lee, S., 1991. A dynamic subgrid-scale model for compressible turbulence and scalar transport. Phys. Fluids A 3, 2746.

Moitra, P., Sonder, I., Valentine, G.A., 2018. Effects of size and temperature-dependent thermal conductivity on the cooling of pyroclasts in air. Geochem. Geophys. Geosyst. 19, 3623–3636.

Montone, P., Amato, A., Chiarabba, C., Buonasorte, G., Fiordelisi, A., 1995. Evidence of active extension in Quaternary volcanoes of Central Italy from breakout analysis and seismicity. Geophys. Res. Lett. 22, 1909–1912. https://doi.org/10.1029/95GL01326.

Morgan, D.J., Blake, S., Rogers, N.W., De Vivo, B., Rolandi, G., Davidson, J.P., 2006. Magma chamber recharge at Vesuvius in the century prior to the eruption of A.D. 79. Geology 34, 845–848.
Munno, R., Petrosino, P., 2004. New constraints on the occurrence of Y-3 Upper Pleistocene tephra marker layer in the Tyrrhenian Sea. Italian J. Quat. Sci. 17, 11–20.
Muschitiello, F., Pausata, F.S.R., Lea, J.M., Mair, D.W.F., Wohlfarth, B., 2017. Enhanced ice sheet 351 melting driven by volcanic eruptions during the last deglaciation. Nat. Commun. 8 (1) https://doi.org/10.1038/s41467-017-01273-1, 352 1–9.
Németh, K., Cronin, S.J., 2009. Phreatomagmatic volcanic hazards where rift-systems meet the sea, a study from Ambae Island, Vanuatu. J. Volcanol. Geotherm. Res. 180 (2–4), 246–258.
Németh, K., Palmer, J., 2019. Geological mapping of volcanic terrains: discussion on concepts, facies models, scales, and resolutions from New Zealand perspective. J. Volcanol. Geotherm. Res. 385, 27–45.
Neri, A., Dobran, F., 1994. Influence of eruption parameters on the thermofluid dynamics of collapsing volcanic columns. J. Geophys. Res. 99, 11833.
Neri, A., Macedonio, G., 1996. Numerical simulation of collapsing volcanic columns with particles of two sizes. J. Geophys. Res. 101, 8153–8174.
Neri, A., Esposti Ongaro, T., Macedonio, G., Gidaspow, D., 2003. Multiparticle simulation of collapsing volcanic columns and pyroclastic flow. J. Geophys. Res. 108, 2202.
Neri, A., Esposti Ongaro, T., Menconi, G., de Michieli Vitturi, M., Cavazzoni, C., Erbacci, G., Baxter, P.J., 2007. 4D simulation of explosive eruption dynamics at Vesuvius. GRL 34. https://doi.org/10.1029/2006GL028597.
Neri, A., Esposti, Ongaro T., de Michieli Vitturi, M., Cerminara, M., 2022. Multiphase Flow Modeling of Explosive Volcanic Eruptions. In: Transport Phenomena in Multiphase Systems. Mechanical Engineering Series. Springer, Cham.
Osanna, M., 2021. Le impronte della morte: l'invenzione dei calchi dei pompeiani. In: Studi e ricerche del Parco archeologico di Pompei, vol. 46, pp. 45–65. Ed. L'Erma di Bretschneider.
Osores, S., Ruiz, J., Folch, A., Collini, E., 2020. Volcanic ash forecast using ensemble-based data assimilation: an ensemble transform Kalman filter coupled with the FALL3D-7.2 model (ETKF-FALL3D version 1.0). Geosci. Model Dev. 13, 1–22.
Palladino, D.M., 2017. Simply pyroclastic currents. Bull. Volcanol. 79, 53.
Papale, P., Dobran, F., 1993. Modeling of the ascent of magma during the plinian eruption of Vesuvius in A.D. 79. J. Volcanol. Geotherm. Res. 58 (1–4), 101–132. https://doi.org/10.1016/0377-0273(93)90104-Y.
Pardini, F., et al., 2020. Ensemble-based data assimilation of volcanic ash clouds from satellite observations: application to the 24 december 2018 Mt. Etna explosive eruption. Atmosphere (Basel). 11, 1–31.
Pepe, F., Di Donato, V., Insinga, D., Molisso, F., Faraci, C., Sacchi, M., Dera, R., Ferranti, L., Passaro, S., 2018. Seismic stratigraphy of upper Quaternary shallow-water contourite drifts in the Gulf of Taranto (Ionian Sea, southern Italy). Mar. Geol. 397, 79–92.
Pfeiffer, T., Costa, A., Macedonio, G., 2005. A model for the numerical simulation of tephra fall deposits. J. Volcanol. Geotherm. Res. 140, 273–294.
Plunkett, G., Sigl, M., Schwaiger, H.F., Tomlinson, E.L., Toohey, M., McConnell, J.R., Pilcher, J.R., Hasegawa, T., Siebe, C., 2022. No evidence for tephra in Greenland from the historic eruption of Vesuvius in 79 CE: implications for geochronology and paleoclimatology. Clim. Past 18, 45–65.
Prata, A.J., Grant, I.F., 2001. Retrieval of microphysical and morphological properties of volcanic ash plumes from satellite data: application to Mt Ruapehu, New Zealand. Q. J. R. Meteorol. Soc. 127, 2153–2179.
Prata, A.J., Kerkmann, J., 2007. Simultaneous retrieval of volcanic ash and SO2 using MSG-SEVIRI measurements. Geophys. Res. Lett. 34, L05813.
Prata, G.S., Ventress, L.J., Carboni, E., Mather, T.A., Grainger, R.G., Pyle, D.M., 2019. A new parameterization of volcanic ash complex refractive index based on NBO/T and SiO2 content. J. Geophys. Res.-Atmos. 124, 1779–1797. https://doi.org/10.1029/2018JD028679.
Principe, C., Rosi, M., Santacroce, R., Sbrana, A., 1987. Explanatory Notes to the Geological Map of Vesuvius, Quaderni de "La Ricerca Scientifica". CNR, Roma.
Pyle, D.M., 1989. The thickness, volume and grainsize of tephra fall deposits. Bull. Volcanol. 51, 1–15.
Pyle, D.M., 2000. Sizes of Volcanic Eruptions. In: Encyclopedia of Volcanoes. Academic Press.
Radiotelevisione Italiana, 2020. Pompei - Ultima Scoperta. Rai Documentari.
Regattieri, E., Giaccio, B., Zanchetta, G., Drysdale, R.N., Galli, P., Nomade, S., Peronace, E., Wulf, S., 2015. Hydrological variability over Apennine during the Early Last Glacial precession minimum, as revealed by a stable isotope record from Sulmona basin, Central Italy. J. Quat. Sci. 30, 19–31.
Ricciardi, G.P., 2009. Diario del Monte Vesuvio. Edizioni Scientifiche e Artistiche.
Ricco, C., Petrosino, S., Aquino, I., Cusano, P., Madonia, P., 2021. Tracking the recent dynamics of Mt. Vesuvius from joint investigations of ground deformation, seismicity and geofluid circulation. Sci. Report. 1–14, 2021 111 11. doi:10.1038/s41598-020-79636-w.
Ripepe, M., De Angelis, S., Lacanna, G., Voight, B., 2010. Observation of infrasonic and gravity waves at Soufrière Hills Volcano, Montserrat. Geophys. Res. Lett. 37, L00E14.
Rivista di Studi Pompeiani - vol. XXXII, 2021 (L'Erma di Bretschneider).
Roche, O., 2015. Nature and velocity of pyroclastic density currents inferred from models of entrainment of substrate lithic clasts. Earth Planet. Sci. Lett. 418, 115–125.
Rolandi, G., Paone, A., Di Lascio, M., Stefani, G., 2007. The 79 AD eruption of Somma: the relationship between the date of the eruption and the southeast tephra dispersion. J. Volcanol. Geotherm. Res. 169, 87–98.
Rose, W.I., Wunderman, R.L., Hoffman, M.F., Gale, L., 1983. Atmospheric hazards of volcanic activity from a volcanologist's point of view: Fuego and Mount St. Helens. J. Volcanol. Geotherm. Res. 17, 133–157.
Rossi, E., Bonadonna, C., 2021. SCARLET-1.0: SpheriCal Approximation for viRtuaL aggrEgaTes. Geosci. Model Dev. 14, 4379–4400.
Ruggieri, N., Galassi, S., Tempesta, G., 2020. The effect of pyroclastic flows of the 79 AD eruption of Mount Vesuvius on the Pompeii's city walls. The case study of the sector near the Tower XI. J. Cult. Herit. 43, 235–241.
Russo, G., Giberti, G., 2004. Numerical modeling of surface deformations on Mt. Vesuvius volcano (Italy) in presence of asymmmetric elastic heterogeneities. J. Volcanol. Geotherm. Res. 133, 41–54.
Russo, G., Giberti, G., Sartoris, G., 1997. Numerical modeling of surface deformation and mechanical stability of Vesuvius volcano, Italy. J. Geophys. Res. Solid Earth 102, 24785–24800. https://doi.org/10.1029/97JB01776.
Sacchi, M., Insinga, D., Milia, A., Molisso, F., Raspini, A., Torrente, M.M., Conforti, A., 2005. Stratigraphic signature of the Vesuvius 79 AD event off the Sarno prodelta system, Naples Bay. Mar. Geol. 222-223, 443–469.
Sacchi, M., Molisso, F., Violante, C., Esposito, E., Insinga, D., Lubritto, C., Porfido, S., Toth, T., 2009. Insights into the flood-dominated fan-deltas: very high-resolution seismic examples off the Amalfi cliffed coasts, eastern Tyrrhenian Sea. Geol. Soc. Lond. Spec. Publ. 322, 33–71.
Samartin, S., Heiri, O., Joos, F., Renssen, H., Franke, J., Brönnimann, S., Tinner, W., 2017. Warm Mediterranean mid-Holocene summers inferred from fossil midge assemblages. Nat. Geosci. 10, 207–212.
Santacroce, R., 1987. Somma-Vesuvius. Quaderni de "La Ricerca Scientifica". CNR, Roma.
Scaillet, B., Pichavant, M., Cioni, R., 2008. Upward migration of Vesuvius magma chamber over the past 20,000 years. Nat. 216–219. https://doi.org/10.1038/nature07232, 2008 4557210 455.
Scandone, R., Giacomelli, L., 2001. The slow boiling of magma chambers and the dynamics of explosive eruptions. J. Volcanol. Geotherm. Res. 110, 121–136.
Scandone, R., Giacomelli, L., Rosi, M., 2019. Death, survival and damaga during the 79 AD eruption of Vesuvius which destroyed Pompeii and Herculaneum. J. Res. Didactics Geogr. 2, 5–30.
Scarpa, R., Tronca, F., Bianco, F., Del Pezzo, E., 2002. High resolution velocity structure beneath Mount Vesuvius from seismic array data. Geophys. Res. Lett. 29 https://doi.org/10.1029/2002GL015576, 36–1.
Scarpati, C., Perrotta, A., Martellone, A., Osanna, M., 2020. Pompeian hiatuses: new stratigraphic data highlight pauses in the course of the AD 79 eruption at Pompeii. Geol. Mag. 157, 695–700.
Sevink, J., De Neef, W., Di Vito, M.A., Arienzo, I., Attema, P.A.J., Van Loon, E.E., Ullrich, B., Den Haan, M., Ippolito, F., Noorda, N., 2020. A multidisciplinary study of an exceptional prehistoric waste dump in the mountainous inland of Calabria (Italy): implications for reconstructions of prehistoric land use and vegetation in Southern Italy. The Holocene. https://doi.org/10.1177/0959683620919974, 9/30 (2020).
Shea, T., Gurioli, L., Houghton, B.F., Cioni, R., Cashman, K.V., 2011. Transition from stable to collapsing column during the 79AD eruption of Vesuvius: the role of pyroclats density. Geology 39 (7), 695–698. https://doi.org/10.1130/G32092.1.
Shea, T., Gurioli, L., Houghton, B.F., 2012. Transitions between fall phases and pyroclastic density currents during the AD 79 eruption at Vesuvius: building a transient conduit model from the textural and volatile record. Bull. Volcanol. 74, 2363–2381. https://doi.org/10.1007/s00445-012-0668-z.
Sheridan, M.F., Malin, M.C., 1983. Application of computer assisted mapping to volcanic hazard evaluation of surge eruptions: Vulcano, Lipari and Vesuvius. J. Volcanol. Geotherm. Res. 17, 187–202.
Sheridan, M.F., Barberi, F., Rosi, M., Santacroce, R., 1981. A model of plinian eruptions of Vesuvius. Nature 289, 282–285.
Shimizu, H.A., et al., 2021. Validation of a two-layer depth-averaged model by comparison with an experimental dilute stratified pyroclastic density current. Bull. Volcanol. 83, 1–12.
Sicre, M.A., Jalali, B., Martrat, B., Schmidt, S., Bassetti, M.A., Kallel, N., 2016. Sea surface temperature variability in the North Western Mediterranean Sea (Gulf of Lion) during the Common Era. Earth Planet. Sc. Lett. 456, 124–133.
Siebe, C., Abrams, M., Macias, J.L., Obenholzner, J., 1996. Repeated volcanic distasters in Prehispanic time at Popocatépetl, Central Mexico: past key to the future? Geology 24, 399–402.
Sigl, M., Winstrup, M., McConnell, J.R., Welten, K.C., Plunkett, G., Ludlow, F., et al., 2015. Timing and 397 climate forcing of volcanic eruptions for the past 2,500 years. Nature 523 (7562). https://doi.org/10.1038/nature14565, 543–549. 398.
Sigurdsson, H., Carey, S., Cornell, W., Pescatore, T., 1985. The eruption of Vesuvius in a. D. 79, Natl. Geogr. Res. 3, 332–397.
Sigurdsson, H., Cornell, W., Carey, S., 1990. Influence of magma withdrawal on compositional gradients during the AD 79 Vesuvius eruption. Nature 345, 519–521.
Sohn, Y.K., Cronin, S.J., Brenna, M., Smith, I.E.M., Németh, K., White, J.D.L., Murtagh, R. M., Jeon, Y.M., Kwon, C.W., 2011. Ilchulbong tuff cone, Jeju Island, Korea, revisited; a compound monogenetic volcano involving multiple magma pulses, shifting vents, and discrete eruptive phases. Geol. Soc. Am. Bull. 124 (3–4), 259–274.
Sparks, R.S.J., et al., 1997. Volcanic Plumes. Wiley, p. 574.
Stefani, G., 2006. La vera data dell'eruzione. Archeo n. 10 (260) pagg. 10-13.
Sulpizio, et al., 2008. Discriminating the long distance dispersal of fine ash from sustained columns or near ground ash clouds: the example of the Pomici di Avellino eruption (Somma-Vesuvius, Italy). J. Volcanol. Geotherm. Res. 177, 263–276.
Sulpizio, et al., 2012. Hazard assessment of far-range volcanic ash dispersal from a violent Strombolian eruption at Somma-Vesuvius volcano, Naples, Italy: implications on civil aviation. Bull. Volcanol. 74, 2205–2218.

Sulpizio, R., Dellino, P., Doronzo, D.M., Sarocchi, D., 2014. Pyroclastic density currents: state of the art and perspectives. J. Volcanol. Geotherm. Res. 283, 36–65.
Suzuki, T., 1983. A theoretical model for dispersion of tephra. In: Shimozuru, D., Yokoyama, I. (Eds.), Volcanism: Physics and Tectonics. Arc, Tokyo, pp. 95–113.
Suzuki, Y.J., Koyaguchi, T., Ogawa, M., Hachisu, I., 2005. A numerical study of turbulent mixing in eruption clouds using a three-dimensional fluid dynamics model. J. Geophys. Res. 110, B08201.
Suzuki, Y.J., et al., 2016a. Inter-comparison of three-dimensional models of volcanic plumes. J. Volcanol. Geotherm. Res. 326, 26–42.
Suzuki, Y.J., Costa, A., Koyaguchi, T., 2016b. On the relationship between eruption intensity and volcanic plume height: Insights from three-dimensional numerical simulations. J. Volcanol. Geotherm. Res. 326, 120–126.
Tadini, A., Bevilacqua, A., Neri, A., Cioni, R., Biagioli, G., de Michieli Vitturi, M., Esposti Ongaro, T., 2021. Reproducing pyroclastic density current deposits of the 79 CE eruption of the Somma–Vesuvius volcano using the box-model approach. Solid Earth 12, 119–139. https://doi.org/10.5194/se-12-119-2021.
Tammaro, U., Riccardi, U., Romano, V., Meo, M., Capuano, P., 2021. Topography and structural heterogeneities in surface ground deformation: a simulation test for Somma-Vesuvius volcano. Adv. Geosci. 52, 145–152. https://doi.org/10.5194/ADGEO-52-145-2021.
Theys, N., Hedelt, P., De Smedt, I., Lerot, C., Yu, H., Vlietinck, J., Pedergnana, M., Arellano, S., Galle, B., Fernandez, D., et al., 2019. Global monitoring of volcanic SO2 degassing with unprecedented resolution from TROPOMI onboard Sentinel-5 Precursor. Sci. Rep. 9, 1–10.
Tierz, P., Stefanescu, E.R., Sandri, L., Sulpizio, R., Valentine, G.A., Marzocchi, W., Patra, A.K., 2018. Towards quantitative volcanic risk of pyroclastic density currents: Probabilistic hazard curves and maps around Somma-Vesuvius (Italy). J. Geophys. Res. Solid Earth 123, 6299–6317. https://doi.org/10.1029/2017JB015383.
Todesco, M., Neri, A., Esposti, Ongaro T., Papale, P., Macedonio, G., Santacroce, R., Longo, A., 2002. Pyroclastic flow hazard assessment at Vesuvius (Italy) by using numerical models. I. Large-scale dynamics. Bull. Volcanol. 64, 155–177.
Toniolo, L., Amoretti, V., Gravina, E., Martinelli, R., Scala, P., Sparice, D., 2021. Da Mumia alle ultime vittime di Pompei: nuove ricerche nella villa di Civita Giuliana. Rivist. Studi Pomp. XXXII, 123–130.
Tramparulo, F.D.A., Vitale, S., Isaia, R., Tadini, A., Bisson, M., Prinzi, E.P., 2018. Relation between alternating open/closed-conduit conditions and deformation patterns: an example from the Somma-Vesuvius volcano (southern Italy). J. Struct. Geol. 112, 138–153. https://doi.org/10.1016/J.JSG.2018.05.008.
Trolese, M., Cerminara, M., Esposti Ongaro, T., Giordano, G., 2019. The footprint of column collapse regimes on pyroclastic flow temperatures and plume heights. Nat. Commun. 10.
Valentine, G.A., 1987. Stratified flow in pyroclastic surges. Bull. Volcanol. 49, 616–630.
Valentine, G.A., Doronzo, D.M., Dellino, P., de Tullio, M.D., 2011. Effects of volcano profile on dilute pyroclastic density currents: numerical simulations. Geology 39, 947–950.
Vazquez, J.A., Ort, M.H., 2006. Facies variation of eruption units produced by the passage of single pyroclastic surge currents, Hopi Buttes volcanic field, USA. J. Volcanol. Geotherm. Res. 154, 222–236.
Wilson, L., Walker, G.P.L., 1987. Explosive volcanic eruptions - VI. Ejecta dispersal in plinian eruptions: the control of eruption conditions and atmospheric properties. Geophys. J.R. Astron.Astron. Soc. 89, 657–679.
Wulf, S., 2000. Das tephrochronologische Referenzprofil des Lago Grande di Monticchio - Eine detaillierte Stratigraphie des suditalienischen explosiven Vulkanismus der letzten 100.000 Jahre. Ph.D. Thesis, University of Potsdam, Germany, Scientific Technical. Report STR01/03, p. 124.
Zanchetta, G., Sulpizio, R., Roberts, N., Cioni, R., Eastwood, W.J., Siani, G., Caron, B., Paterne, M., Santacroce, R., 2011. Tephrostratigraphy, chronology and climatic events of the Mediterranean basin during the Holocene: an overview. The Holocene 21, 33–52.
Zanchetta, G., Giraudi, C., Sulpizio, R., Magny, M., Drysdale, R.N., Sadori, L., 2012a. Constraining the onset of the Holocene “Neoglacial” over the Central Italy using tephra layers. Quat. Res. 78, 236–247.
Zanchetta, G., van Welden, A., Baneschi, I., Drysdale, R.N., Sadori, L., Roberts, N., Giardini, M., Beck, C., Pascucci, V., 2012b. Multiproxy record for the last 4500 years from Lake Shkodra (Albania/Montenegro). J. Quat. Sci. 27, 780–789.
Zanchetta, G., Regattieri, E., Isola, I., Drysdale, R.N., Bini, M., Baneschi, I., Hellstrom, J. C., 2016. The so-called “4.2 event” in the Central Mediterranean and its climatic teleconnections. Alpine Medit. Quat. 29 (1), 5–17.
Zanchetta, G., Bini, M., Di Vito, M.A., Sulpizio, R., Sadori, L., 2019. Tephrostratigraphy of paleoclimatic archives in Central Mediterranean during the Bronze Age. Quat. Int. 499, 186–194.
Zanchetta, G., et al., 2020. I livelli vulcanoclastici: analisi chimica e considerazioni deposizionali. Il Musteriano di Grotta del Cavallo nel Salento (Scavi 1986-2005). Cultura e ambienti.
Zanella, E., Gurioli, L., Pareschi, M.T., Lanza, R., 2007. Urban fabric influences on pyroclastic density currents at Pompeii (Italy): deposit temperature (part II). J. Geophys. Res. 112 (B5) https://doi.org/10.1029/2006JB004775.
Zanella, E., Sulpizio, R., Gurioli, L., Lanza, R., 2014. Temperatures of the pyroclastic density currents deposits emplaced in the last 22 kyr at Somma-Vesuvius (Italy) Geological Society special Publications. In: Ort, M.H., Porreca, M., Geissman, J.W. (Eds.), The Use of Palaeomagnetism and Rock Magnetism to Understand Volcanic Processes, 396. Special Publications, Geological Society, London, pp. 13–33.
Zollo, A., Gasparini, P., Virieux, J., Le Meur, H., De Natale, G., Biella, G., Boschi, E., Capuano, P., De Franco, R., Dell’Aversana, P., De Matteis, R., Guerra, I., Iannaccone, G., Mirabile, L., Vilardo, G., 1996a. Seismic evidence for a low-velocity zone in the upper crust beneath mount vesuvius. Science (80). 274, 592–594. https://doi.org/10.1126/science.274.5287.592.
Zollo, A., Gasparini, P., Biella, G., De Franco, R., Buonocore, B., Mirabile, L., De Natale, G., Milano, G., Pingue, F., Vilardo, G., Bruno, P., De Matteis, R., Le Meur, H., Iannaccone, G., Deschamps, A., Virieux, J., Nardi, A., Frepoli, A., Hunstad, I., Guerra, I., 1996b. 2D seismic tomography of Somma-Vesuvius: description of the experiment and preliminary results. Ann. Geofis. 39, 471–486. https://doi.org/10.4401/ag-3983.
Zollo, A., Marzocchi, W., Capuano, P., Lomax, A., Iannaccone, G., 2002. Space and Time Behavior of Seismic activity at Mt. Vesuvius Volcano, Southern Italy. Bull. Seismol. Soc. Am. 92, 625–640. https://doi.org/10.1785/0120000287.
Zuccaro, G., Ianniello, D., 2004. Interaction of pyroclastic flows with building structures in an urban settlement: a fluid-dynamic simulation impact model. J. Volcanol. Geotherm. Res. 133, 345–352.